## ABSTRACT

# MODIFICATION OF SCATTERING FROM THICK CYLINDERS AND RADIATION FROM LOOPS BY IMPEDANCE LOADING

By

John R. Short

The modification of the scattering from a thick, slotted cylinder and the radiation and circuit properties of a circular loop antenna by impedance loading are investigated in this thesis.

The modification and control of the scattering of a plane electromagnetic wave by a thick, conducting, infinitely long cylinder loaded with several impedance-backed longitudinal slots is investigated in Part I of this thesis. The incident plane wave is polarized with its electric field vector perpendicular to the cylinder axis. The slots are electrically narrow and the electric fields across them are assumed to be constant. Within this assumption an exact theory is developed. Synthesis procedures are developed to find load impedances and purely reactive load impedances that cause the scattered field to vanish in one or more desired directions. Synthesis procedures are also developed for finding a single purely reactive load impedance that produces minimum scattering in one direction and load impedances which result in zero scattering in one direction at several frequencies. The frequency dependence and bandwidths of the different loadings are also considered. Extensive numerical results are presented. The theoretical predictions are confirmed with an experiment.

The modification of the radiation fields and circuit properties (impedance) of a loaded, circular-loop antenna is investigated in Part II of this thesis. An improved theory for the loop antenna is developed which includes a finite gap excitation. "Effective" gap widths are defined for the cases of a loop antenna driven by a two-wire line or a coaxial line. Excellent agreement between theoretical antenna admittances is found. The maximum and minimum gain attainable from a

loop loaded by a single impedance is presented for loops up to five wavelengths in circumference. A procedure is developed to facilitate the design of loaded loop antennas that have specified radiation patterns. Several examples of loaded loop antennas which have relatively directive patterns with respect to unloaded loop antennas are given. A scheme for matching a loop antenna to a transmission system is presented and its efficiency is compared to that of a conventional base tuning network.

# MODIFICATION OF SCATTERING FROM THICK CYLINDERS AND RADIATION FROM LOOPS BY IMPEDANCE LOADING

by

John R. Short

A THESIS

Submitted to
Michigan State University
in partial fulfillment of the requirements
for the degree of

DOCTOR OF PHILOSOPHY

Department of Electrical Engineering and Systems Science

1971

To My Parents

## ACKNOWLEDGMENTS

The author wishes to express his deep appreciation to his major professor, Dr. K. M. Chen, for his guidance and never-ending support through the course of this work. He also wishes to thank the other members of his guidance committee, Drs. D. P. Nyquist, J. S. Frame, J. Asmussen, and G. Kemeny for their time and interest in this work.

A special note of thanks is extended to Dr. D. P. Nyquist who introduced the author to electromagnetics and stimulated him with many enlightening discussions throughout his graduate education.

The research reported in this thesis was supported in part by the Air Force Cambridge Research Laboratory under Contract No. F19(628)-70-C-0072.

Finally, the author thanks his fiance, Mary, for correcting the spelling in the manuscript.

# TABLE OF CONTENTS

LIST OF FIGURES

PART I

| Figure | | Page |
|---|---|---|

Figure Page

| Figure | | Page |
|---|---|---|



PART II

## LIST OF TABLE

## PART II

# PART I

# MODIFICATION OF EM SCATTERING FROM A THICK CYLINDER BY MULTI-SLOT IMPEDANCE LOADING

# CHAPTER I

# INTRODUCTION

The modification of the electromagnetic wave scattered by a thick infinite cylinder using the technique of impedance loading is investigated in this study.

When a conducting body is illuminated by an electromagnetic wave a surface current is induced on the conducting body. This surface current, in turn, reradiates a scattered field. Distributed or lumped impedances can be installed on the surface of the conducting body which will alter the amplitude and phase of the induced surface current, thus modifying the scattered field. This method of modifying the field scattered by a conducting body is known as impedance loading. The modification or control of electromagnetic scattering has applications in the areas of antenna design, electromagnetic compatibility, scattering cross section modification and others.

The history and development of the impedance loading technique can be found in a review paper by Schindler, Mack, and Blacksmith.[1] Since the writing of this review paper, scattering modification by the impedance loading technique has received considerable attention.[2-17] A review of the literature shows that nearly all the studies have been concerned with impedance loaded thin wire rods or loops. To present, there have been only two published studies on impedance loading of electrically thick objects. Liepa and Senior[18] considered a conducting sphere loaded with a single impedance backed circumferential slot,* and the authors[15] considered a thick cylinder loaded with a single impedance backed longitudinal slot. There is a noticeable lack of any information on the modification and control of the field scattered by a thick object loaded with more than one impedance.

---

*Chen and Vincent[6,10] also loaded a sphere with two loaded wires which is another technique of loading an object. This differs from the discreet surface loading considered in this study.

This study is concerned with an electrically thick conducting cylinder loaded with N impedance-backed longitudinal slots. The cylinder is illuminated with a normally incident plane electromagnetic wave polarized with its electric field vector perpendicular to the cylinder axis. The incident field induces a circumferential surface current on the surface of the cylinder. The control of the surface current, which in turn controls the scattering, is accomplished by the longitudinal loaded slots which intersect the induced current.

The purposes of this study are 1) to determine the extent of the control over the scattering that can be accomplished with different types of loading, 2) to develop and analyze procedures for determining optimal loadings which result in zero or minimum scattering in desired directions, 3) to determine what procedures lead to broad band loadings and 4) to develop broad banding techniques.

In Chapter II the basic theory used in analyzing the scattering from the loaded cylinder is developed. The theory is of a general form into which all multi-loaded scatters fall.[19, 20]

Chapter III deals with general synthesis procedures for finding optimal impedances that result in zero or minimum scattering in one or more desired directions. First, a procedure is developed for finding N load impedances which cause zero field to be scattered in N directions. This synthesis procedure is similar to the one used by Strait[21, 22, 23] in synthesizing radiation patterns of loaded antennas and arrays. Secondly, a procedure is developed for finding N purely reactive load impedances that result in zero field scattered in N/2 desired directions. After this, procedures are developed for finding a single purely reactive load impedance that produces minimum scattering in one direction and a set of N load impedances which result in zero scattering in one direction at N different frequencies.

Numerical results of these procedures and other loading schemes are presented and discussed in Chapter IV. The frequency dependence and bandwidths of these loading techniques are also considered.

The theoretical predictions are confirmed with an experiment. This is described in Chapter V.

Chapter VI summarizes the work presented in this study.

## CHAPTER II

## THEORETICAL FORMULATION OF PLANE WAVE SCATTERING BY A MULTI-LOADED, SLOTTED CYLINDER

### 2.1. Formulation of the Problem and Boundary Conditions

A perfectly conducting cylinder of infinite length and radius a has N impedance-backed longitudinal slots cut on its surface as indicated in Figure 2.1. The center of the nth slot is located at $\theta = \theta_n$. The nth slot has angular width $\delta_n$ and is loaded with an impedance $Z_n$ that is lumped in this slot region on the cylinder surface. The cylinder is illuminated by a plane electromagnetic wave which is linearly polarized with its $\vec{E}$-field vector perpendicular to the cylinder axis. This incident wave induces a circumferential surface current $K_\theta(\theta)$ on the cylinder, which in turn, radiates a scattered electromagnetic field.

The tangential $\vec{E}$-field must vanish at the cylinder surface except in the slot regions since the cylinder is assumed to be perfectly conducting. The slots are taken to be electrically narrow and thus the tangential $\vec{E}$-field is assumed to have a constant, uniform distribution within each slot region. The potential difference across the nth slot is

$$V_n = -\int_{\theta_n + \delta_n/2}^{\theta_n - \delta_n/2} E_\theta(r=a^-)\, a\, d\theta = a\delta_n E_\theta(r=a^-, \theta=\theta_n)$$

and is a slot voltage since the slots are electrically narrow so that the quasi-static approximation is valid. The boundary condition on the tangential $\vec{E}$-field at the surface of the illuminated slotted cylinder is

$$E_\theta^i(r=a^+) + E_\theta^s(r=a^+) = \begin{cases} \dfrac{V_n}{a\delta_n} & \text{for } |\theta - \theta_n| < \delta_n/2 \\ & n=1, 2, \ldots, N \\ 0 & \text{elsewhere} \end{cases} \qquad (1)$$

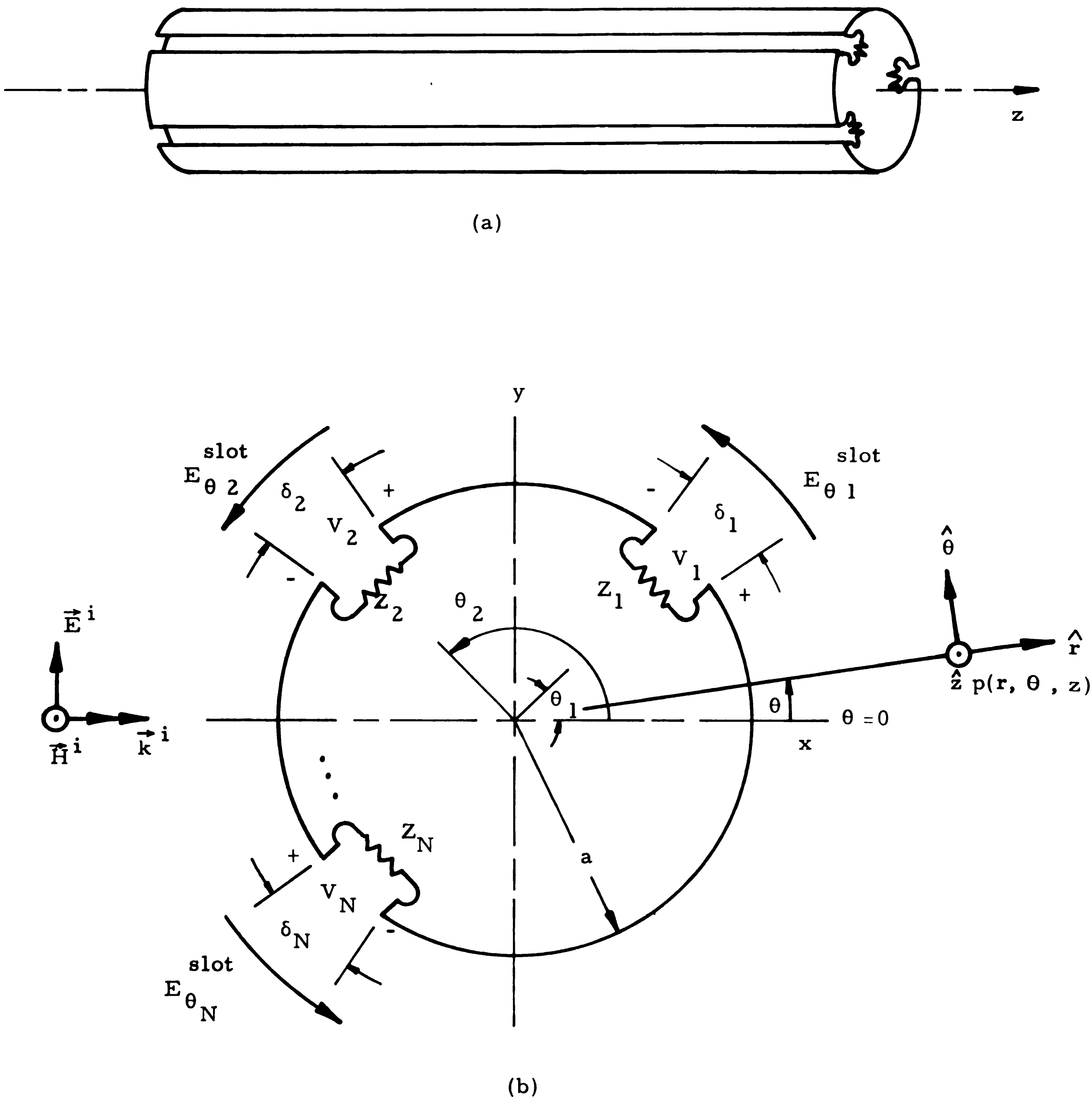


Figure 2. 1. An infinite cylinder with N longitudinal slots illuminated by a plane EM wave with its $\vec{E}$ -field vector perpendicular to the cylinder axis.
(a) Front view. (b) Cross Section view.

where $E^i_\theta$ and $E^s_\theta$ are the $\theta$ components of the incident and scattered $\vec{E}$-fields, respectively. The nth load impedance is defined by

$$V_n = Z_n K_\theta \;(\theta = \theta_n)$$

$$= -Z_n H_z(r=a,\; \theta = \theta_n) \quad . \tag{2}$$

It is noted that the physical dimension of the load impedance $Z_n$ is ohm-meter.

2.2. Superposition

The field scattered by a cylinder with N impedance-backed, longitudinal slots can be obtained by the superposition of the field scattered by an unloaded solid cylinder illuminated by a plane wave and the field radiated by a cylinder with N longitudinal slots having slot voltages $V_n$, $n = 1, 2, \ldots, N$ impressed across the slots. A mathematical statement of this superposition is

$$\vec{E}^s = \vec{E}^c + \vec{E}^r \tag{3}$$

$$\vec{H}^s = \vec{H}^c + \vec{H}^r \tag{4}$$

where $\vec{E}^s$ and $\vec{H}^s$ represent the field scattered by a slotted cylinder illuminated by a normally incident plane wave, $\vec{E}^c$ and $\vec{H}^c$ represent the field scattered by a solid cylinder illuminated by the same incident plane wave, and $\vec{E}^r$ and $\vec{H}^r$ represent the fields radiated by a slotted cylinder driven by slot voltages $V_n$. The excitation of the nth slot, $V_n$, must be determined in accordance with the total surface current on the illuminated slotted cylinder at the location of the slot and the impedance backing the slot. This superposition is indicated schematically in Figure 2.2.

The boundary condition (1) for the illuminated slotted cylinder can be separated into the boundary condition for the illuminated solid cylinder

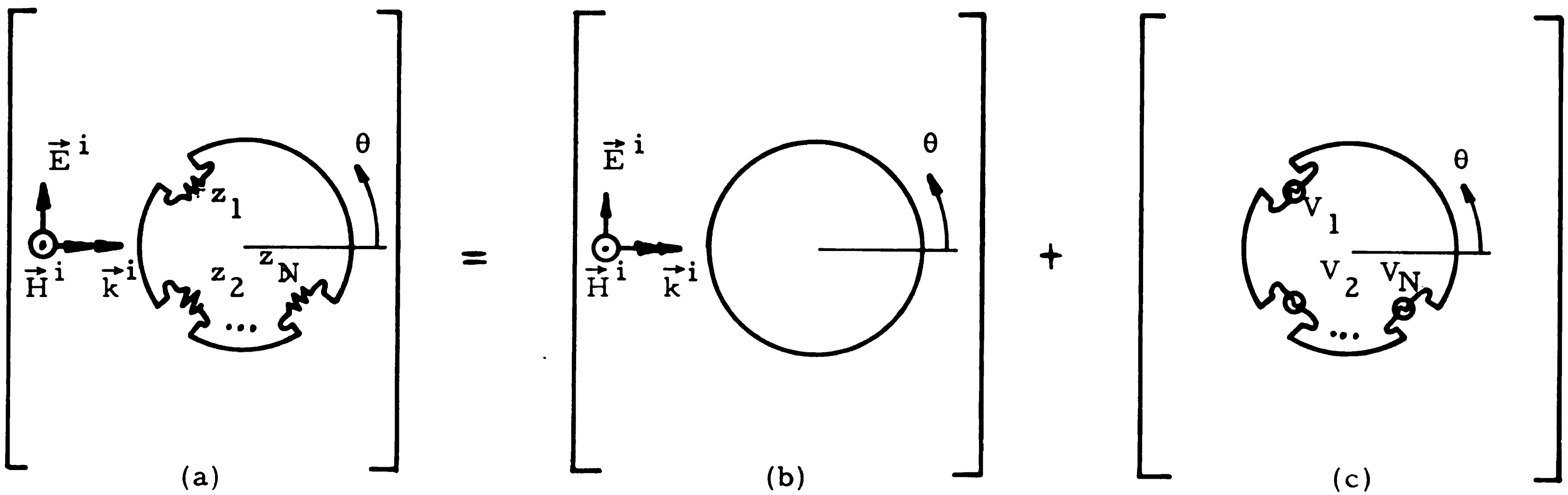


Figure 2. 2. Superposition for an illuminated cylinder with N loaded slots.
(a) Illuminated slotted cylinder. (b) Illuminated solid cylinder.
(c) Driven slotted cylinder.

$$E_\theta^i\ (r=a^+) + E_\theta^c\ (r=a^+) = 0 \tag{5}$$

and the boundary condition for the driven slotted cylinder

$$E_\theta^r\ (r=a^+) = \begin{cases} \dfrac{V_n}{a\delta_n} \text{ for } |\theta - \theta_n| < \dfrac{\delta_n}{2} \\ \qquad n = 1, 2, \ldots, N \\ \\ 0 \qquad \text{elsewhere} \end{cases} \tag{6}$$

Boundary conditions (5) and (6) define the scattering and radiation problems to be discussed in the following two sections.

## 2. 3. Scattering from a Solid Cylinder

Consider a perfectly conducting cylinder of radius a which is illuminated by a normally incident plane electromagnetic wave with an $\vec{E}$-field vector perpendicular to the cylinder axis. The geometry of the problem is defined in Figure 2. 2(b).

The incident plane wave can be represented by the following field expansions[24]:

$$H_z^i = e^{-jkx} = e^{-jkr\cos\theta}$$

$$= \sum_{n=0}^{\infty} \epsilon_{0n} (-j)^n \cos(n\theta)\, J_n(kr) \tag{7}$$

$$H_\theta^i = H_r^i = E_z^i = 0 \tag{8}$$

$$E_\theta^i = \frac{j}{\omega\epsilon_0} \frac{\partial}{\partial r} H_z^i$$

$$= j\zeta_0 \sum_{n=0}^{\infty} \epsilon_{0n} (-j)^n \cos(n\theta)\, J_n'(kr) \tag{9}$$

$$E_r^i = \frac{-j}{\omega \epsilon_0} \frac{1}{r} \frac{\partial}{\partial \theta} H_z^i$$

$$= \frac{j}{\omega \epsilon_0} \frac{1}{r} \sum_{n=0}^{\infty} \epsilon_{0n} (-j)^n n \sin(n\theta) J_n(kr) \tag{10}$$

where $J_n(kr)$ is the nth-order Bessel function of the first kind and $\epsilon_{0n}$ is the Neumann factor and equals unity for n=0 and is equal to 2 otherwise. The impedance of free-space $\zeta_0$ is $120\pi$ ohms, and k is the free-space wavenumber. The $e^{j\omega t}$ time-dependence factor is implied.

The solution for the fields scattered by a perfectly conducting infinite cylinder illuminated by a plane wave are well known[25, 26] and are given by

$$H_z^c = -\sum_{n=0}^{\infty} \epsilon_{0n} (-j)^n \cos(n\theta) J_n'(ka) \frac{H_n^{(2)}(kr)}{H_n^{(2)'}(ka)} \tag{11}$$

$$H_r^c = H_\theta^c = E_z^c = 0 \tag{12}$$

$$E_r^c = \frac{1}{\omega \epsilon_0} \frac{1}{r} \sum_{n=0}^{\infty} \epsilon_{0n} (-j)^{n+1} n \sin(n\theta) J_n'(ka) \frac{H_n^{(2)}(kr)}{H_n^{(2)'}(ka)} \tag{13}$$

$$E_\theta^c = \zeta_0 \sum_{n=0}^{\infty} \epsilon_{0n} (-j)^{n+1} \cos(n\theta) J_n'(ka) \frac{H_n^{(2)'}(kr)}{H_n^{(2)'}(ka)} \tag{14}$$

where $H_n^{(2)}(kr)$ is the nth-order Hankel function of the second kind.

## 2.4. Radiation from a Cylinder with N Driven Slots

The field radiated by a cylinder with N longitudinal slots which have voltages $V_1, V_2, \ldots, V_N$ impressed across them [see Figure 2.2 (c)] can be found by solving the boundary value problem subject to boundary condition (6).

The magnetic field has only a z component which is governed by the wave equation,

$$(\nabla^2 + k^2)\, H_z^r = 0 \tag{15}$$

The cylinder and slots are infinitely long and the excitation is assumed uniform axially, thus the radiated field has no z-dependence, that is $\frac{\partial}{\partial z} \equiv 0$ . The wave equation for $H_z^r$ becomes

$$\left[\frac{\partial^2}{\partial r^2} + \frac{1}{r}\frac{\partial}{\partial r} + \frac{1}{r^2}\frac{\partial^2}{\partial \theta^2} + k^2\right] H_z^r = 0 \; .$$

This partial differential equation can be solved by the method of separation of variables. The appropriate solution is

$$H_z^r = \sum_{n=0}^{\infty} \left[A_n \cos(n\theta) + B_n \sin(n\theta)\right] H_n^{(2)}(kr) \tag{16}$$

where $A_n$ and $B_n$ are unknown coefficients to be determined by boundary condition (6) and $H_n^{(2)}(kr)$ is the nth order Hankel function of the second kind which represents an outward traveling cylindrical wave. The other components of the radiated field can be determined from Equation (16) and Maxwell's equations. Coefficients $A_n$ and $B_n$ are found by applying boundary condition (6) to the $E_\theta^r$ component of the field [See Appendix A] and are

$$A_n = \frac{\epsilon_{0n}}{j2\pi a\zeta_0} \frac{1}{H_n^{(2)'}(ka)} \sum_{m=1}^{N} V_m \frac{\sin\left(\frac{n\delta_m}{2}\right)}{\left(\frac{n\delta_m}{2}\right)} \cos(n\theta_m) \tag{17}$$

$$B_n = \frac{\epsilon_{0n}}{j2\pi a\zeta_0} \frac{1}{H_n^{(2)'}(ka)} \sum_{m=1}^{N} V_m \frac{\sin\left(\frac{n\delta_m}{2}\right)}{\left(\frac{n\delta_m}{2}\right)} \sin(n\theta_m) \tag{18}$$

The field radiated from the cylinder with N driven slots is now completely determined and is given by

$$E_\theta^r = \frac{1}{2\pi a} \sum_{n=0}^{\infty} \epsilon_{0n} \frac{H_n^{(2)'}(kr)}{H_n^{(2)'}(ka)} \sum_{m=1}^{N} V_m \frac{\sin\left(\frac{n\delta_m}{2}\right)}{\left(\frac{n\delta_m}{2}\right)} \cos(n(\theta - \theta_m)) \tag{19}$$

$$E_r^r = \frac{1}{\pi akr} \sum_{n=1}^{\infty} n \frac{H_n^{(2)}(kr)}{H_n^{(2)'}(ka)} \sum_{m=1}^{N} V_m \frac{\sin\left(\frac{n\delta_m}{2}\right)}{\left(\frac{n\delta_m}{2}\right)} \sin(n(\theta - \theta_m)) \tag{20}$$

$$E_z^r = H_r^r = H_\theta^r = 0 \tag{21}$$

$$H_z^r = \frac{-j}{2\pi a\zeta_0} \sum_{n=0}^{\infty} \epsilon_{0n} \frac{H_n^{(2)}(kr)}{H_n^{(2)'}(ka)} \sum_{m=1}^{N} V_m \frac{\sin\left(\frac{n\delta_m}{2}\right)}{\left(\frac{n\delta_m}{2}\right)} \cos(n(\theta - \theta_m)) \tag{22}$$

2. 5. Scattering from a Cylinder with N Loaded Slots

The slot voltages $V_n$ which excite the slots of the driven cylinder must now be determined in view of our intent to combine the results of the preceding two sections. The voltages $V_n$ can be expressed in terms of the impedances backing the slots, $Z_n$, and the total surface current on the illuminated slotted cylinder. From Equation (2).

$$\begin{aligned} V_n &= -Z_n H_z(r=a, \theta=\theta_n) \\ &= -Z_n [H_z^i + H_z^c + H_z^r] \Big|_{\substack{r=a \\ \theta=\theta_n}} \\ &= -Z_n \left[-K_{n0} + \sum_{m=1}^{N} V_m y_{nm}\right] \end{aligned} \tag{23}$$

where

$$K_{n0} = -[H_z^i + H_z^c]\Big|_{\substack{r=a \\ \theta=\theta_n}}$$

$$= -\sum_{p=0}^{\infty} \epsilon_{0p} (-j)^p \cos(p\,\theta_n) \left[ J_p(ka) - J_p'(ka) \frac{H_p^{(2)}(ka)}{H_p^{(2)'}(ka)} \right]$$

$$= -\frac{2}{\pi ka} \sum_{p=0}^{\infty} \epsilon_{0p} (-j)^{p+1} \frac{\cos(p\theta_n)}{H_p^{(2)'}(ka)} \tag{24}$$

which is the value of the surface current on the unloaded solid cylinder evaluated at the position of the nth slot, and the terms

$$y_{nm} = \frac{-j}{2\pi a \zeta_0} \sum_{p=0}^{\infty} \epsilon_{0p} \frac{\sin(\frac{p\delta_m}{2})}{(\frac{p\delta_m}{2})} \frac{H_p^{(2)}(ka)}{H_p^{(2)'}(ka)} \cos(p(\theta_n - \theta_m)) \tag{25}$$

are the self and mutual short circuit radiation admittances of the slots. The dimensions of these admittances are mho/meter.

Equation (23) can be written in matrix form as

$$\begin{bmatrix} y_{11}+Y_1 & y_{12} & \cdots & y_{1N} \\ y_{21} & y_{22}+Y_2 & \cdots & y_{2N} \\ \vdots & & & \\ y_{N1} & y_{N2} & \cdots & y_{NN}+Y_N \end{bmatrix} \begin{bmatrix} V_1 \\ V_2 \\ \vdots \\ V_N \end{bmatrix} = \begin{bmatrix} K_{10} \\ K_{20} \\ \vdots \\ K_{N0} \end{bmatrix} \tag{26}$$

where $Y_n = 1/Z_n$ and is the load admittance of the nth slot. The voltages $V_n$ are found by solving the above matrix equation. From the superposition picture it is seen that the voltages, $V_n$, depend on the short circuited radiation admittances of the driven slotted cylinder and the surface current on the illuminated solid cylinder.

The fields scattered by an infinitely long, perfectly conducting cylinder with N impedance loaded longitudinal slots is now completely determined and can be obtained by the superposition of the results of the preceding two sections in accordance with Equations (3) and (4), and the solution to Equation (26).

In the radiation zone the scattered field behaves as an outward traveling TEM cylindrical wave, which can be observed by replacing $H_n^{(2)}(kr)$ and its derivative with their principal asymptotic forms for large arguments.[27] This procedure yields

$$E_\theta^{sr} = -\sqrt{\frac{2}{\pi kr}}\, e^{-j(kr-\pi/4)} \sum_{p=0}^{\infty} \left[ \zeta_0\, \epsilon_{0p} \cos(p\theta) \frac{J_p'(ka)}{H_p^{(2)'}(ka)} + \frac{\epsilon_{0p}}{2\pi a} \frac{(j)^{p+1}}{H_p^{(2)'}(ka)} \sum_{m=0}^{N} V_m \frac{\sin\left(\frac{p\delta_m}{2}\right)}{\left(\frac{p\delta_m}{2}\right)} \cos(p(\theta-\theta_m)) \right] \tag{27}$$

$$E_r^{sr} = E_z^{sr} = H_r^{sr} = H_\theta^{sr} = 0 \tag{28}$$

$$H_z^{sr} = E_\theta^{sr}/\zeta_0 \tag{29}$$

where the second superscript denotes radiation zone fields.

## 2.6. Bistatic Scattering Cross Section

The bistatic scattering cross section per unit length of the illuminated slotted cylinder is given by

$$\sigma(\theta) = \lim_{r\to\infty} 2\pi r \left| \frac{\vec{E}^{s}(\theta)}{\vec{E}^{i}} \right|^2 \tag{30}$$

where $\theta$ defines the direction in which the scattered field is received, and the illuminating plane wave is incident from the direction $\theta = 180°$.

Using Equation (27), the bistatic scattering cross section can be written

$$\sigma(\theta) = \frac{4}{k} \left| S_0 + \sum_{m=1}^{N} V_m S_m \right|^2 \tag{31}$$

where

$$S_0 = \sum_{p=0}^{\infty} \epsilon_{0p} \cos(p\theta) \frac{J_p'(ka)}{H_p^{(2)}(ka)} \tag{32}$$

and

$$S_m = \frac{1}{2\pi a \zeta_0} \sum_{p=0}^{\infty} \epsilon_{0p} (j)^{p+1} \frac{\sin\left(\frac{p\delta_m}{2}\right)}{\left(\frac{p\delta_m}{2}\right)} \frac{\cos(p(\theta - \theta_m))}{H_p^{(2)'}(ka)} \tag{33}$$

Looking at Equation (31) from the superposition picture, $S_0$ corresponds to the contribution of the solid cylinder to the bistatic scattering cross section. The $S_m$ coefficients multipled by the appropriate slot voltages correspond to the contribution of the driven slotted cylinder to the bistatic cross section.

## 2.7. Generalizing the Theory

The physical interpretation of the quantities $K_{n0}$, $y_{nm}$, $S_o$, and $S_m$ allows the theory just developed to be interpretated in a more general manner. Consider, from the point of view of superposition, the scattering of an EM wave by a multi-loaded conducting body of any arbitrary shape. If the geometry of the loading is such that unique load voltages can be defined, then a matrix equation, having a form identical to Equation (26), relating the load voltages to the short circuit radiation admittances of the structure and the surface current on a similar unloaded structure can be formulated. The values of the radiation admittances and the surface current may be found exactly, as was done in this chapter, or by some approximate method. Similarly a result for the bistatic scattering cross section of the multi-loaded body can be formulated in terms of the load voltages as was done in Equation (31). Harrington[19, 20] has pursued this idea in his multiport network parameter representation.

The loading techniques and synthesis procedures developed in the next chapter are completely general and can be applied to conducting bodies of arbitrary shapes.

CHAPTER III

# THE SYNTHESIS OF LOAD IMPEDANCES THAT RESULT IN ZERO OR MINIMUM SCATTERING FOR ONE OR MORE DIRECTIONS OR FREQUENCIES

In this chapter procedures are developed for finding load impedances that result in zero scattering in one or more directions and load impedances that result in zero scattering in one direction at several frequencies. Procedures are also developed to find purely reactive load impedances that result in zero or minimum scattering in one or more directions.

## 3.1. Zero Scattering in N Directions

A set of N load impedances that causes the field scattered by the N-slotted, loaded cylinder to vanish in N directions may be determined by the following synthesis procedure.

If the load admittances $Y_1, Y_2, \ldots, Y_N$ are assumed to be unknowns, matrix Equation (26) contains 2N complex unknowns, the N load admittances and the N slot voltages. Since matrix Equation (26) contains only N complex equations, N complex constraint equations may be chosen to completely determine the problem.

It can be seen from Equation (31) that

$$S_0(\theta = \theta_{01}) + \sum_{m=1}^{N} V_m S_m(\theta = \theta_{01}) = 0 \qquad (34)$$

implies the radiation zone field scattered by the loaded cylinder will vanish in the direction $\theta = \theta_{01}$. Similarly a system of N complex constraint equations, involving the N unknown slot voltages, which force the radiation zone scattered field to vanish in directions $\theta_{01}, \theta_{02}, \ldots, \theta_{0N}$ can be expressed as

$$\begin{bmatrix} C_{11} & C_{12} & \cdots & C_{1N} \\ C_{21} & C_{22} & \cdots & C_{2N} \\ \cdot & & & \\ \cdot & & & \\ \cdot & & & \\ C_{N1} & C_{N2} & & C_{NN} \end{bmatrix} \begin{bmatrix} V_1 \\ V_2 \\ \cdot \\ \cdot \\ \cdot \\ V_N \end{bmatrix} = - \begin{bmatrix} C_{10} \\ C_{20} \\ \cdot \\ \cdot \\ \cdot \\ C_{N0} \end{bmatrix} \tag{35}$$

where $C_{ij} = S_j\ (\theta = \theta_{0i})$.

The load admittances that result in zero scattering in the N directions are found from Equation (23) to be

$$Y_n = [\,K_{n0} - \sum_{m=1}^{N} y_{nm} V_m]\ /V_n \qquad n = 1, 2, \ldots, N \tag{36}$$

where $V_1$, $V_2$, ..., $V_N$ are the slot voltages found by solving Equation (35).

The admittances found by the above procedure may have negative real parts which are difficult to physically realize. If the positions of the slots are free to be changed, it is possible in many cases to find to slot positions such that the load admittances will have positive real parts. This topic will be considered in Section 4. 3.

In some cases when the load admittances have negative real parts it may be more practical to consider purely reactive loading.

## 3. 2. Zero Scattering in N/2 Directions Using Purely Reactive Load Impedances

In the previous section, the introduction of N complex load admittances led to the elimination of the scattered field in N directions because N complex constraint equations were allowed to be introduced. If N purely reactive load impedances are considered, it is possible to eliminate the scattered field in N/2 directions only. This is due to the fact that N purely reactive load impedances gives the same number of

degrees of freedom as N/2 complex load impedances and thus only N/2 complex constraint equations for zero scattering are permitted.

A set of N purely reactive load impedances that result in zero field scattered in N/2 directions may be determined by the following synthesis procedure.

The condition that the N load admittances be purely reactive is equivalent to N real constraint equations, and may be written

$$Y_n + Y_n^* = 0 \qquad n = 1, 2, \ldots, N$$

where $Y_n^*$ is the complex conjugate of $Y_n$. Using Equation (36) this condition can be written

$$(K_{n0} V_n^* + K_{n0}^* V_n) - \sum_{m=1}^{N} (y_{nm} V_m V_n^* + y_{nm}^* V_m^* V_n) = 0$$
$$n = 1, 2, \ldots, N \qquad (37)$$

which is a set of N real nonlinear constraint equations involving the slot voltages. (Note: N real equations are equivalent to N/2 complex equations.) To completely determine the problem N/2 complex constraint equations must still be chosen.

The scattered field will vanish in the N/2 directions $\theta_{01}$, $\theta_{02}$, . . . , $\theta_{0N/2}$ if the slot voltages satisfy

$$\begin{bmatrix} C_{11} & C_{12} & \cdots & C_{1N} \\ \cdot & & & \\ \cdot & & & \\ \cdot & & & \\ C_{N/2\,1} & C_{N/2\,2} & \cdots & C_{N/2\,N} \end{bmatrix} \begin{bmatrix} V_1 \\ V_2 \\ \cdot \\ \cdot \\ \cdot \\ V_N \end{bmatrix} = - \begin{bmatrix} C_{10} \\ \cdot \\ \cdot\cdot \\ \cdot \\ C_{N/2\,0} \end{bmatrix} \qquad (38)$$

Equations (37) and (38) comprise a system of nonlinear equations which can be solved for the slot voltages, provided a solution exists. Once again, the load admittances may be found by substituting the solution of Equations (37) and (38) into Equation (36). These load admittances will be purely susceptive and will cause the scattered field to vanish in directions $\theta_{01}$, $\theta_{02}$, ... $\theta_{0N/2}$.

The special case of two slots (i.e., N=2) is worked out in detail in Appendix B. The admittances are found to be the solutions to a quadratic equation. The position of the slots on the cylinder surface is a crucial factor in determining whether or not solutions to this problem exist. This topic is discussed in detail in Section 4.4.

The non-existence of a purely reactive loading that results in zero scattering in one or more directions does not imply that the reduction of the scattering to levels other than zero in these directions by a purely reactive loading is impossible. In many cases the scattering can be significantly reduced below the unloaded level by purely reactive loading.

### 3.3. Minimum Scattering Using Purely Reactive Load Impedances

In general, the field scattered by a loaded cylinder cannot be reduced to zero in a given direction when the load impedances are purely reactive and all equal (i.e., $jX = Z_1 = Z_2 = \ldots = Z_N$). This does not, however, rule out the possibility of reducing the scattered field to a minimum in a given direction by a suitable choice of the loading reactance. An optimum reactance, $X_{0p}$, for minimum bistatic scattering cross section can be determined by differentiating the bistatic scattering cross section with respect to X and setting this derivative equal to zero. The optimum reactance is found by solving the resulting equation.

Applying this procedure to the case N=1 yields the following result.

$$X_{0p} = 1/2\left[G \pm \sqrt{G^2 + 4I}\right] \tag{39}$$

where

$$G = \frac{(E^2 + F^2) - (C^2 + D^2)(A^2 + B^2)}{(C^2 + D^2)(BE - FA) + D(E^2 + F^2)}$$

$$I = \frac{D(A^2 + B^2) + (BE - FA)}{(C^2 + D^2)(BE - FA) + D(E^2 + F^2)}$$

and the constants on the right hand side of the above two equations are real and defined by

$$A + jB = S_0 (\theta_0)$$

$$C + jD = y_{11} (\theta_0)$$

$$E + jF = (y_{11} S_0 + K_{10} S_1)\Big|_{\theta = \theta_0} .$$

Equation (39) yields two solutions one of which results in a minimum and the other a maximum bistatic scattering cross section in the direction $\theta = \theta_0$.

Other procedures can also be developed for determining the optimal loading reactances for minimum scattering by cylinders with more general configurations of purely reactive loadings.

## 3.4. Zero Scattering at N Different Frequencies.

Many times it is of interest to modify the scattering properties of an object at several different frequencies or over a large band of frequencies. Consider the problem of the synthesis of N load impedances that reduce the scattered field to zero in one direction at N different frequencies $\omega_1, \omega_2, \ldots, \omega_N$.

At the first frequency, $\omega_1$, the constraint equation is

$$C_{10} + \sum_{m=1}^{N} V_m(\omega_1) C_{1m} = 0$$

where $C_{1j} = S_j(\theta = \theta_0, \omega = \omega_1)$.
The second constraint equation is

$$C_{20} + \sum_{m=1}^{N} V_m(\omega_2) C_{2m} = 0$$

where $C_{2j} = S_j\ (\theta = \theta_0,\ \omega = \omega_2)$. The slot voltages in the first equation, $\{V_m(\omega_1),\ m=1, 2, \ldots, N\}$, and the slot voltages in the second equation $\{V_m(\omega_2),\ m=1, \ldots, N\}$ are in general not equal and must be considered as independent variables. Likewise all other slot voltages at the other frequencies must be treated as independent variables.

Using matrix Equation (26) all the voltages can be eliminated from the problem and the constraint equations written directly in terms of the admittances. Consider the nth constraint equation

$$C_{n0} + \sum_{m=1}^{N} C_{nm} V_m(\omega_n) = 0 .$$

Evaluating matrix Equation (26) at $\omega = \omega_n$ and augmenting it with the above constraint equation yields

$$\begin{bmatrix} y_{11} + Y_1 & y_{12} & \cdots & y_{1N} \\ y_{21} & y_{22} + Y_2 & \cdots & y_{2N} \\ \cdot & & & \\ \cdot & & & \\ \cdot & & & \\ y_{N1} & y_{N2} & \cdots & y_{NN} + Y_N \\ C_{n1} & C_{n2} & \cdots & C_{nN} \end{bmatrix} \begin{bmatrix} V_1(\omega_n) \\ V_2(\omega_n) \\ \cdot \\ \cdot \\ \cdot \\ \\ V_N(\omega_n) \end{bmatrix} = \begin{bmatrix} K_{10} \\ K_{20} \\ \cdot \\ \cdot \\ \cdot \\ K_{N0} \\ -C_{n0} \end{bmatrix} \tag{40}$$

where all the coefficients $y_{nm}$ and $K_{n0}$ are evaluated at $\omega = \omega_n$ and the load admittances $Y_n$ are assumed to be frequency independent. The first matrix in Equation (40) becomes N by N+1 at this step. Equation (40) however, can be rewritten as

$$\begin{bmatrix} y_{11}+Y_1 & y_{12} & \cdots & y_{1N} & -K_{10} \\ y_{21} & y_{22}+Y_2 & \cdots & y_{2N} & -K_{20} \\ \cdot & & & & \\ \cdot & & & & \\ \cdot & & & & \\ y_{N1} & y_{N2} & \cdots & y_{NN}+Y_N & -K_{N0} \\ C_{n1} & C_{n2} & \cdots & C_{nN} & C_{n0} \end{bmatrix} \begin{bmatrix} V_1(\omega_n) \\ V_2(\omega_n) \\ \cdot \\ \cdot \\ \cdot \\ V_N(\omega_n) \\ 1 \end{bmatrix} = 0$$

which will have a solution only if the determinant of the coefficient matrix vanishes. Similar arguments hold for all N frequencies and this gives a system of N nonlinear equations in terms of the N load admittances.

$$\begin{vmatrix} y_{11}+Y_1 & y_{12} & \cdots & y_{1N} & -K_{10} \\ y_{21} & y_{22}+Y_2 & \cdots & y_{2N} & -K_{20} \\ \cdot & & & & \\ \cdot & & & & \\ \cdot & & & & \\ y_{N1} & y_{N2} & \cdots & y_{NN}+Y_N & -K_{N0} \\ C_{n1} & C_{n2} & \cdots & C_{nN} & C_{n0} \end{vmatrix} = 0 \qquad (41)$$

for $n = 1, 2, \ldots, N$ with all the $y_{nm}$ and $K_{n0}$ coefficients evaluated at $\omega = \omega_n$.

Provided a solution exists, this set of equations can be solved for the load admittances $Y_1, Y_2, \ldots, Y_n$ which will give zero scattering in the direction $\theta = \theta_0$ at the frequencies $\omega_1, \omega_2, \ldots, \omega_N$.

The special case of zero scattering in one direction at two frequencies is examined in detail in Appendix C. The impedances are found to be solutions to a quartic equation.

Throughout this section it has been assumed that the scattering was forced to zero in the same direction, $\theta = \theta_0$, at all N frequencies. Examining the theory shows that this restriction is not necessary.

The scattering can be reduced to zero in one direction at one frequency, a different direction at the second frequency, and so forth. However, at any one frequency the scattering is still reduced to zero in only one direction.

An assumption has been made through the development of this last procedure that the load impedances are constants with respect to frequency. The practical application of this procedure as a broad band technique is thus limited by the frequency dependence of the load impedances actually available for implementation.

## CHAPTER IV

## NUMERICAL RESULTS AND DISCUSSION

In order to gain a firm understanding of the theory and procedures developed in the previous two chapters a considerable amount of numerical results were calculated. This chapter deals with the presentation, interpretation, and discussion of these results.

### 4.1. Numerical Method

The series $S_0$, $S_m$, $y_{nm}$, and $K_{n0}$ involved in the expressions for the bistatic scattering cross section and the slot impedances were evaluated on the Michigan State University CDC 6500 computer. Series $S_0$, $S_m$, and $K_{n0}$ converged rapidly and the computations were straight forward. Thirty terms were retained in these series. This gave eight-digit accuracy over the range of cylinder size considered (i.e., $1 \leq ka \leq 13$). The theory is not limited to this range but for larger cylinders it may be necessary to retain more terms to attain this accuracy.

The evaluation of series $y_{nm}$, the self and mutual radiation admittance of the slots, is complicated by the slow convergence of its imaginary part. Mathematically the imaginary part of $y_{nm}$ approaches infinity as the slot width $\delta_m$ approaches zero. Physically this implies an infinite stray capacitance existing at the slot with an infinitesimal gap width. The real part of $y_{nm}$ remains finite for any slot width corresponding to the existence of a finite radiation resistance for a slot radiator. Thus the numerical calculation of $y_{nm}$ requires special attention.

The actual computation of $y_{nm}$ is accomplished by summing 300 terms of the series. The first M terms of the series are treated exactly, where M depends on ka and varies from 95 to 149. In the next (150-M) terms the approximation

i
t
i

w
w
b

4

fi
ex
s
c
va
ob
fe
is

sc
wi

of
si
δa
fo

$$\frac{H_n^{(2)}(ka)}{H_n^{(2)'}(ka)} \simeq \frac{Y_n(ka)}{Y_n'(ka)} = \left[\frac{Y_{n-1}(ka)}{Y_n(ka)} - \frac{n}{ka}\right]^{-1}$$

is made since $|Y_n(ka)| >> |J_n(ka)|$ for $n>>ka$. The Bessel functions are replaced by their asymptotic expressions for large order[28] in the last 150 terms. This leads to the approximation

$$\frac{H_n^{(2)}(ka)}{H_n^{(2)'}(ka)} \simeq \left[\left(\frac{n-1}{n}\right)^{n-1/2}\left(\frac{eka}{2n}\right) - \frac{n}{ka}\right]^{-1}$$

where $e = 2.71828\ldots$ . The real part of $y_{nm}$ has eight-digit accuracy while the imaginary part may be in error by as much as one per cent, but in most cases the error is much less than this.

4.2. Effect of the Slot Width

As discussed in the previous section, the slot width has a significant effect on the imaginary part of $y_{nm}$. It is thus reasonable to expect the slot width to have some effect on the load admittances resulting from the synthesis procedures. Numerically, extensive calculations were performed for different load configurations at several values slot width $\delta$. It was found the real parts of the load admittances obtained from the impedance synthesis procedure are only slightly affected by the slot width, however, its effect on their imaginary parts is more significant.

It was also found that the bistatic scattering patterns for zero scattering in several directions are nearly identical for different slot widths.

One more remark on the slot width is also important. The value of $\delta$ limits the size of a cylinder that can be considered with this theory since the slot width $\delta a$ is assumed to be electrically narrow. If $\delta a < \lambda/10$ the slot can be considered to be electrically narrow and it follows that the electrical cylinder size is limited by

$$ka < \frac{\pi}{5\delta} \quad .$$

### 4.3. Zero Scattering in Several Directions

Numerical results of the impedance synthesis procedure of Section 3.1 are presented and discussed in this section. The slot configuration and the directions in which zero scattering is desired are specified and the impedances necessary to realize these scattering modifications are calculated using Equations (35) and (36). It is of interest to examine numerically the effect the number of slots and their location (relative to the incident wave and directions of zero scattering) have on the synthesized load impedances.

The superposition picture is useful in interpreting the numerical results. It should be remembered, the modified scattered field of a loaded cylinder is the superposition of the field scattered from a solid cylinder and the fields radiated by a series of driven slotted cylinders whose driven slots are located at positions corresponding to the loaded slots on the loaded cylinder [See Equation (31)]. The slot voltages driving the slotted cylinders are determined by the surface current on the unloaded cylinder, the short circuit radiation admittances of the slots, and the load impedances [See Equation (26)]. The impedance synthesis procedure yields impedances such that the radiation zone field "radiated" by the driven slotted cylinders has exactly the same amplitude and is 180° out of phase with the field scattered from the unloaded cylinder in directions where the total scattered field has been constrained to be zero.

Consider a brief description of the surface current and the bistatic scattering pattern of a thick solid cylinder illuminated by a plane wave whose $\vec{E}$-field vector is polarized perpendicular to the cylinder's axis.[25, 26] The amplitude of the surface current is nearly constant in the region about the center of the illuminated side of the cylinder. Progressing toward the shadow region, it decreases nearly linearly until it becomes slightly irregular in the center of the shadow region. The backscattering and forward scattering cross section as a function of electrical cylinder size ka are displayed in Figure 4.1 and the bistatic scattering cross section patterns for ka equal to 2, 5, and 10 are shown in Figure 4.2. The backscattering cross section, forward scattering cross section, and bistatic scattering cross section are normalized to the geometric-optics value of the backscattering cross

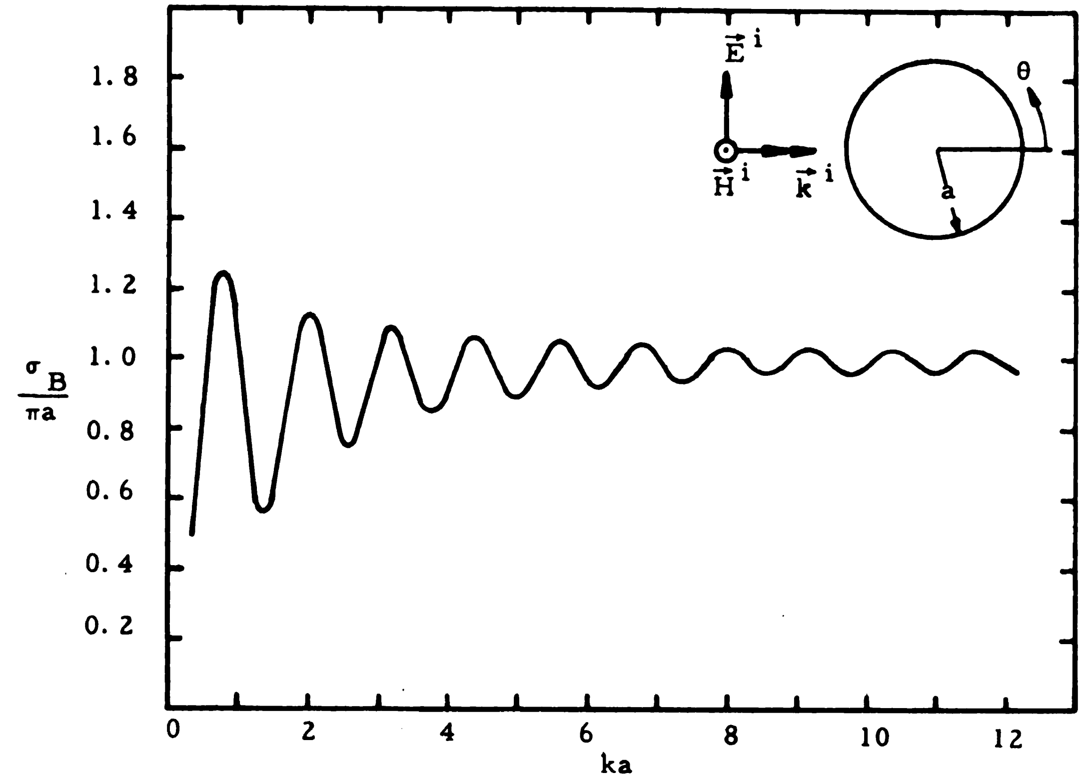


(a)

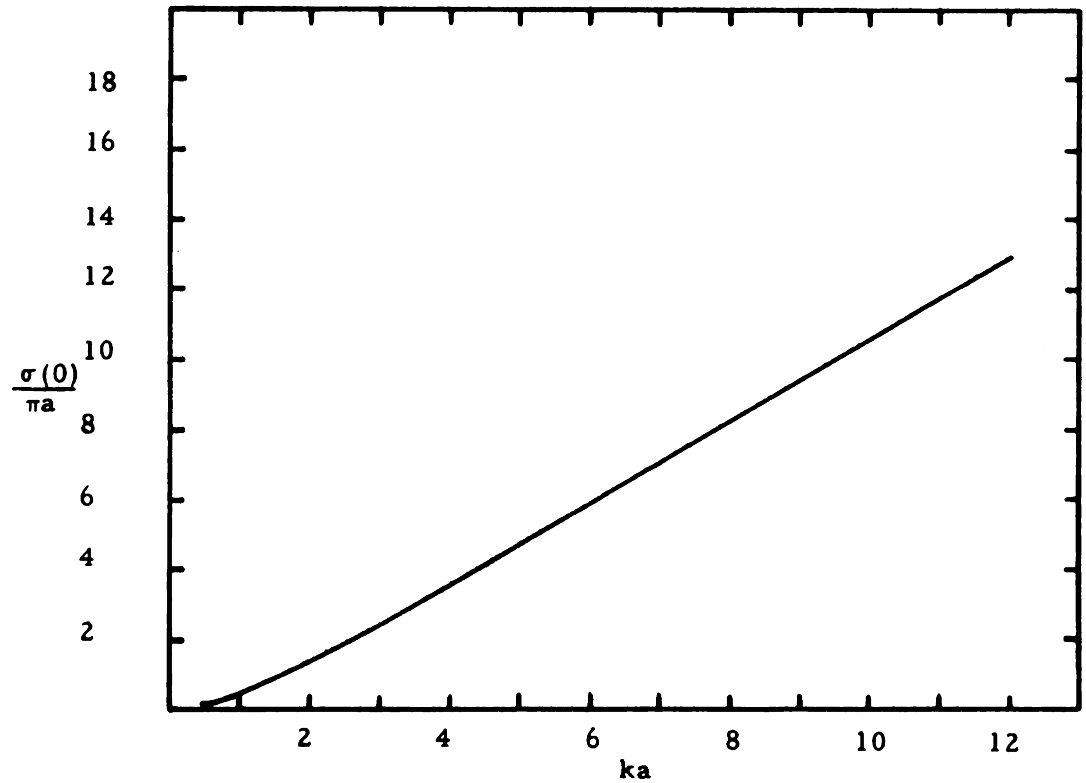


(b)

Figure 4. 1. (a) Normalized backscattering cross section and (b) Normalized forward scattering cross section, for a solid cylinder as a function of cylinder size, ka.

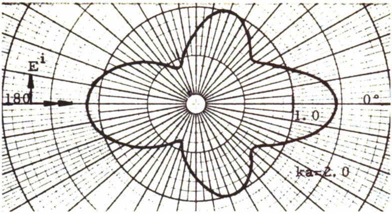


(a)

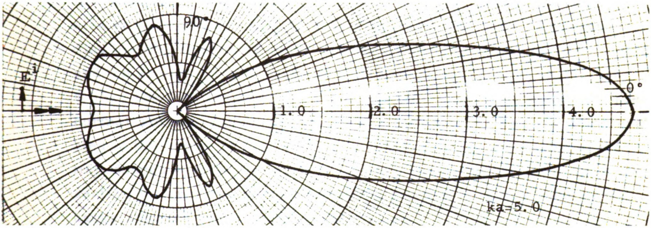


(b)

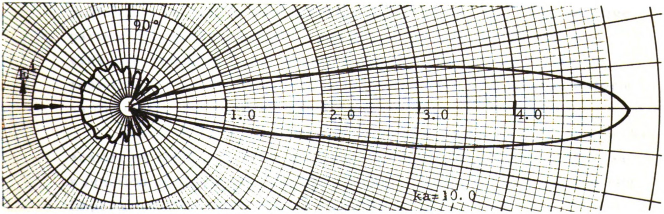


(c)

Figure 4. 2. Normalized bistatic scattering cross section patterns, $\sigma(\theta)/\pi a$, for solid thick cylinder with (a) ka= 2. 0, (b) ka=5. 0, and (c) ka= 10. 0 .

section, $\pi a$. It is seen that the bistatic scattering pattern of a thick cylinder is fairly uniform in the region around the backscattered direction while the remainder of the pattern consists of many sublobes with one very large lobe in the forward scattered direction.

The final component in the superposition picture is the radiation pattern of a thick driven slotted cylinder.[29, 30] The pattern has a fairly uniform amplitude over a region of about 60° on either side of the slot, then falls off to a much smaller value and becomes nonuniform on the side of the cylinder opposite the slot.

Slot loading impedances, calculated by the procedure described in Section 3.1, that result in zero scattering in one, two, three and four directions are displayed as a function of electrical cylinder size ka in Figures 4.3, 4.5, 4.7, 4.9, 4.11, and 4.13. Corresponding bistatic scattering cross section patterns for ka equal to two, five, and ten are shown in Figures 4.4, 4.6, 4.8, 4.10, 4.12, 4.14, and 4.15. The load impedances are normalized to the slot width $\delta a$. These normalized impedances are the wave impedances of the slot fields evaluated at the center of the slots. It should be noted, the scales of the impedances vary from figure to figure. The bistatic scattering cross section patterns are normalized to the geometric-optics value of the backscattering cross section, $\pi a$.

The resistive parts of the load impedances are negative over a large range of cylinder size for many slot configurations. This means that a device with negative resistance characteristics such as a tunnel-diode must be used in implementing these impedances. The reactive parts are in general inductive and decrease in amplitude with increasing frequency (i.e., negative slope). In most cases both the resistive and reactive parts become increasingly smooth and uniform as the cylinder size increases.

Figure 4.3 displays the slot impedance necessary for zero backscattering from a cylinder with one loaded slot located at $\theta = 180°$ as a function of electrical cylinder size ka. Figure 4.5 displays the slot impedances necessary for zero scattering in directions $\theta = 170°$ and 190° from a cylinder with two slots which are located at $\theta = 170°$ and 190°. The resistive and reactive parts of the load impedance in Figure 4.5 are more nonuniform than those in Figure 4.3. The load

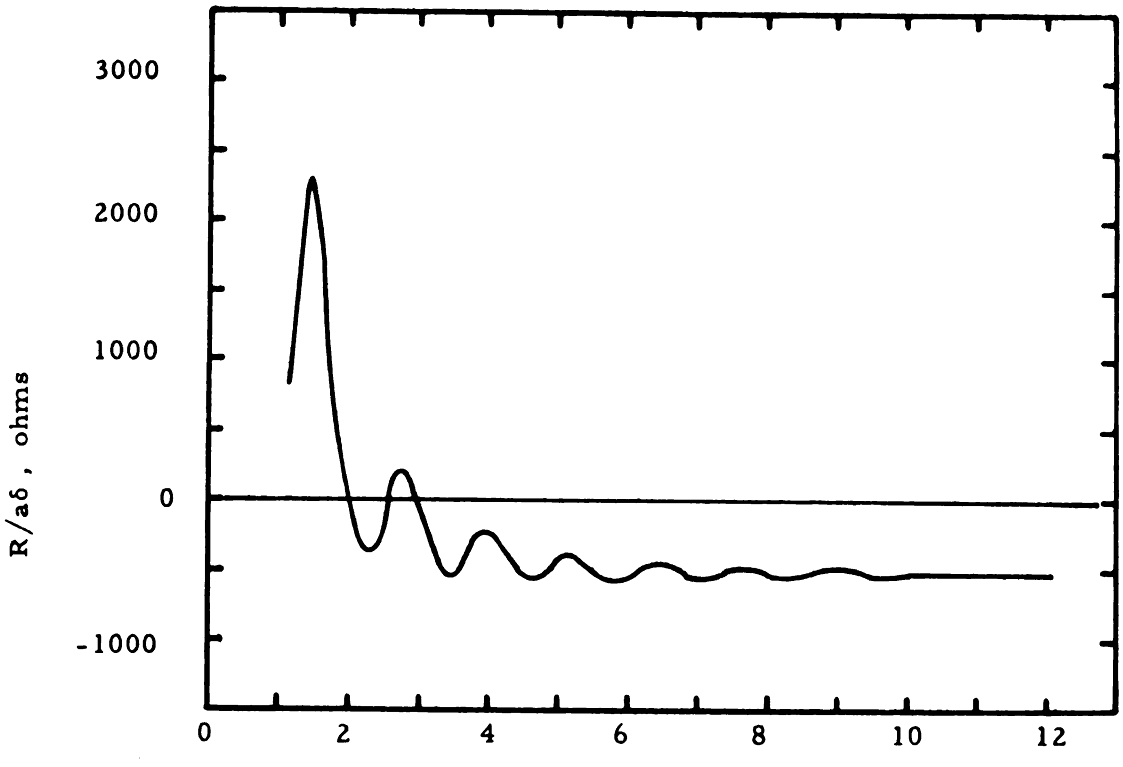


(a)

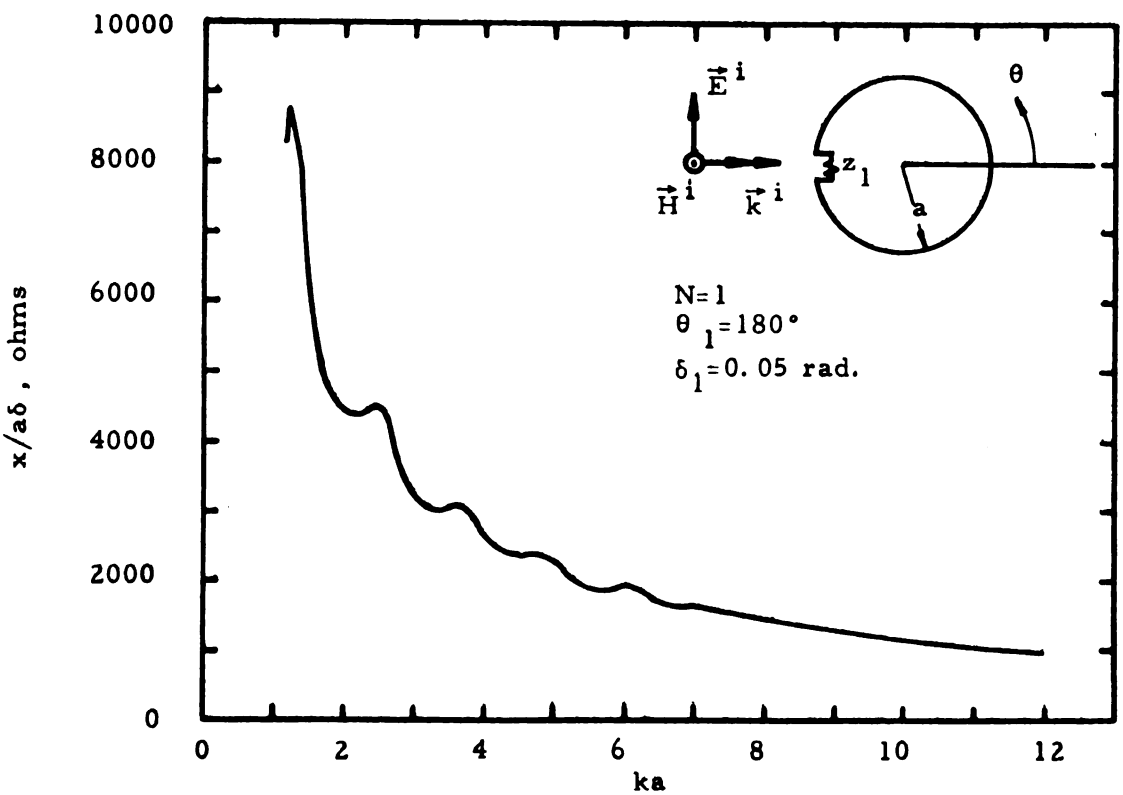


(b)

Figure 4. 3. Slot impedance for zero backscattering as a function of cylinder size ka.
(a) Normalized resistive part of load impedance.
(b) Normalized reactive part of load impedance.

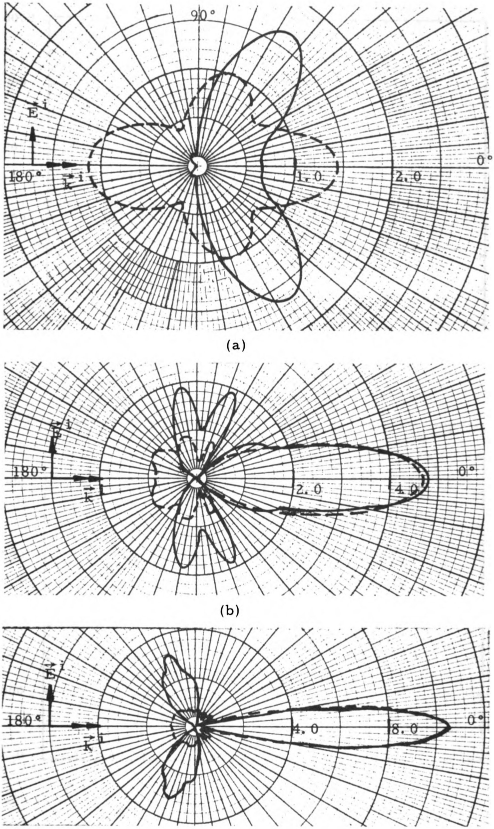


(a)



(b)



(c)

Figure 4.4. Normalized bistatic scattering cross section patterns, $\sigma(\theta)/\pi a$, for a thick cylinder loaded with one load at $\theta = 180°$ with (a) ka=2.0, (b) ka=5.0, and (c) ka=10.0 .

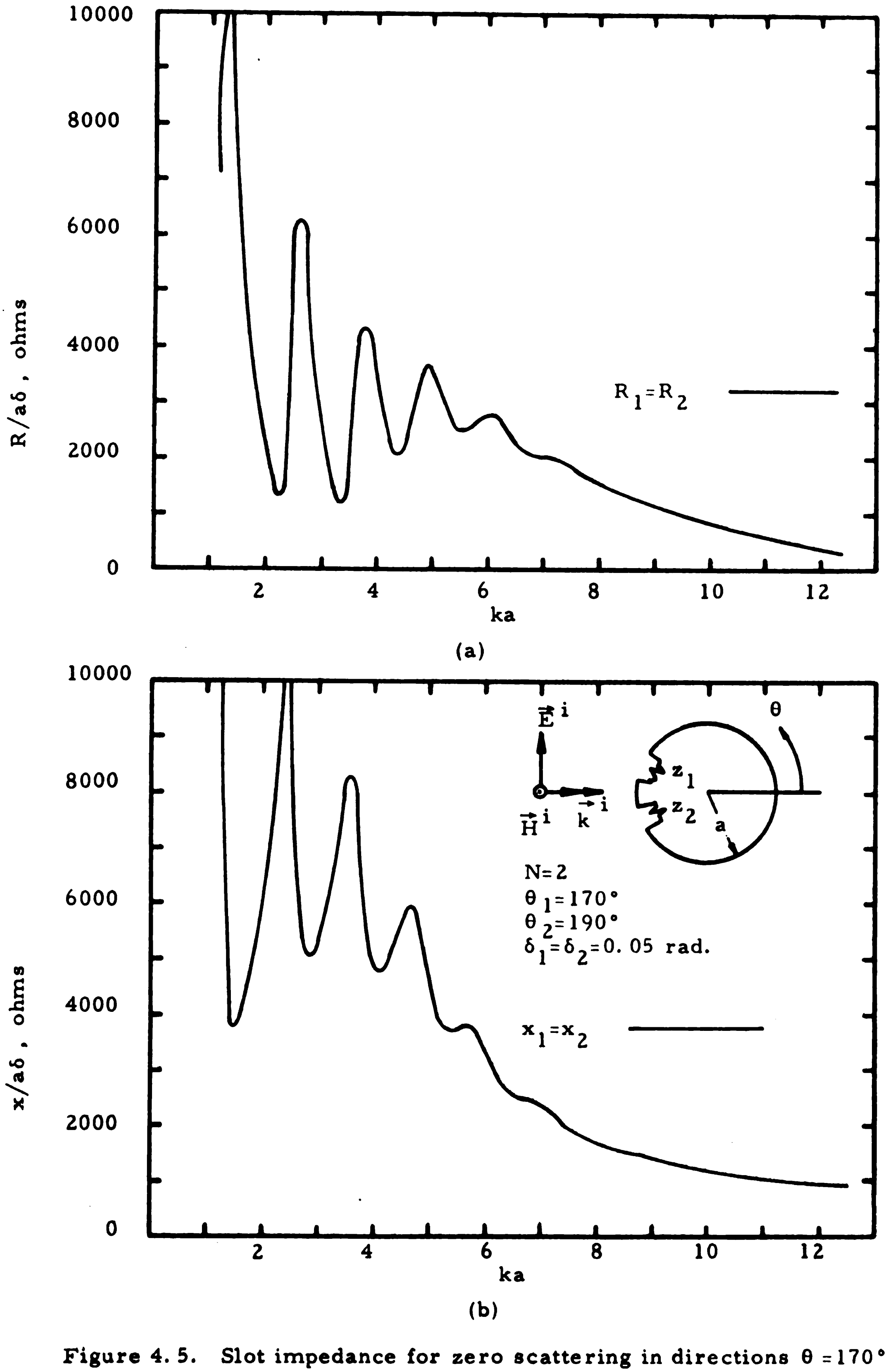


Figure 4.5. Slot impedance for zero scattering in directions θ = 170° and 190° as a function of cylinder size ka.
(a) Normalized resistive part of load impedance.
(b) Normalized reactive part of load impedance.

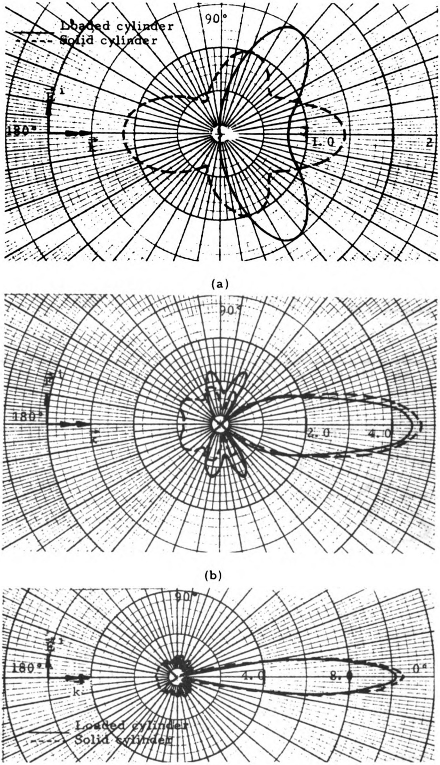


(a)

(b)

(c)

**Figure 4.6.** Normalized bistatic scattering cross section patterns, $\sigma(\theta)/\pi a$, for a thick cylinder loaded with two loads at $\theta = 170°$ and $\theta = 190°$ with (a) ka=2.0, (b) ka=5.0, and (c) ka=10.0 .

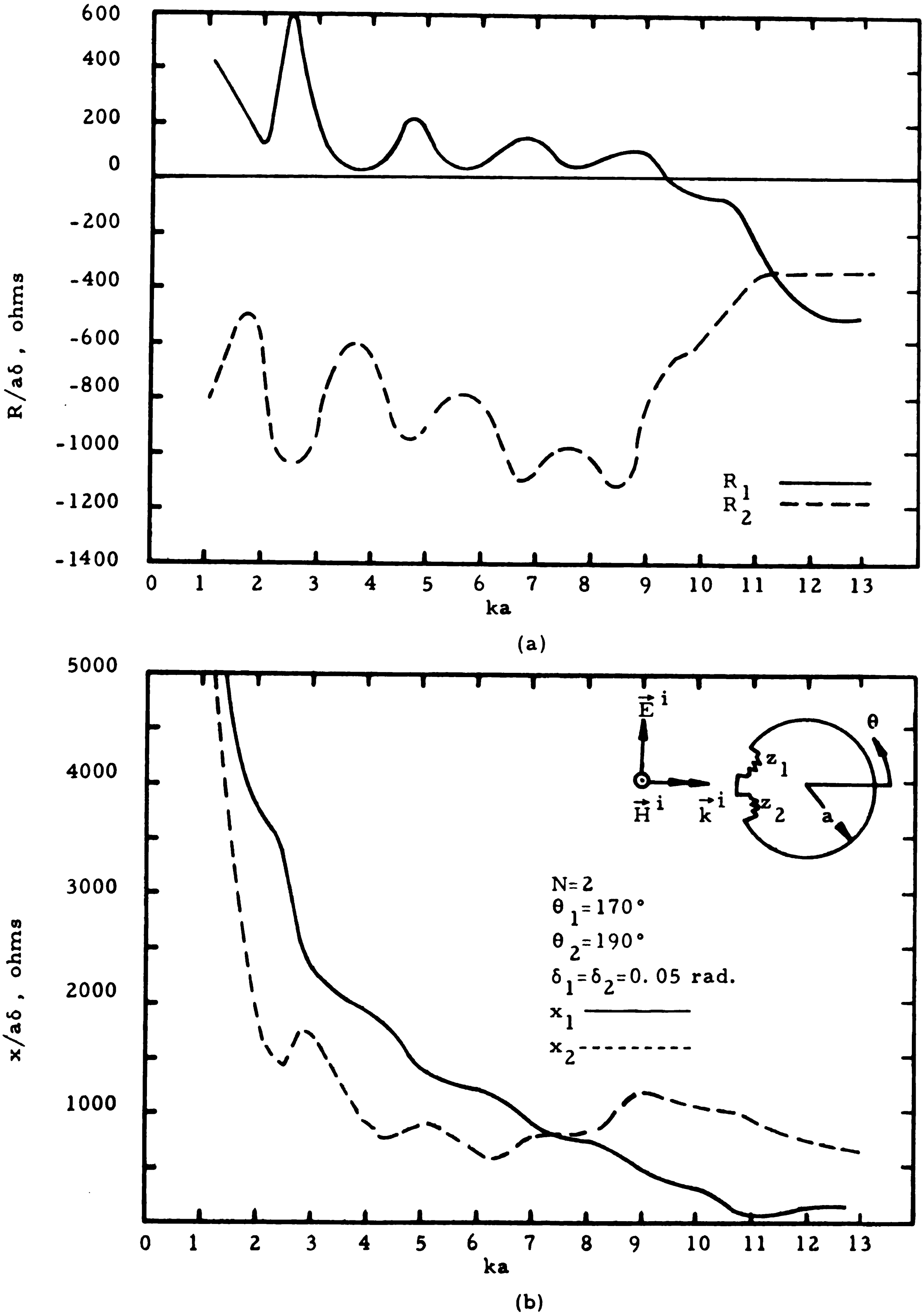


Figure 4. 7. Slot impedance for zero scattering in directions $\theta = 90°$, and 180° as a function of cylinder size ka. (a) Normalized resistive part of load impedance. (b) Normalized reactive part of load impedance.

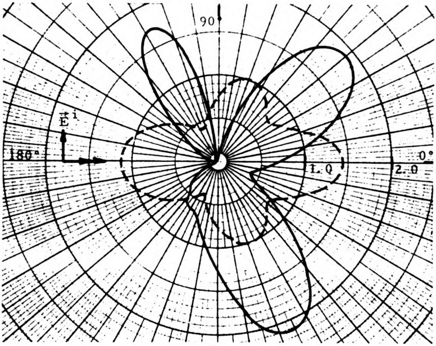


(a)

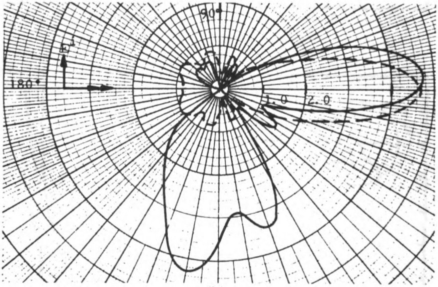


(b)

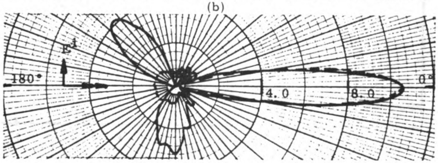


(c)

**Figure 4.8.** Normalized bistatic scattering cross section patterns, $\sigma(\theta)/\pi a$, for a thick cylinder loaded with two loads at $\theta = 170°$ and $190°$ for zero scattering in the directions $\theta = 90°$ and $180°$ with (a) ka=2.0, (b) ka=5.0, and (c) ka=10.0 .

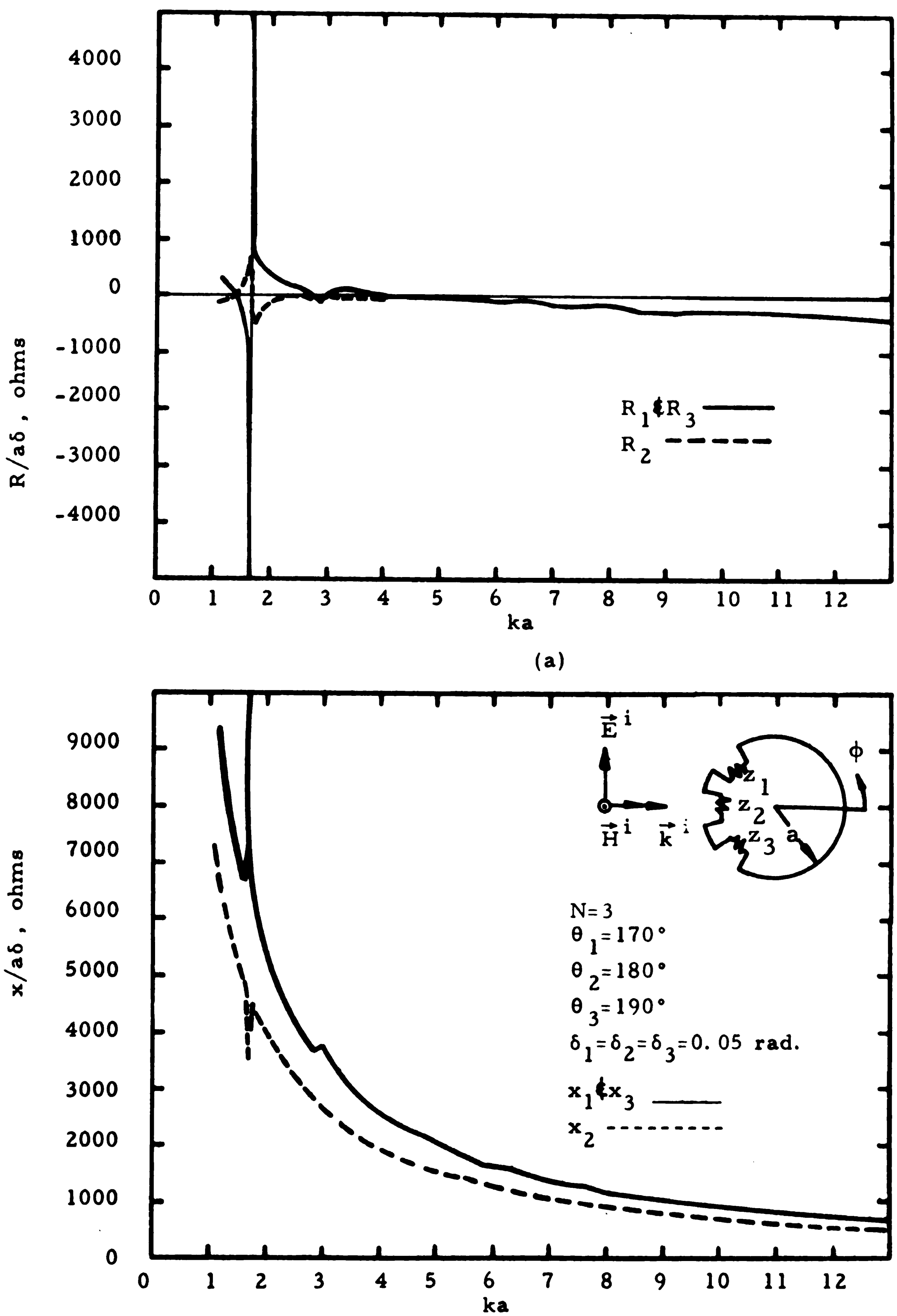


(b)

Figure 4.9. Slot impedance for zero scattering in the directions $\theta = 135°$, $180°$, and $225°$ as a function of cylinder size ka.
(a) Normalized resistive part of load impedance.
(b) Normalized Reactive part of load impedance.

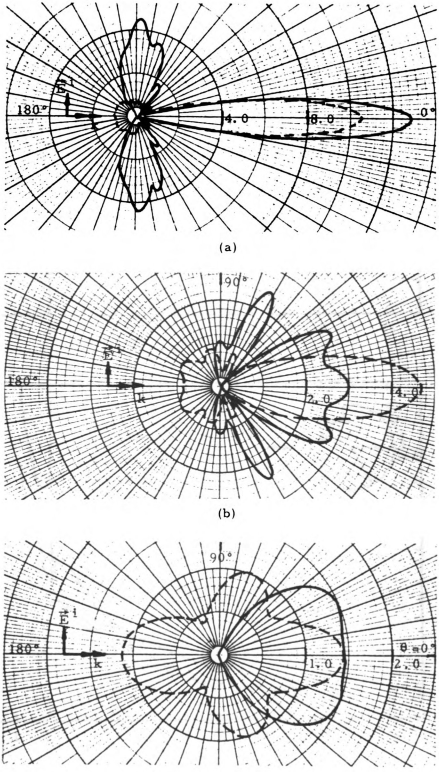


**Figure 4.10.** Normalized bistatic scattering cross section patterns, $\sigma(\theta)/\pi a$, for a thick cylinder loaded with three loads at $\theta = 170°$, $180°$, and $190°$ for zero scattering in the directions $\theta = 135°$, $180°$, and $225°$ with (a) ka = 10.0, (b) ka = 5.0, and (c) ka = 2.0 .

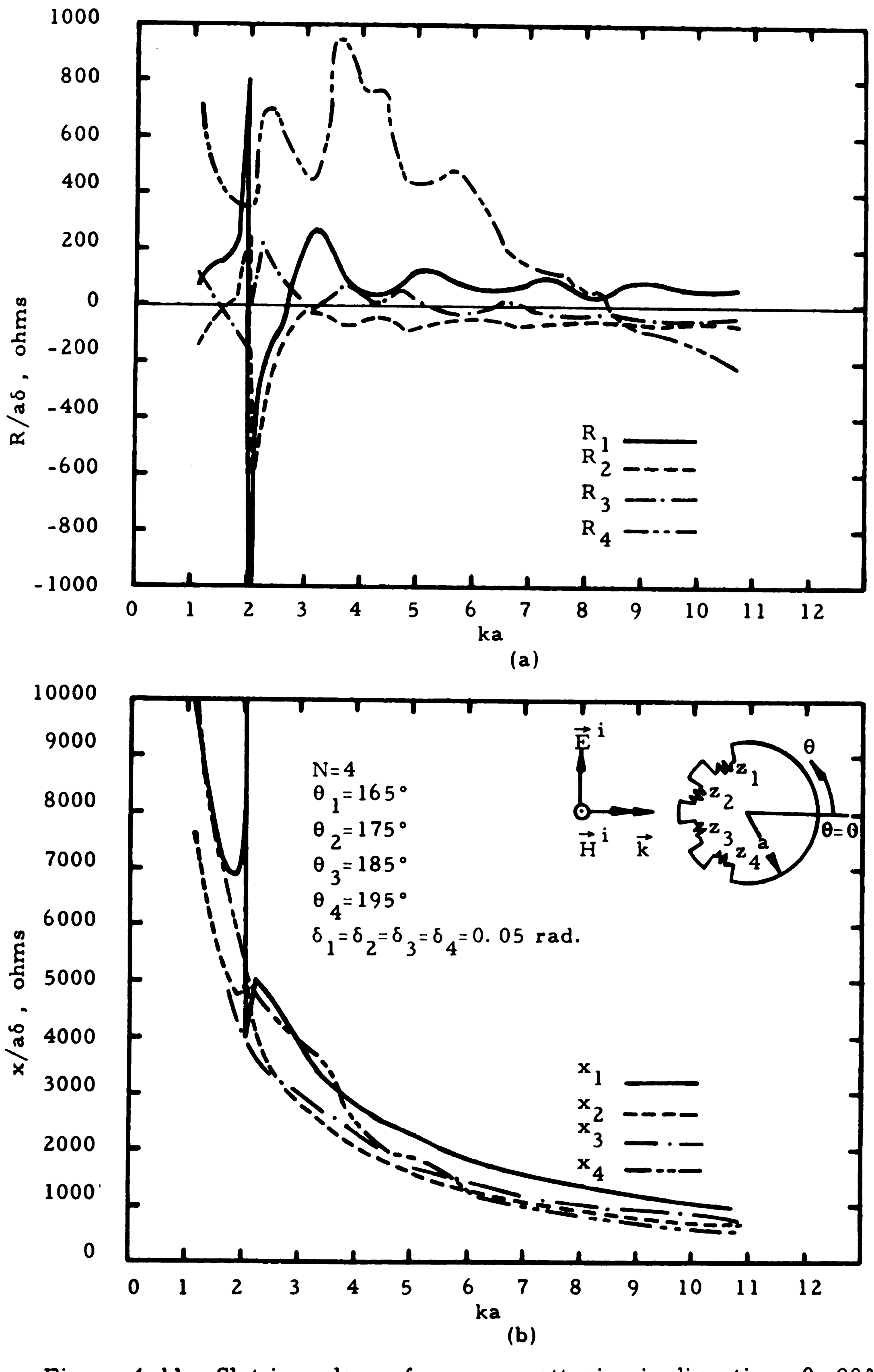


Figure 4.11. Slot impedance for zero scattering in directions θ = 90°, 135°, 180°, and 225° as a function of cylinder size ka.
(a) Normalized resistive part of load impedance.
(b) Normalized reactive part of load impedance.

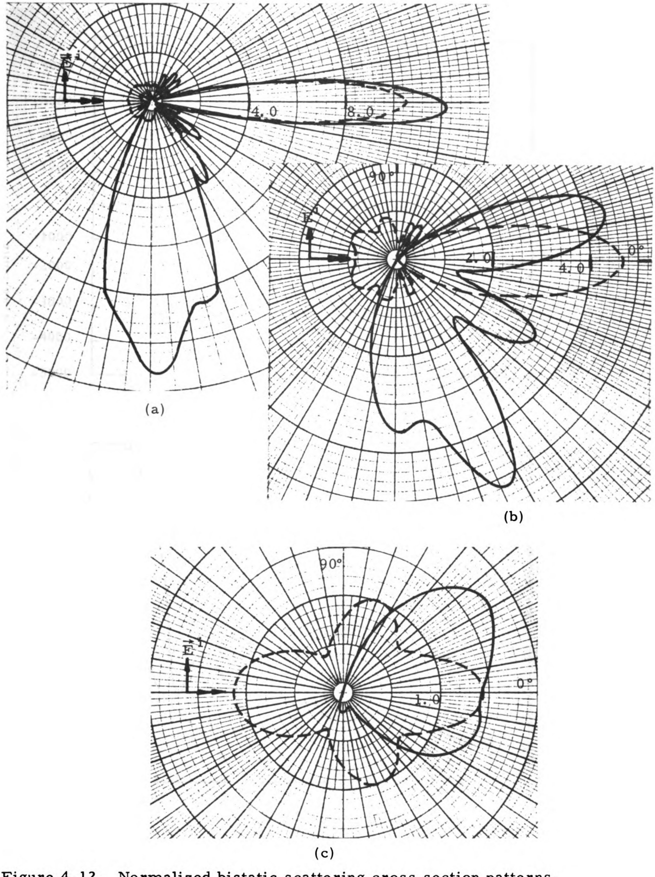


Figure 4.12. Normalized bistatic scattering cross section patterns, $\sigma(\theta)/\pi a$, for a thick cylinder loaded with four loads at $\theta = 165°$, $175°$, $185°$, and $195°$ for zero scattering in the directions $\theta = 90°$, $135°$, $180°$, and $225°$ with (a) ka=10.0, (b) ka=5.0, and (c) ka=2.0 .

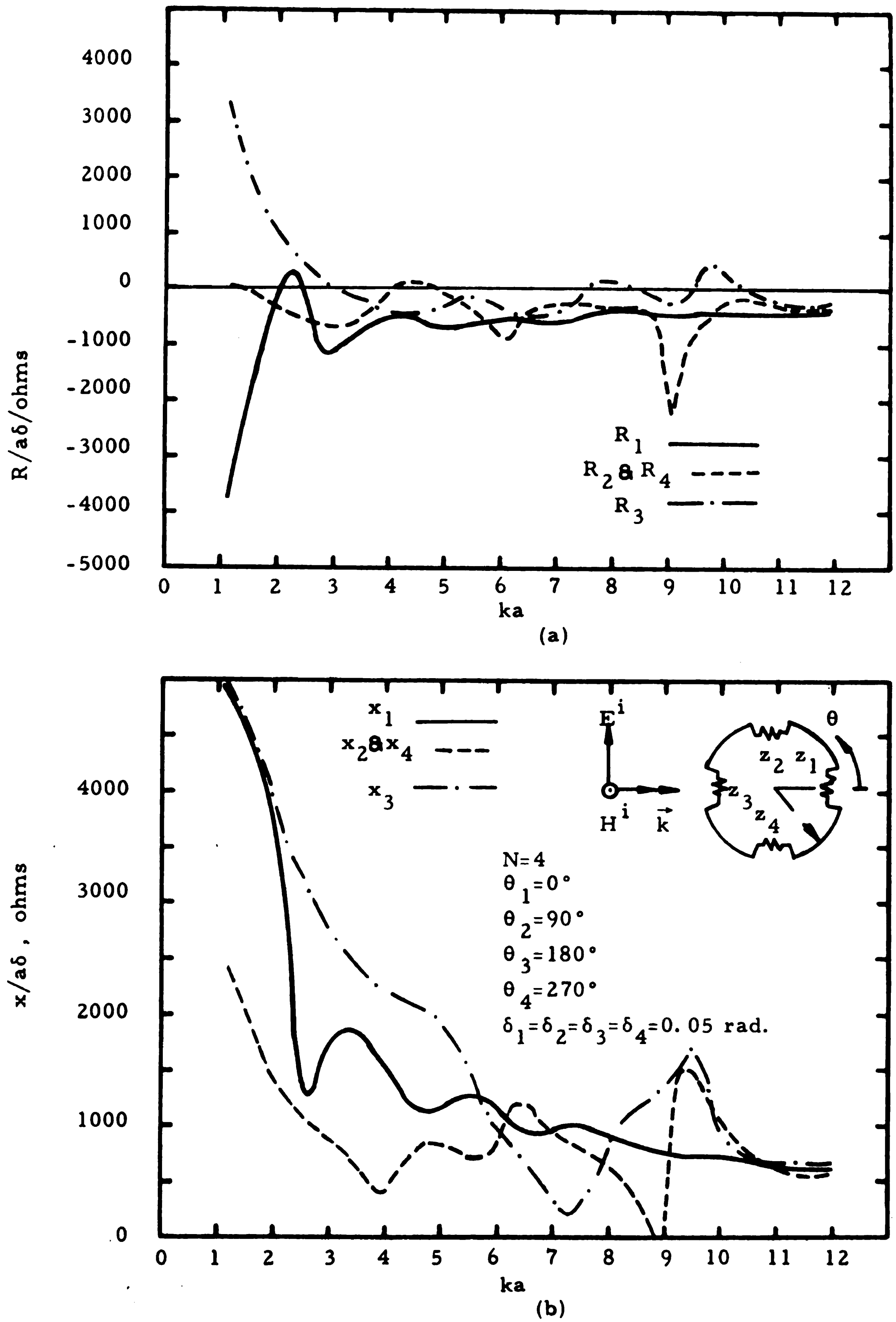


Figure 4.13. Slot impedance for zero scattering in directions θ = 90°, 135°, 180°, and 225° as a function of cylinder size ka.
(a) Normalized resistive part of load impedance.
(b) Normalized reactive part of load impedance.

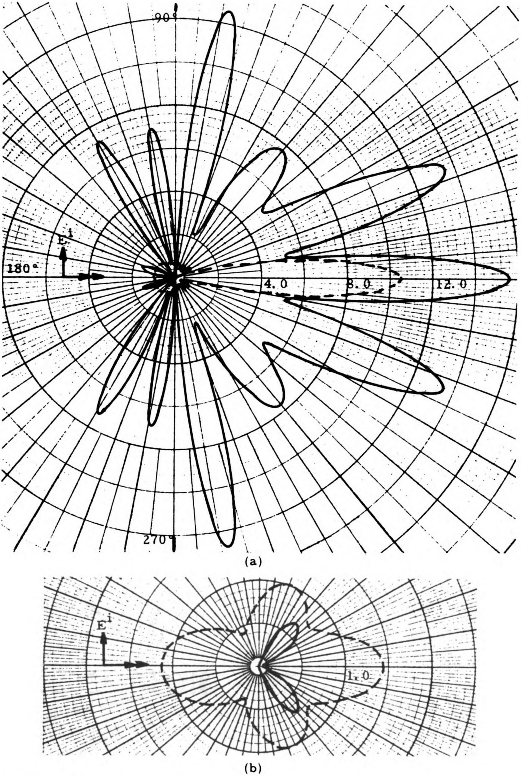


**Figure 4.14.** Normalized bistatic scattering cross section patterns, $\sigma(\theta)/\pi a$, for a thick cylinder loaded with four loads at $\theta = 0°$, $90°$, $180°$, and $225°$ for zero scattering in the directions $\theta = 90°$, $135°$, $180°$, and $225°$ with (a) ka= 10. and (b) ka= 2.0.

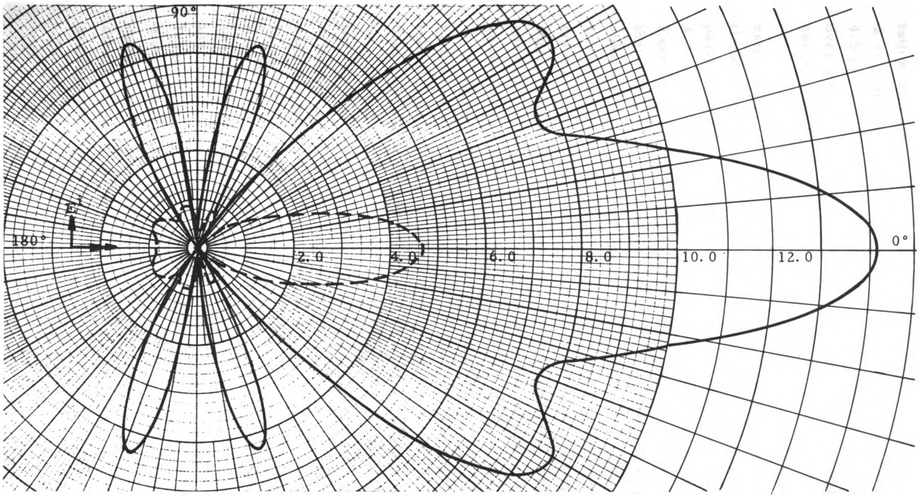


Figure 4.15. Normalized bistatic scattering cross section pattern, $\sigma(\theta)/\pi a$, for a thick cylinder $ka = 5.0$ loaded with four loads at $\theta = 0°$, $90°$, $180°$, and $270°$ for zero scattering in the directions $\theta = 90°$, $135°$, $180°$, and $225°$.

resistance in Figure 4.5 is always positive which makes the implementation of this impedance easier than the impedances shown in Figure 4.3. The bistatic scattering patterns corresponding to Figures 4.3 and 4.5 are nearly identical, but with a reduction of the scattered field over a slightly larger angular excursion (i.e., null width) in the second case.

The cylinder considered in Figure 4.7 has the same slot configuration as the cylinder considered in Figure 4.5, however, the directions of zero scattering are now taken to be $\theta = 90°$ and $180°$. Comparison of these two figures shows that the load resistance in Figure 4.7 is no longer always positive, but takes on large negative values. Examining the corresponding bistatic scattering patterns indicates that forcing the scattered field to be zero at $\theta = 90°$ has produced large enhanced scattering in directions other than those constrained to have zero scattering. The null widths have also markedly decreased. The enhancement of the scattering is to be expected whenever the load impedances have large negative resistive parts since this will, in general, result in an increase in scattered power above that scattered by the unloaded solid cylinder.

This enhancement of the scattering, as shown in Figure 4.8, can also be explained by the superposition picture. The field scattered from the thick solid cylinder and the fields "radiated" from two slotted cylinders with slots located at $\theta = 170°$ and $190°$, respectively, must sum to zero at $\theta = 90°$ and $180°$. The scattering enhancement arises from the condition that the fields sum to zero at $\theta = 90°$. The "driven" slots are located at $170°$ and $190°$ so that $90°$ is in the region where their radiation patterns have fallen off to a small value. Large driving voltages are thus necessary to produce enough radiation in the direction $\theta = 90°$ to cancel the field scattered from the solid cylinder. Hence in directions other than those constrained to have zero total scattering, the total scattered field from the loaded cylinder may be very large. This type of argument indicates that large negative load resistances and enhanced scattering in some directions other than those constrained to have zero scattering might be expected whenever the directions of zero scattering do not lay in the same region as the slots are located. Figures 4.12, 4.14, and 4.15 can also be explained by this type of argument.

Figure 4. 9 displays the slot impedances necessary for zero scattering in directions $\theta = 135°$, $180°$, and $225°$ from a cylinder with three slots located at $\theta = 170°$, $180°$, and $190°$ as a function of ka. The load resistances are in general negative but are very flat and have fairly small amplitudes. The absolute value of the normalized load resistances are less than 400 ohms for $2 < ka < 13$ and in particular $|R_2|/a\delta < 10$ ohms for $5 < ka < 13$. Impedances that have a very similar form to these have been realized using Negative Impedance Converters.[31] The corresponding bistatic scattering patterns are shown in Figure 4. 10 and exhibit the widest null widths considered. It should be noted that in this case the directions of zero scattering and the slot positions lay in the same region and furthermore the slot positions are in the center of the illuminated region of the cylinder.

Figures 4. 11 and 4. 13 display impedances that result in zero scattering in directions $\theta = 90°$, $135°$, $180°$, and $225°$ from a cylinder with four slots. The cylinder considered in Figure 4. 11 has all its slots located in the center of the illuminated region of the cylinder while the cylinder considered in Figure 4. 13 has its four slots equally spaced around the cylinder so that one slot is in the center of the illuminated region, one in the center of the shadow region, and the remaining two slots are located on the borders between the two regions. The load resistances in Figure 4. 13 are predominantly more negative than those in Figure 4. 11. Also, the load reactances are more irregular in Figure 4. 13 where all the slots are not located in the center of the illuminated region. Considering the corresponding bistatic scattering patterns, again it is seen that the larger the amplitude of the negative load resistances is, the greater the enhanced scattering is in directions other than those constrained to have zero scattering.

Figures 4. 16, 4. 17, and 4. 18 examine the change in backscattering cross section when a loaded cylinder is rotated while the load impedances and relative slot positions are held constant. The cylinder considered in Figure 4. 16 has a load configuration identical to the one considered in Figure 4. 3 and cylinder size of ka=5. 0. The load impedance is taken to have the value of the impedance shown in

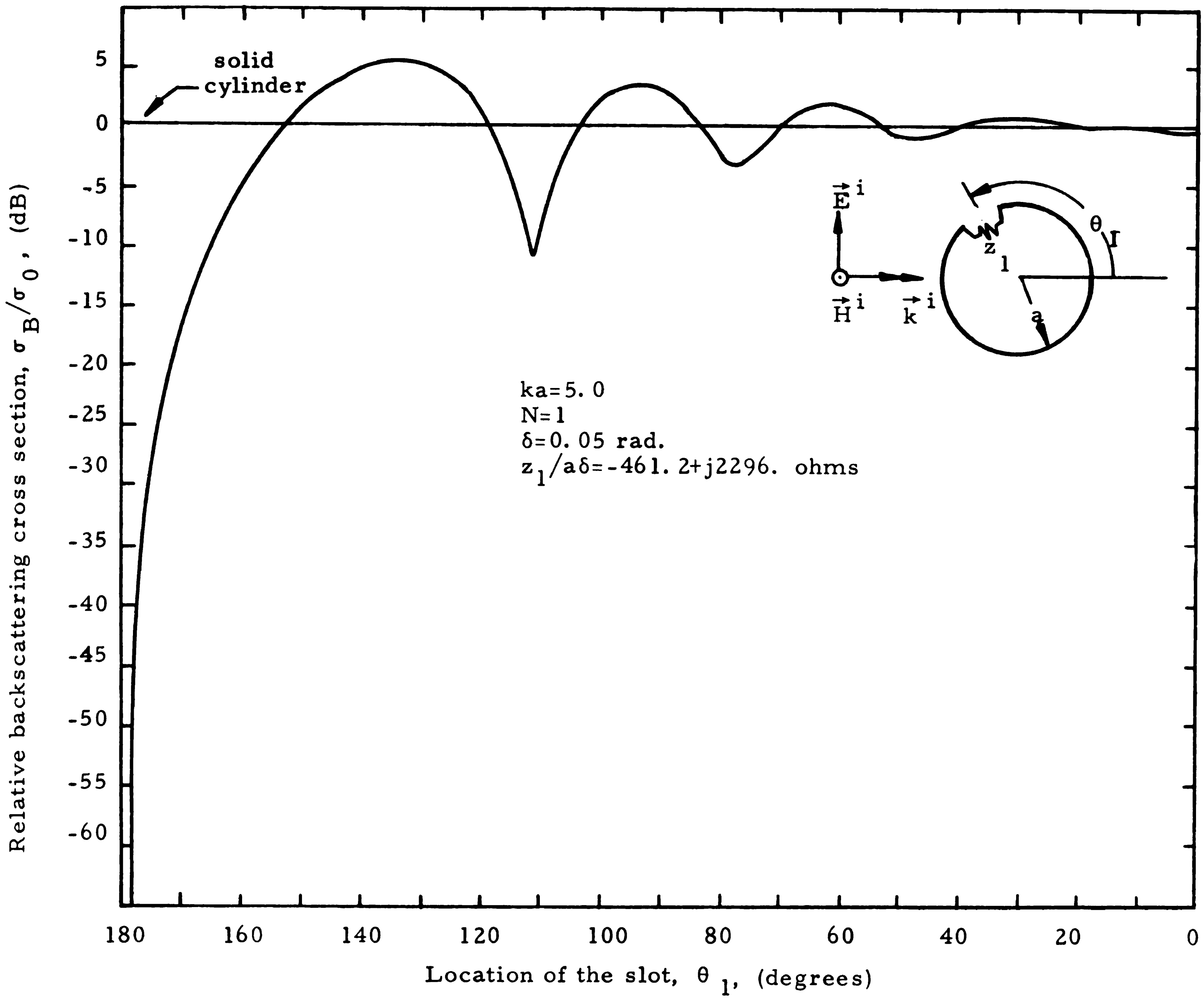


Figure 4.16. Relative backscattering cross section as a function of slot position with ka=5.0 .

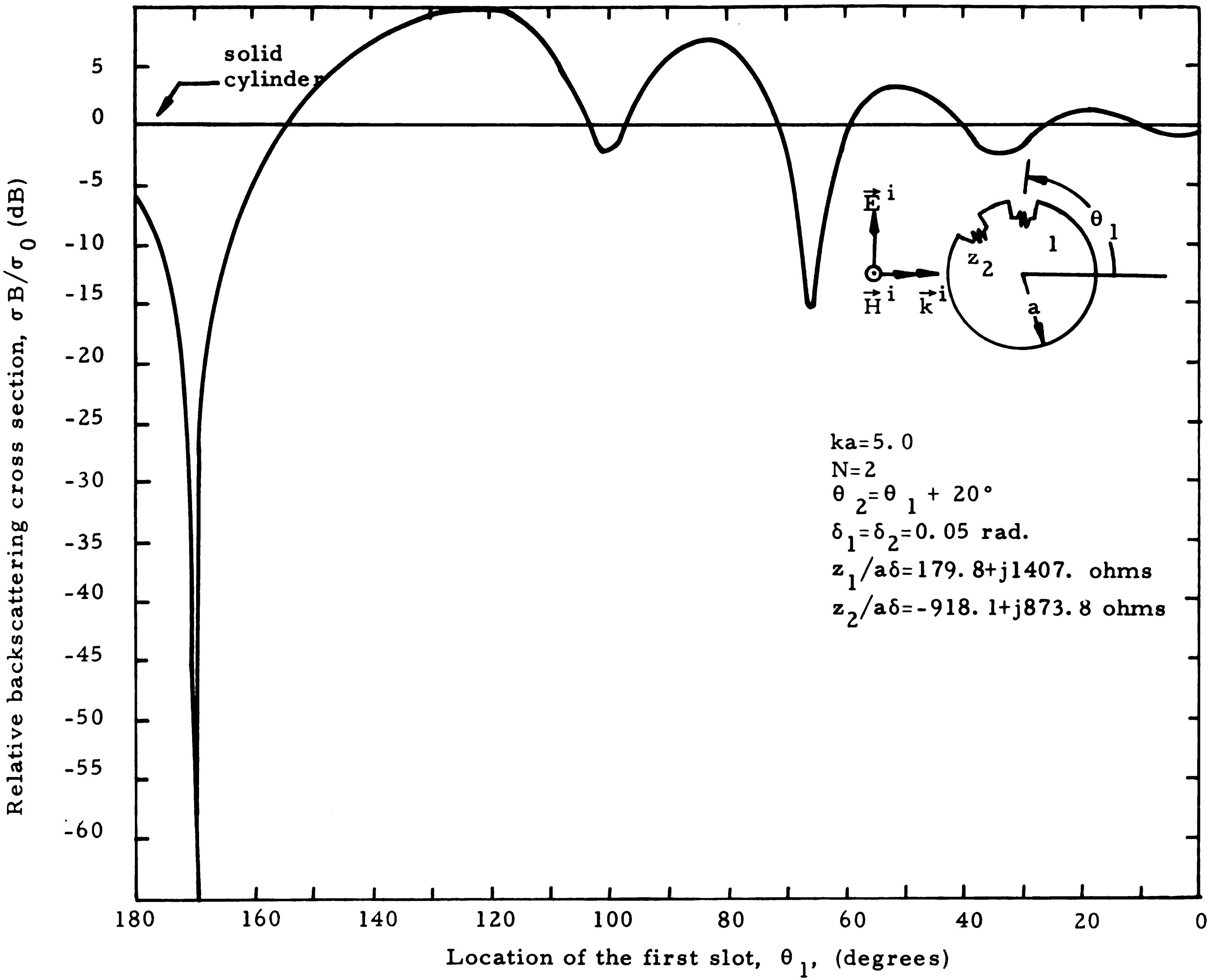


Figure 4.17. Relative backscattering cross section as a function of the first slot position with ka=5.0 .

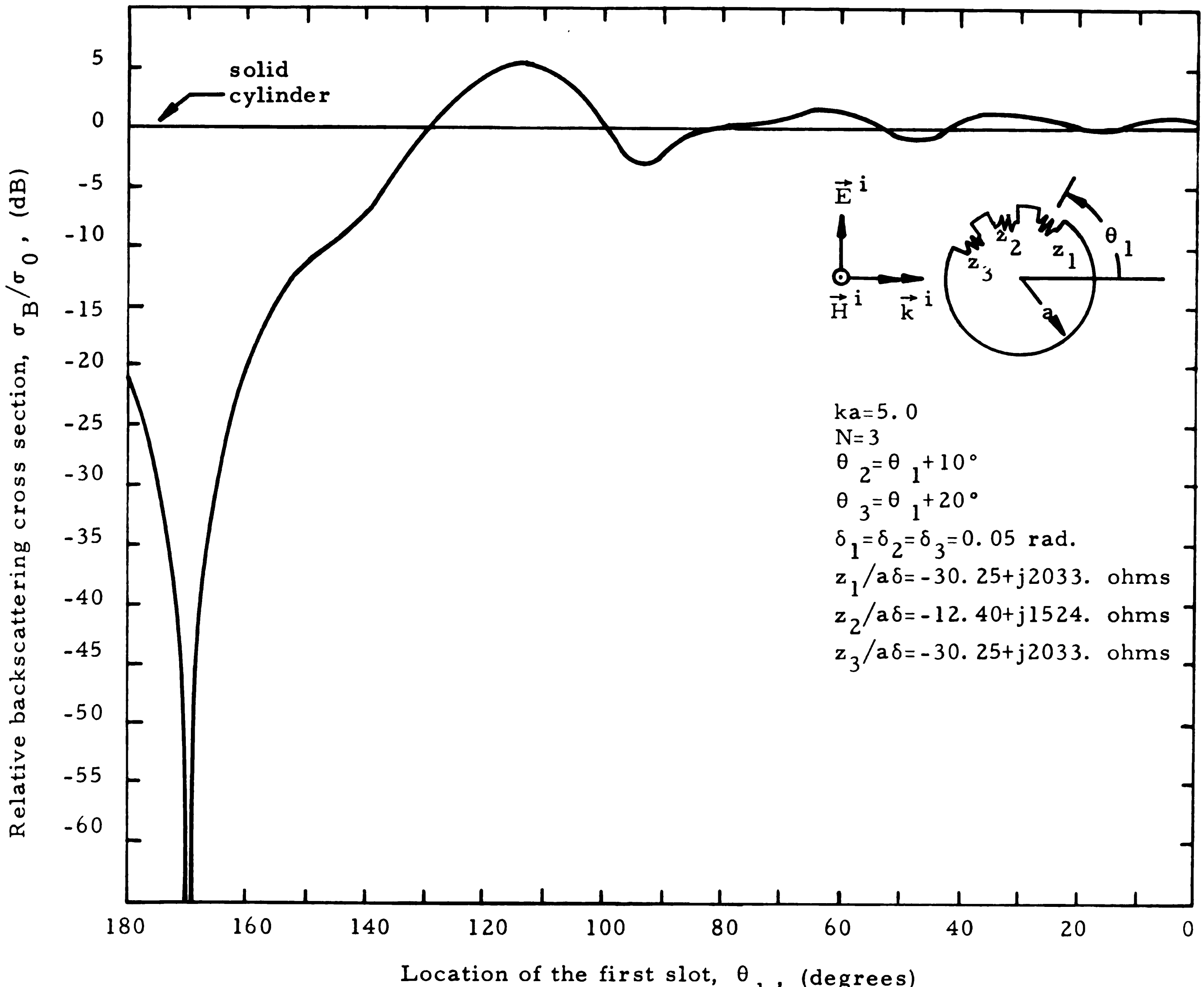


Figure 4.18. Relative backscattering cross section as a function of slot position with ka=5.0 .

Figure 4. 3 when ka=5. 0, hence, the backscattering is zero when $\theta = 180°$. Likewise Figures 4. 17 and 4. 18 correspond to the load configurations and impedances described in Figures 4. 7 and 4. 9 when ka=5. 0. It is seen that changing the number of slots does not significantly change the result. These results are typical of the results obtained for other cylinder sizes.

### 4. 4. Zero Backscattering by a Cylinder Loaded With Two Purely Reactive Impedances

Numerical results of the impedance synthesis procedure of Section 3. 2 for the case of two slots (N=2) are presented in this section. This synthesis procedure yields purely reactive load impedances. The difficulty with this procedure is that the constraint equations are nonlinear.

The load reactances for the case of two slots may be found in terms of a quadratic equation which is derived in Appendix B. Since the load reactances are solutions to a quadratic equation, real solutions do not always exist. The existence of a solution depends on the cylinder size, slot configuration, and direction of zero scattering. The existence of solutions to Equation (B-7) for zero backscattering from several different size cylinders each having one slot located at $\theta = 180°$ and the second slot's position varied from $\theta = 0°$ to $\theta = 170°$ is indicated in Figure 4. 19. An "x" indicates a solution exists for the particular position of the second slot and cylinder size described by the position of the "x". Likewise, the absence of an "x" indicates no solution exists for that particular geometry. Examining this figure it appears that there is an area on the shadow side of the cylinder where no solution exists when the second slot is located in this area. As the cylinder size increases, the size of this area also increases. This trend was examined and found to continue for larger values of ka than shown in this figure.

Solutions for purely reactive loading impedances that result in zero backscattering from a cylinder with slots located at $\theta = 160°$ and 180° exist over the entire range of cylinder size $1 \leq ka \leq 12$. These reactances are displayed in Figure 4. 20. The two solutions to

| ka \ $\theta_2$ | 170° | 160° | 150° | 140° | 130° | 120° | 110° | 100° | 90° | 80° | 70° | 60° | 50° | 40° | 30° | 20° | 10° | 0° |
|---|---|---|---|---|---|---|---|---|---|---|---|---|---|---|---|---|---|---|
| 1.5 | X | X | X | X | X | X | | | | X | X | X | X | | | | | |
| 2.0 | X | X | X | X | X | | X | X | X | X | X | X | X | | | X | X | X |
| 2.5 | X | X | X | X | X | X | X | X | | X | X | X | X | X | | X | X | X |
| 3.0 | X | X | X | X | X | X | X | | X | X | X | X | | X | X | X | | |
| 3.5 | | X | X | X | X | X | | | X | X | | | | X | | | | |
| 4.0 | | X | X | X | X | X | | X | X | X | | X | X | | | | | |
| 4.5 | | X | X | X | X | | | X | X | | | | | | | | | |
| 5.0 | | X | X | X | X | | X | X | | | X | | | | | | | |
| 5.5 | | X | X | X | | | X | | | X | | | | | | | | |
| 6.0 | | X | X | X | | X | X | | | X | | | | | | | | |
| 6.5 | | X | X | X | | X | X | | X | | | | | | | | | |
| 7.0 | | X | X | | | X | | | X | | | | | | | | | |

Figure 4.19. Existence of a solution for zero backscattering from a cylinder loaded with two purely reactive loads with $\theta_1=180°$ and $\delta_1=\delta_2=0.10$ rad.

the quadratic equation which determines these load reactances are labeled $(X_1, X_2)$ and $(X_1', X_2')$. The unprimed reactances are considerably smoother than the primed set. The reactances have negative slope and thus can not be realized by passive elements[32], but work has been done on realizing such reactances using active elements.[31]

Comparison of the bistatic scattering patterns resulting from cylinders loaded with the two different sets of reactances is made in Figures 4.21, 4.22, and 4.23. The shape of the scattering patterns and the null widths differ considerably between the two cases.

Figure 4.24 displays the reactances that produce zero backscattering from a cylinder with slots located at $\theta = 175°$ and $185°$. A solution exists only in the regions $1 \le ka \le 2.11$ and $2.53 \le ka \le 3.04$ and it is very irregular. Due to the symmetry of the two slot locations with respect to the incident wave and the directions of zero scattering the two solutions are degenerate and thus only one distinct set of load reactances exists. Comparison of Figures 4.20 and 4.24 shows that a relatively small change in a slot configuration may drastically change the region over which solutions for zero backscattering exist.

Purely reactive loading impedances that result in zero backscattering from a cylinder whose two slots are located 20° apart are displayed as a function of the first slot position in Figure 4.25. Solutions exist over only a small region mainly in the center of the illuminated side of the cylinder. Although not shown by the figure, no solutions exist in the region $0 \le \theta_1 \le 40°$.

Figure 4.26 examines the change in backscattering cross section when a cylinder loaded with two reactive slots located 20° apart is rotated with respect to the incident wave. The load reactances are held constant and are chosen to give zero backscattering when $\theta_1 = 160°$ [See Figure 4.20]. The two curves represent the two different solutions that are produced by the synthesis procedure. It can be seen that the position of the slots is considerably more critical in the case of the second solution.

An examination of the numerical results of this section seems to indicate that the best positions the slots can be located in, such that a solution to the synthesis procedure exists, are in the center of the illuminated region of the cylinder. Of the slot configurations

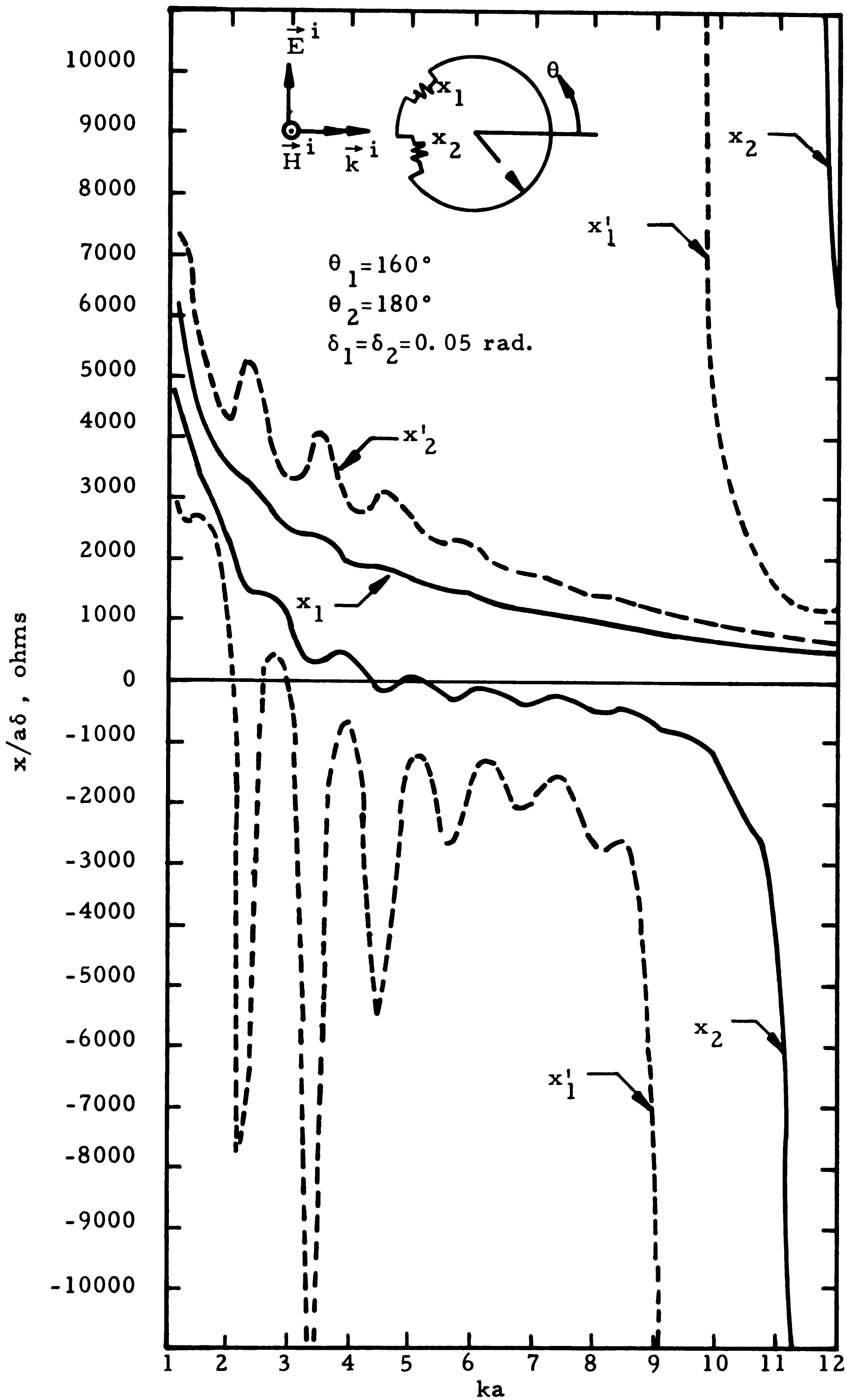


Figure 4. 20. Purely reactive impedances for zero backscattering from a two-slot cylinder as a function of cylinder size ka. $(x_1, x_2)$ is first solution and $(x'_1, x'_2)$ is the second solution.

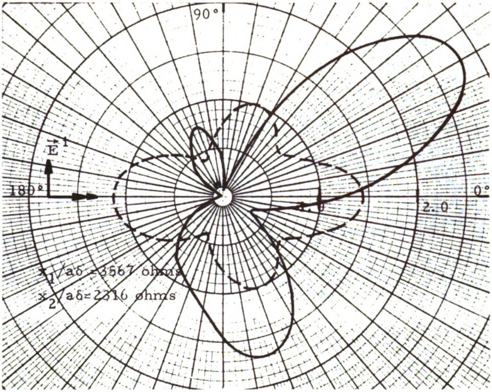


(a)

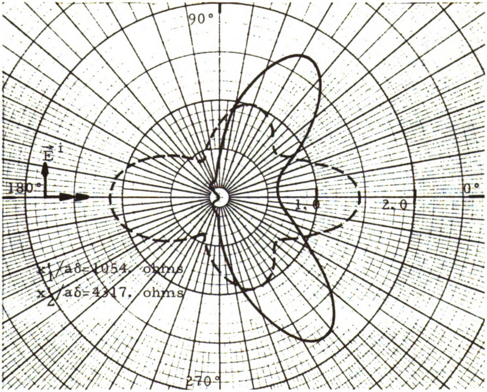


(b)

Figure 4. 21. Normalized bistatic scattering cross section patterns, $\sigma(\theta)/\pi a$, for a thick cylinder, ka=2. 0, with two purely reactive loads located at $\theta = 160°$ and 180°. (a) First solution. (b) Second solution.

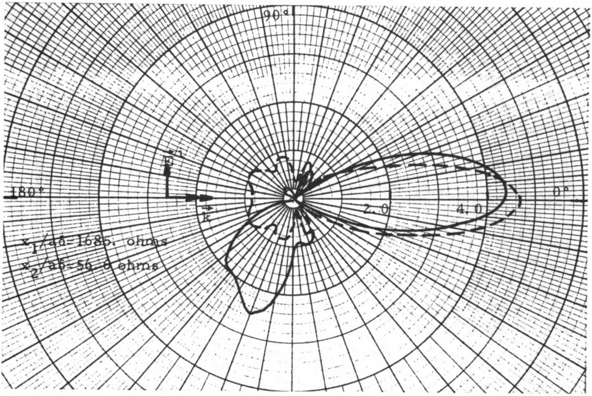


(a)

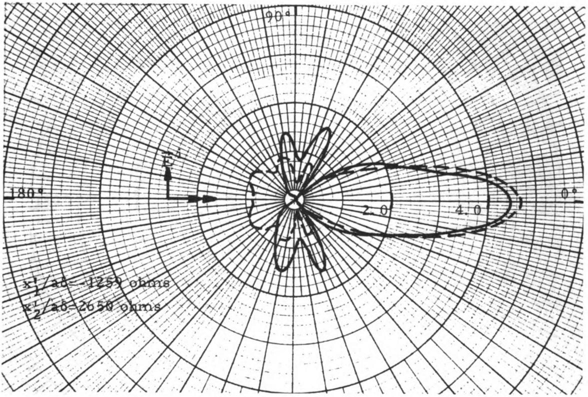


(b)

Figure 4. 22. Normalized bistatic scattering cross section patterns, $\sigma(\theta)/\pi a$ for a thick cylinder, ka=5. 0, with two purely reactive loads located at $\theta = 160°$ and 180°. (a) First solution. (b) Second solution.

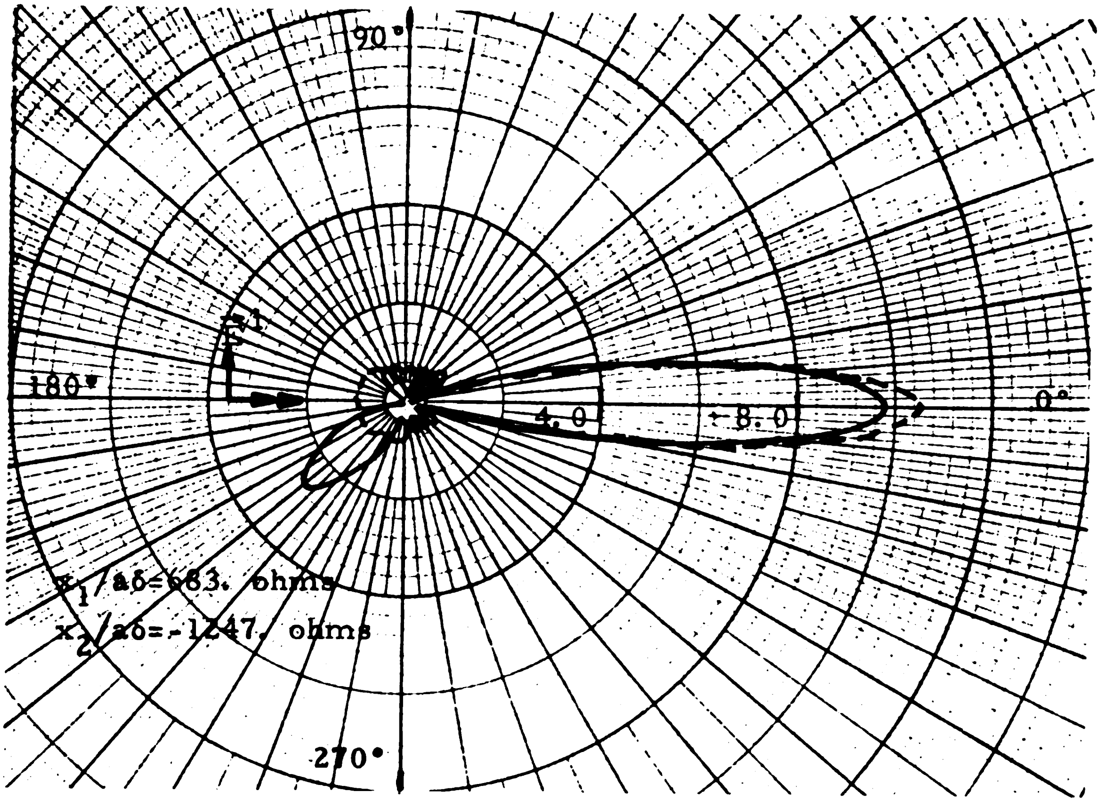


(a)

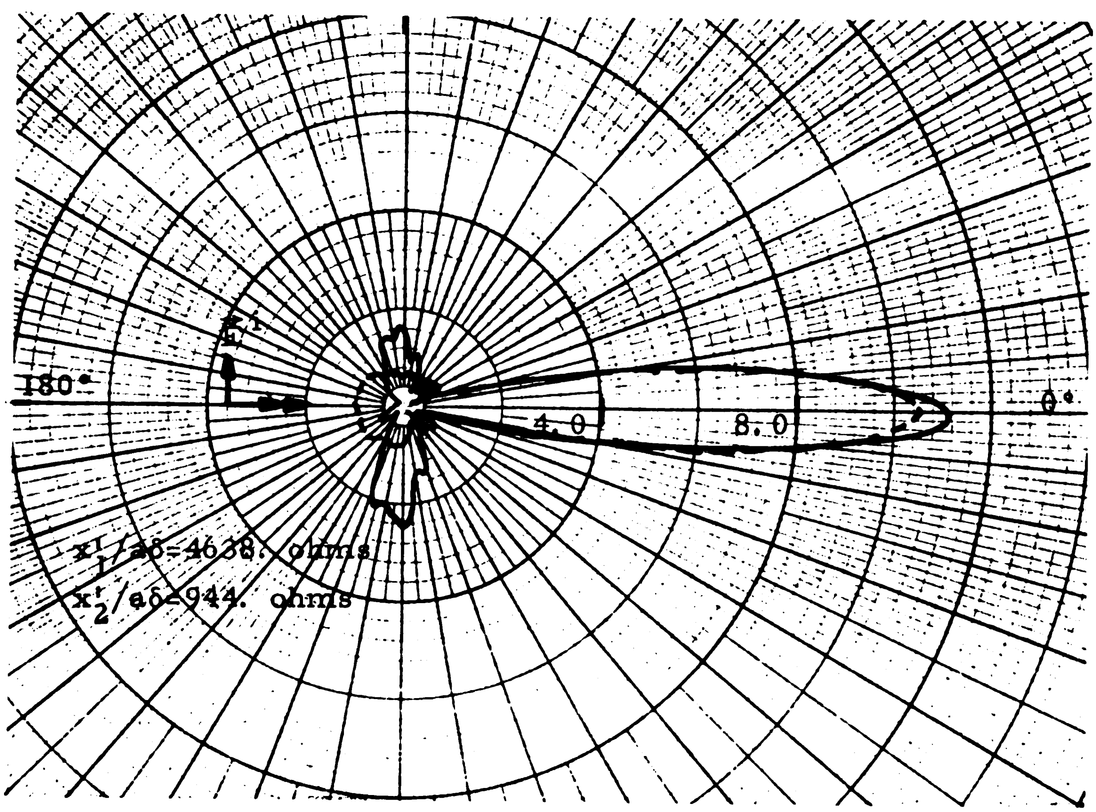


(b)

Figure 4.23. Normalized bistatic scattering cross section patterns, $\sigma(\theta)/\pi a$ for a thick cylinder, ka=10.0, with two purely reactive loads located at $\theta$ =160° and 180°. (a) First solution. (b) Second solution.

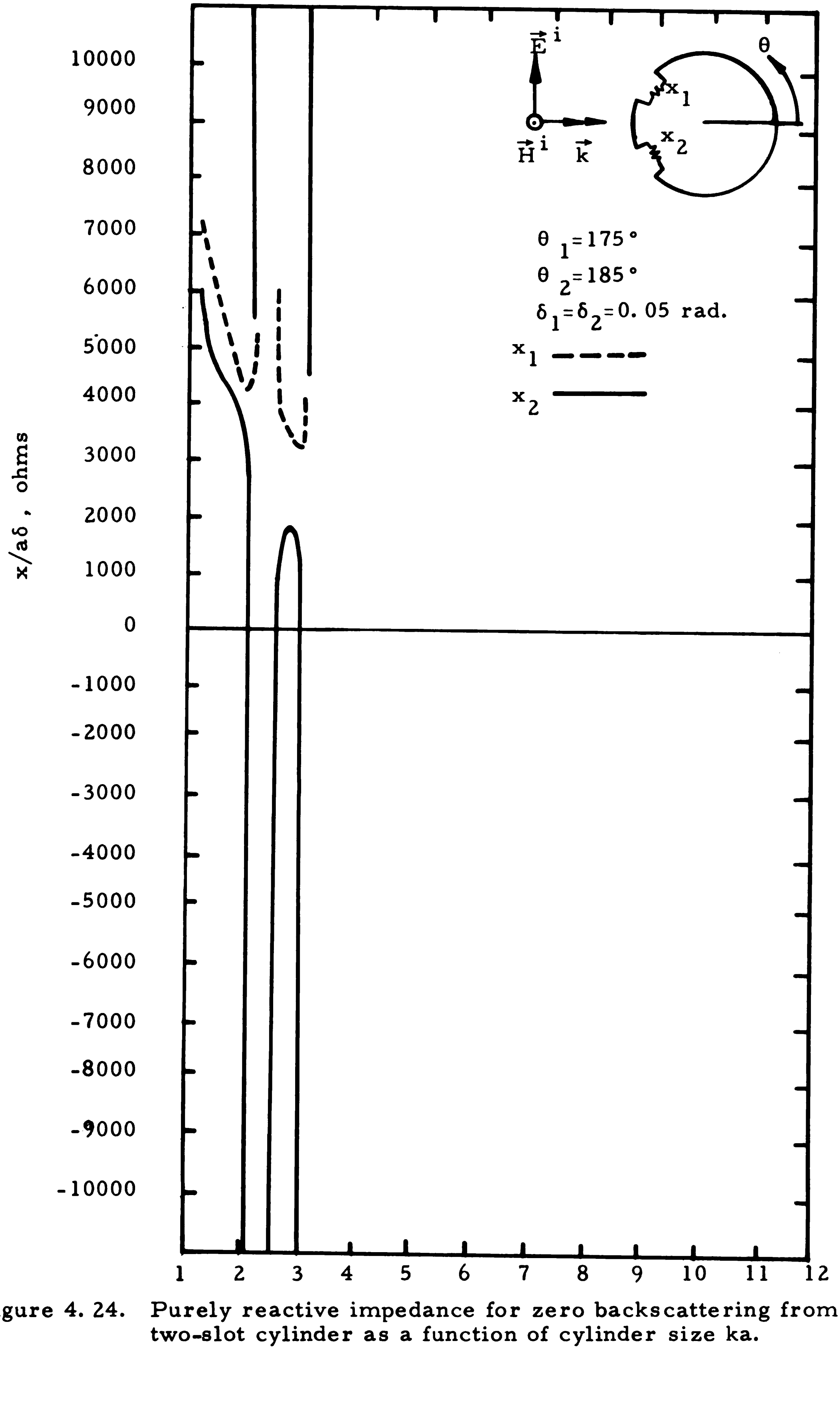


Figure 4.24. Purely reactive impedance for zero backscattering from a two-slot cylinder as a function of cylinder size ka.

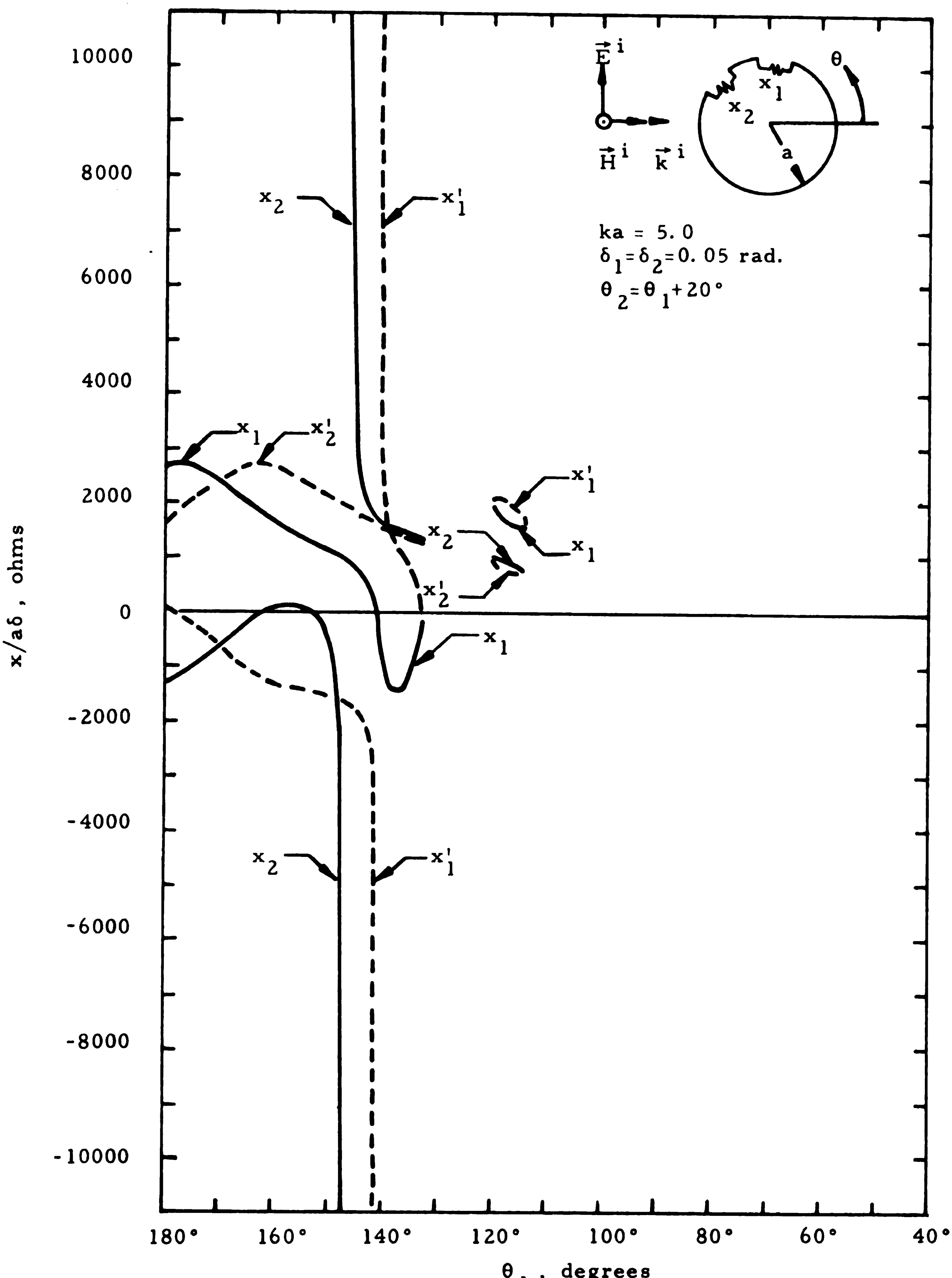


Figure 4.25. Purely reactive impedances for zero backscattering from a two-slot cylinder, as a function of slot position. $(x_1, x_2)$ is one solution and $(x_1', x_2')$ is the second solution.

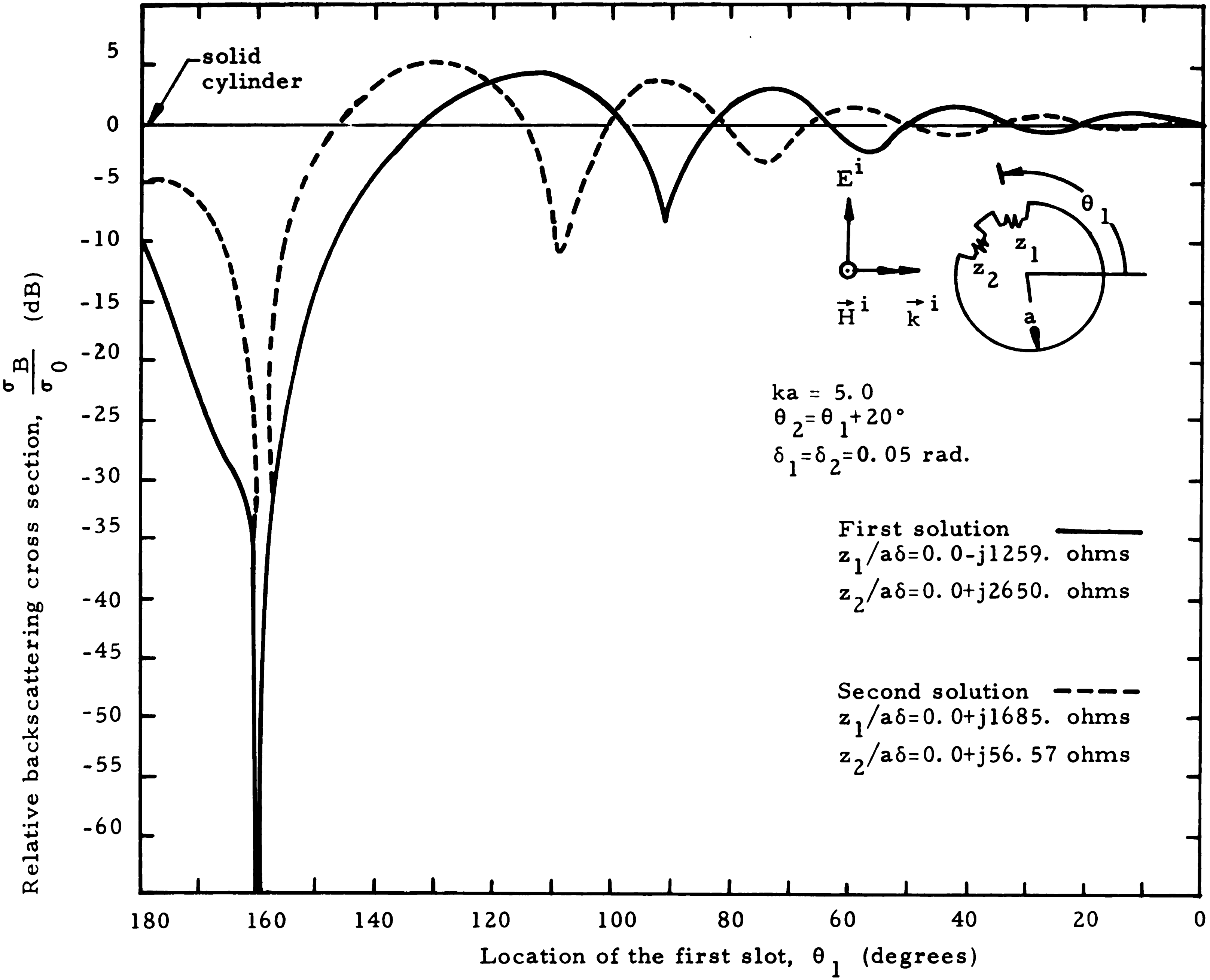


Figure 4.26. Relative backscattering cross section as a function of slot position with purely reactive loading and ka = 5.0.

considered, one was found that yielded solutions over the entire region $1 \leq ka \leq 13$.

It should be pointed out, that even though no solution exists for a purely reactive loading that results in zero backscattering, a suitable set of load reactances can usually be found which significantly reduces the backscattering.

### 4.5. Scattering By a Cylinder Symmetrically Loaded With Equal Purely Reactive Impedances

It has been shown that the backscattering cross section of a discretely loaded cylinder is strongly dependent on the orientation of the cylinder with respect to the incident wave. Thus if a cylinder is slowly rotating about its axis, or is randomly orientated with respect to the incident wave, the impedance loading schemes previously discussed must be modified to remain effective. One method to overcome this problem is to adjust the loading impedances as the position of the cylinder changes. A second, simpler method might be to symmetrically load the cylinder with several loadings in an attempt to reduce the sensitivity of the backscattering to the cylinder orientation. This second method is now considered.

This section examines the scattering modifications that can be obtained by a cylinder loaded with one, two, three, and four purely reactive slots located symmetrically around the cylinder. Furthermore, the restriction is added that all the reactances loading a cylinder are to be equal (i.e., $X=X_1=X_2=X_3=X_4$).

Figure 4.27 displays the relative backscattering cross section of cylinders of size $ka=2.2$ having one, two, three, and four symmetrically located, purely reactive loaded slots. Since all the slots of a cylinder are loaded by reactances having equal value, the net effect is very similar to that of a single load. The result for $N=3$ is superimposed and indistinguishable from the result for $N=1$ over the portion of the curve where $X < 0$. The curves approach asymptotic values ranging from approximately -7db for the case $N=2$ to -5db for $N=4$ for large values of inductive and capacitive loading. The greatest minimization of the backscattering is attained by the cylinder with two slots. The ability of the loading to minimize the

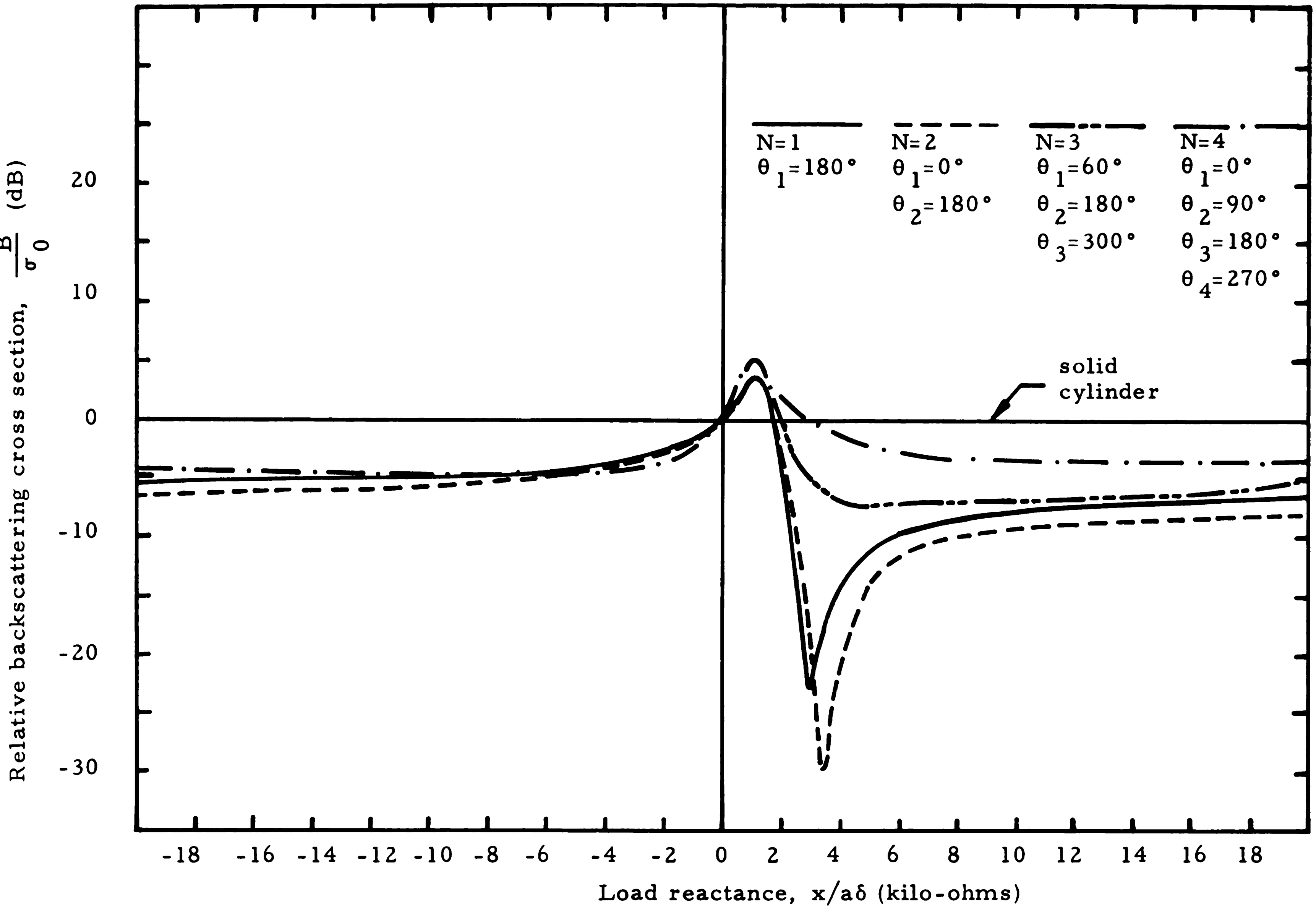


Figure 4. 27. Relative backscattering cross section as a function of purely reactive load impedances for cases N=1, 2, 3, 4 with $z_1=z_2=z_3=z_4=jx$ .

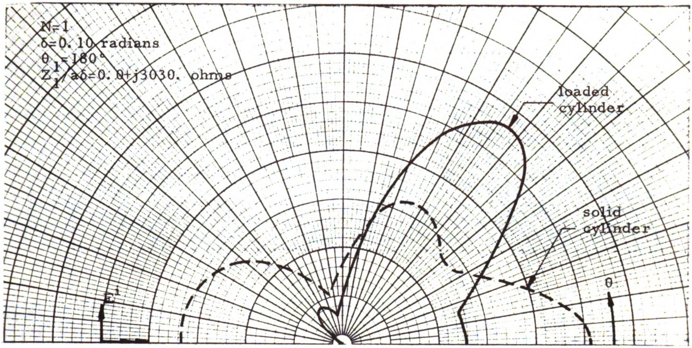


(a)

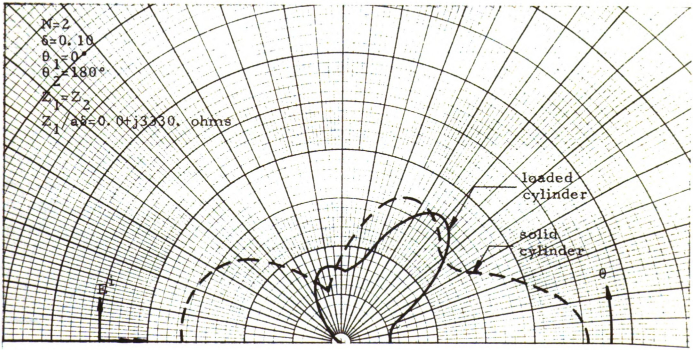


(b)

Figure 4.28. Normalized bistatic scattering cross section patterns for thick cylinders, ka= 2.20, loaded with purely reactive loads.
(a) Minimum backscattering when N= 1.
(b) Minimum backscattering when N= 2.

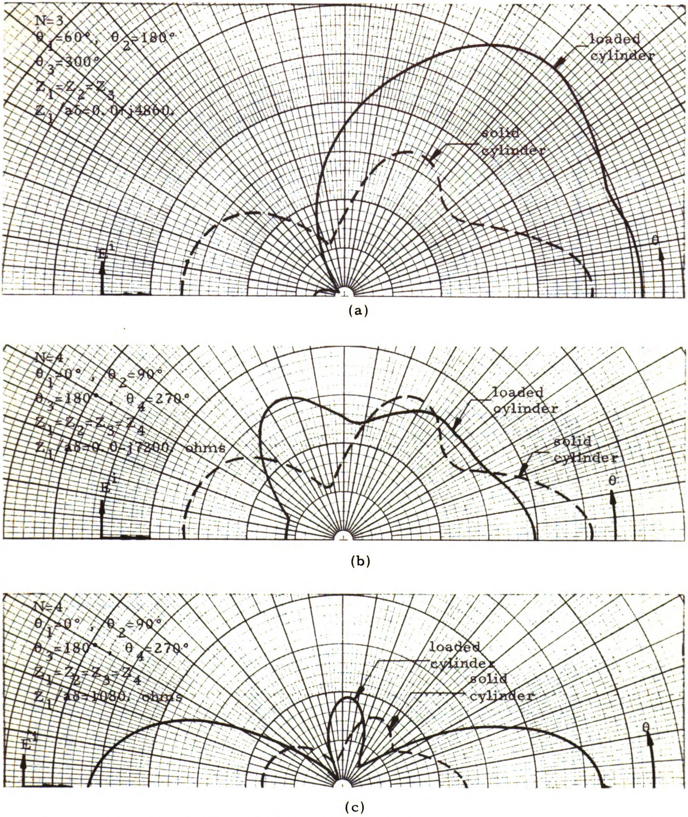


Figure 4.29. Normalized bistatic scattering cross section patterns for thick cylinders, ka=2.20, loaded with purely reactive loads. δ=0.10 radians in all cases. (a) Minimum backscattering when N=3. (b) Minimum backscattering when N=4. (c) Maximum backscattering when N=4.

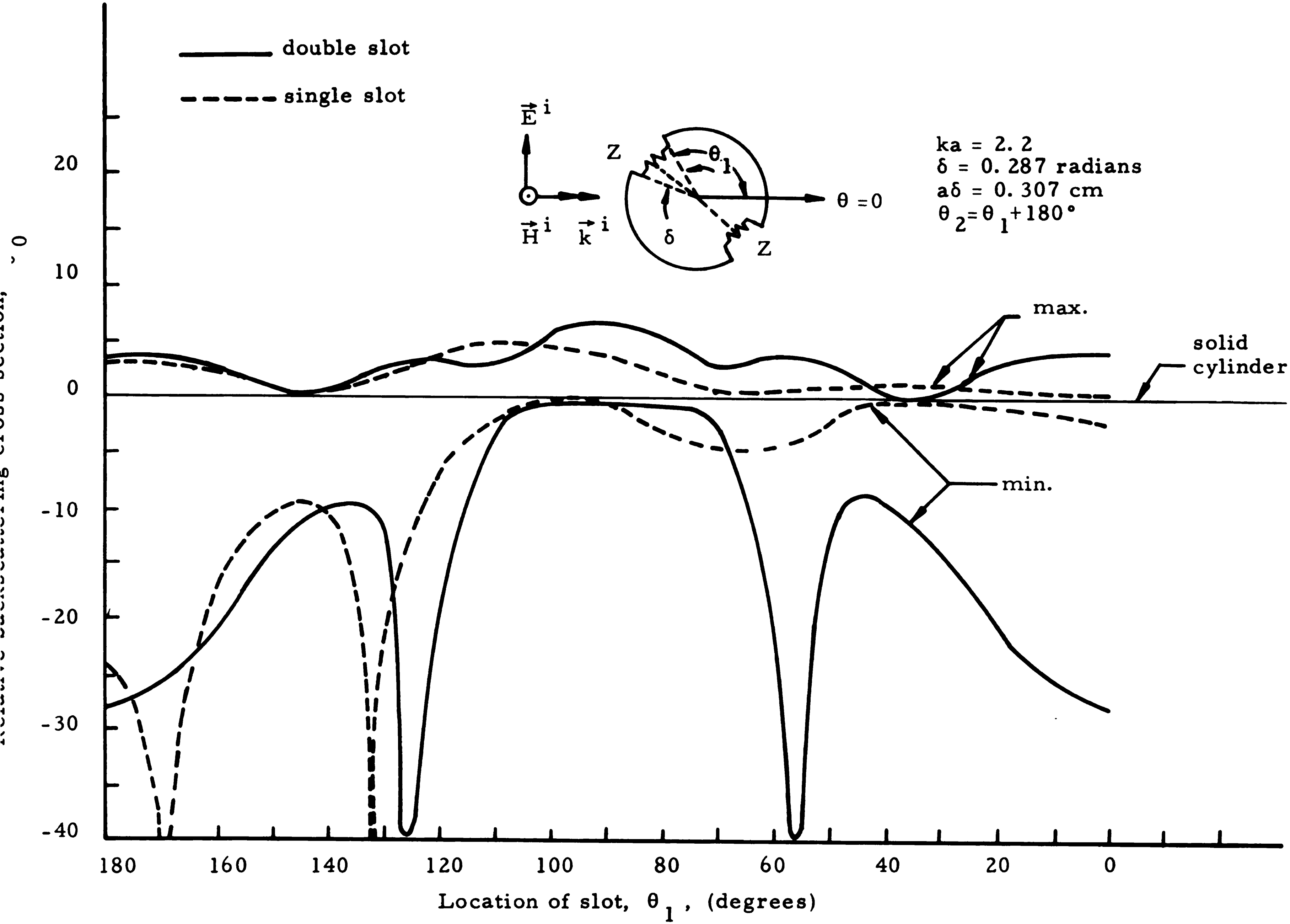


Figure 4.30. Optimum minimum and maximum backscattering cross section as a function of slot position for doubly and singly loaded cylinders.

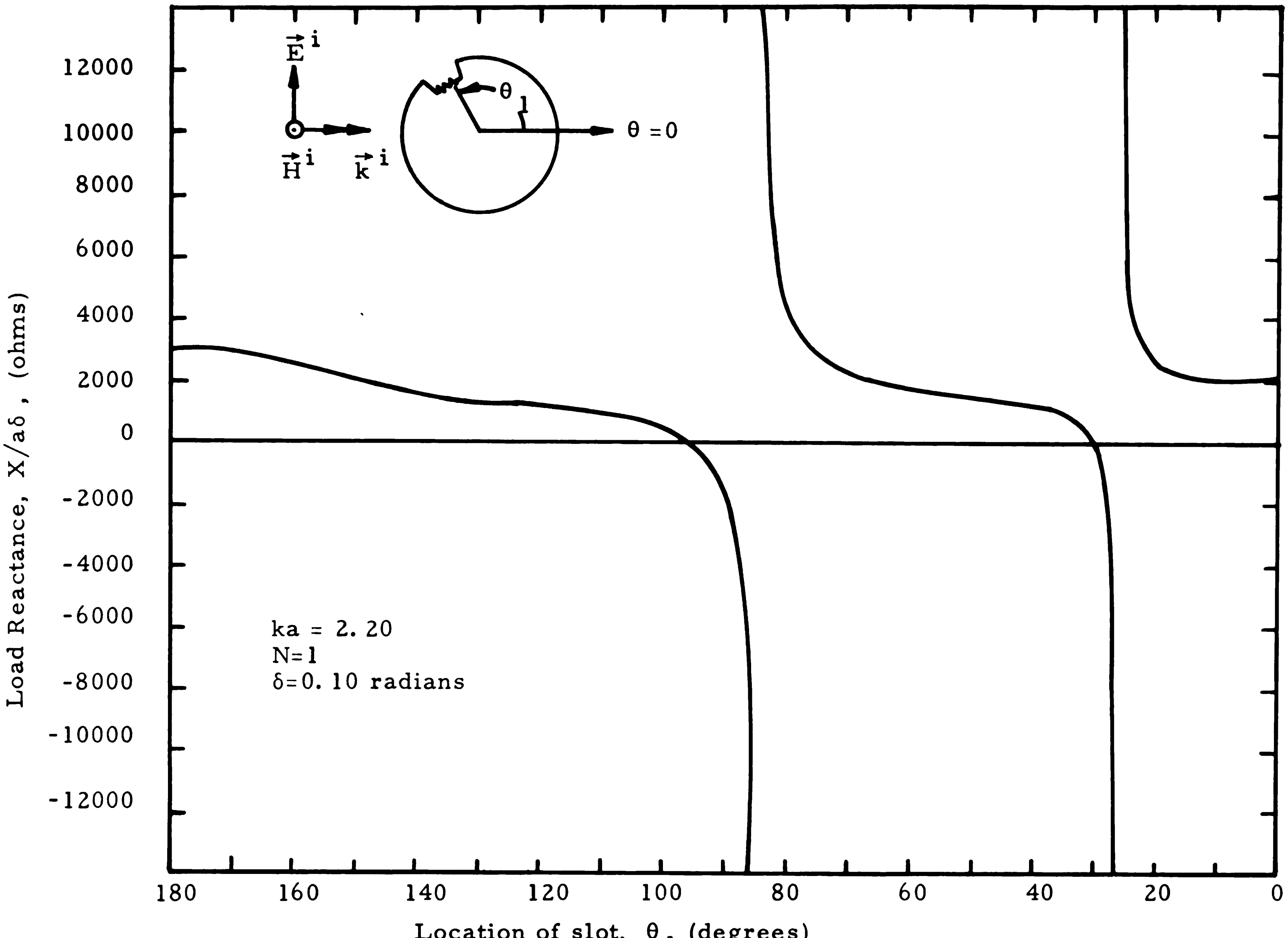


Figure 4. 31. Optimum slot reactance for minimum backscattering cross section as a function of slot position.

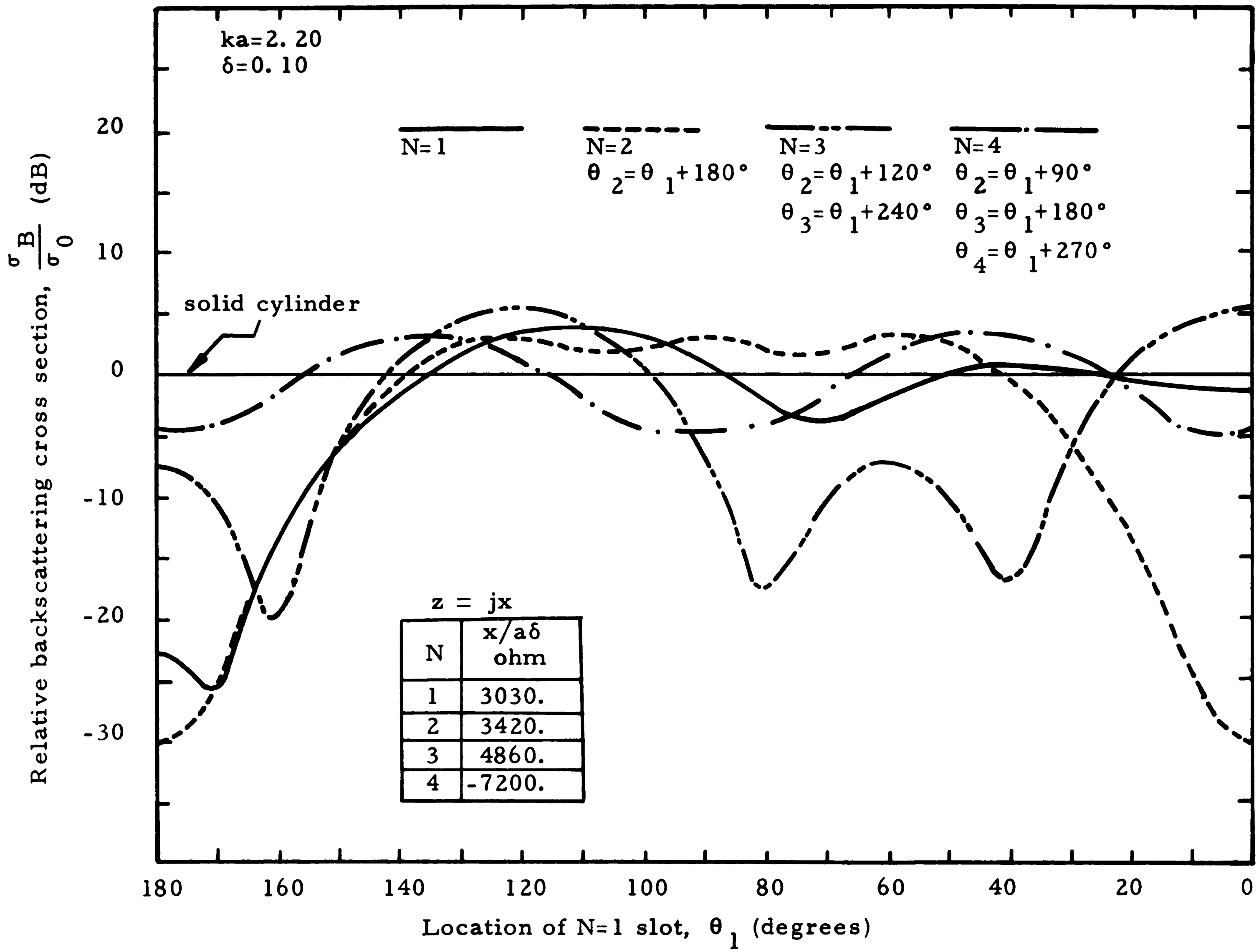


Figure 4.32. Relative backscattering cross section as a function of the first slot position, $\theta_1$ for one through four slots with fixed equal purely reactive loading impedances, $z_1=z_2=z_3=z_4=jx$.

backscattering degenerates as the number of slots is increased to three and then four. Figures 4.28 and 4.29 display the corresponding bistatic scattering cross section patterns for the cases of minimum backscattering when N=1, 2, 3, and 4 and maximum backscattering when N=4. Only the upper half of the scattering patterns are displayed since the lower halves are identical to the upper halves due to symmetry.

Figure 4.30 displays the optimum minimum and maximum backscattering cross section as a function of slot position for cylinders of size ka=2.20 loaded with one and two purely reactive slots. In the case of a single slot, it was found in general, the control over the scattering was markedly decreased for ka>5 and also when the slot is located in the shadow region of the cylinder. The introduction of the second slot considerably increases the slot positions where significant reduction in backscattering can be accomplished. Figure 4.31 displays the load reactance required to obtain the optimum minimum backscattering from a single slotted cylinder as described in the previous figure. The technique described in Section 3.3 was employed in calculating the results in the last two figures.

The backscattering cross section as a function of slot orientation for fixed, purely reactive loading is displayed in Figure 4.32. Cylinders with one, two, three, and four slots are considered and in all cases the load reactances are chosen to minimize the backscattering at $\theta_1 = 180°$. Significant reduction of the backscattering is obtained over the largest region of slot orientations when the cylinder with three slots is considered. In all cases some slot orientations exist where enhancement rather than reduction of the backscattering is experienced.

## 4.6. The Frequency Dependence of the Modified Scattered Field

The techniques that have been discussed in this chapter are concerned with modifying the field scattered by a cylinder at one frequency only. It is usually desired, however, that the scattering be modified over a band of frequencies. In this section the frequency dependence of the fields scattered by loaded cylinders will be discussed.

The frequency dependence of the field scattered by a loaded cylinder depends directly on the frequency dependence of the load impedances. For example, if a set of load impedances can be found that have exactly the same frequency dependence as the desired loading that results in zero backscattering, zero backscattering will be attained at all frequencies.

Three types of load impedances will be considered: (1) the short circuited TEM parallel plane line; (2) the short circuited TEM parallel plane line in series with a resistance; and (3) the constant impedance (i.e., an impedance that is constant with respect to frequency).

The geometry of the short circuited TEM parallel plane line is shown in Figure 4.33. The input impedance of the line is purely reactive and given by[33]

$$Z_{in} = j\, Z_0 \tan k\ell \qquad \text{ohm-meter}$$

where

$$Z_0 = \zeta_0\, d \qquad \text{ohm-meter}$$

is the characteristic impedance of the line, $\ell$ is the length of the line, d is the separation between the parallel planes and $\zeta_0$ is the impedance of the medium between the parallel planes. This type of impedance is easily implemented behind the slots in a cylinder surface as a load impedance. This topic is discussed in detail in Chapter 5.

The short circuited TEM parallel plane line with a resistance in series yields an impedance with a constant resistance and a reactance which behaves as a short circuited line. This type of impedance could be easily implemented by installing a narrow resistive strip along each input terminal of the parallel plane line discussed above.

No attempt is made to explain the implementation of a constant impedance. It is presented to give a comparison of the frequency dependences of differing cylinders and loadings. All end effects at the junction of the load impedance and the cylinder surface are neglected.

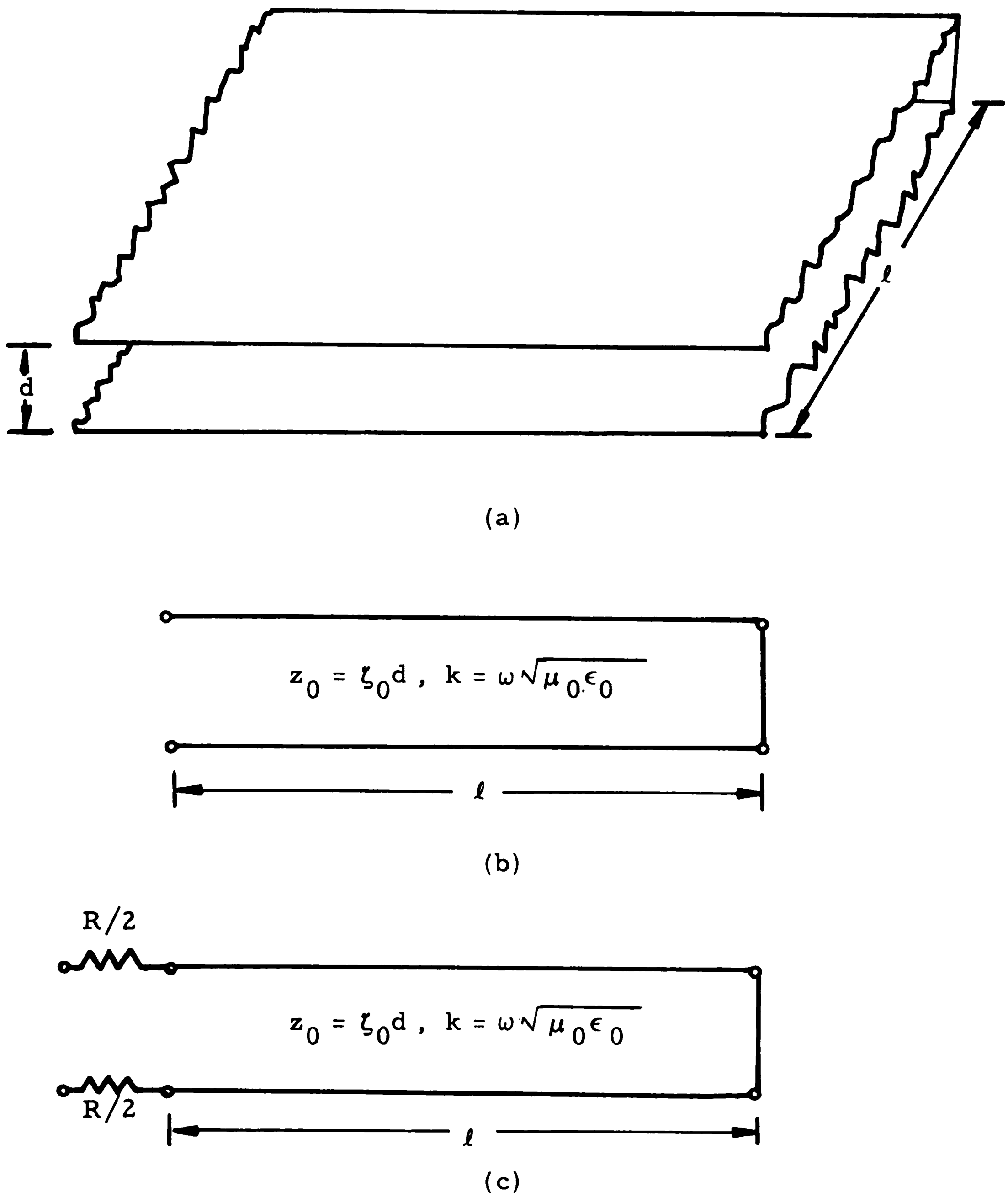


Figure 4.33. Short circuited TEM parallel plane line. (a) Geometry (b) Schematic (c) Short circuited line with series resistance.

The bandwidth of a loaded scatterer is defined as the frequency band over which the backscattering cross section is reduced by 10db or more below the level of the backscattering cross section of an unloaded cylinder of the same size. The backscattering vs. frequency curves are not symmetric about the point of zero or minmum backscattering. Hence, it is convenient to define an upper half bandwidth, UHBW, which is the portion of the bandwidth above the point of zero or minimum backscattering and similarly a lower half bandwidth, LHBW. The bandwidths are given in percent of the frequency of zero or minimum backscattering.

The frequency dependence of the backscattering from a one-slot cylinder loaded with a constant impedance is shown in Figure 4.34(a). The backscattering cross section of the loaded cylinder is normalized to the backscattering cross section of an unloaded cylinder of the same size and plotted as a function of ka, which is linearly proportional to frequency. The load impedance is obtained from Figure 4.3 with ka=6.5 which results in zero backscattering at this frequency. The UHBW is 43% while the LHBW is 18% for an overall bandwidth of 61%. Figure 4.34(b) displays the frequency dependence of a three-slot cylinder loaded with a constant impedance obtained from Figure 4.9 with ka=6.5. The bandwidth is extremely narrow. Comparing Figures 4.3 and 4.9, the impedances necessary for zero backscattering, shows them to be very similar for ka>4, yet the correponding curves in Figure 4.34 differ greatly.

Figure 4.35(a) compares the frequency dependence of the backscattering from a two-slot cylinder loaded first with a TEM line in series with a constant resistance and secondly a constant impedance. In both cases the value of the load impedances at ka=6.4 is set equal to the value obtained from Figure 4.5. This results in zero scattering in directions $\theta = 170°$ and $190°$ at ka=6.4. The characteristic impedance of the TEM line is $Z_0/a\delta = 240\pi$ ohms which corresponds to an air-filled parallel plane line with the planes separated by twice the slot width, that is $d = 2a\delta$.

In the case of the TEM line in series with a constant resistance the UHBW is 14% and the LHBW is 25%, while in the case of the constant impedance, the UHBW is 49% and the LHBW is 43% which is a

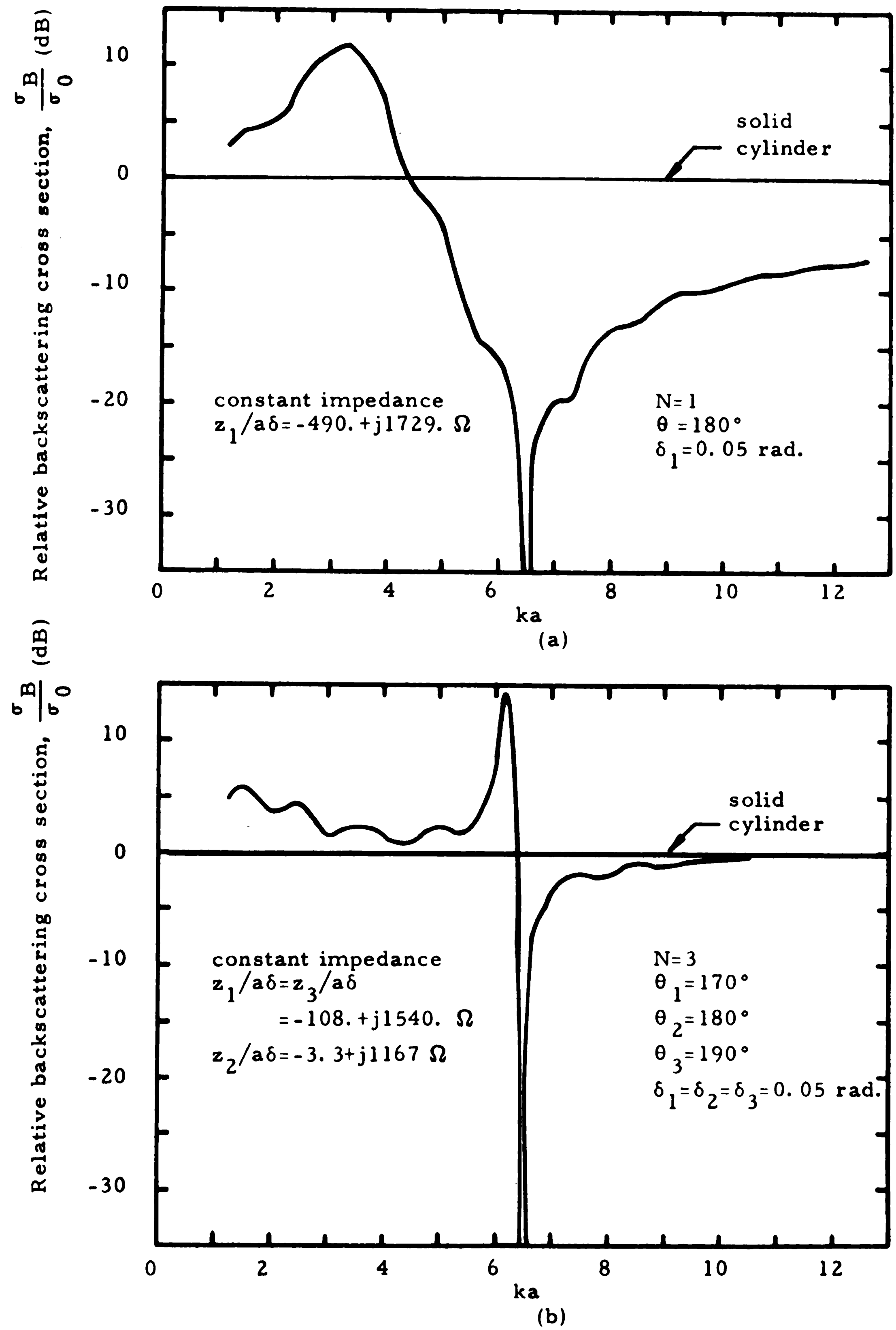


**Figure 4.34.** Relative backscattering cross section as a function of cylinder size ka for cylinders with (a) one slot, (b) three slots.

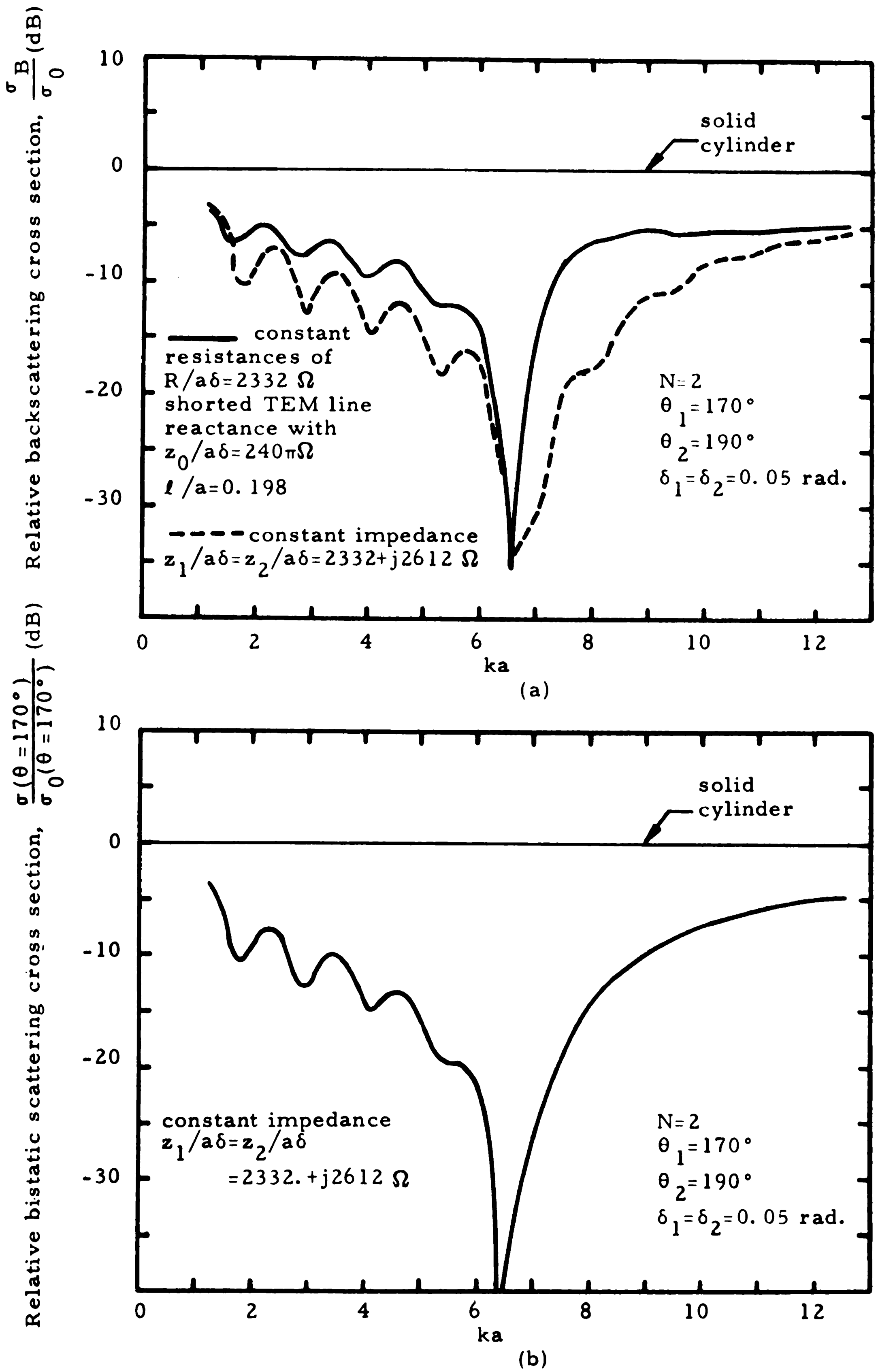


Figure 4.35. Relative scattering cross section as a function of cylinder size ka. (a) Backscattering cross section. (b) Bistatic scattering cross section of $\theta = 170°$.

significant improvement. Comparing the frequency dependence of the short circuited line (i. e., tank$\ell$ which has a positive slope) and the constant reactance to the reactance in Figure 4. 5(b) (which has a negative slope), shows that the constant reactance matches the desired reactance in Figure 4. 5(b) better than the short circuited line does. This explains the wider bandwidth in the case of the constant impedance. Figure 4. 35(b) displays the bistatic scattering cross section at $\theta = 170°$ as a function of frequency for the same constant impedance loading used in Figure 4. 35(a). The UHBW is 38% and the LHBW is 58% with general shape of the curve similar to the backscattering cross section curve shown above.

Figures 4. 36 and 4. 37 describe the frequency dependence of the bistatic scattering pattern of a cylinder loaded with the same constant impedance load configuration that was a consideration in the previous figure. The bistatic scattering patterns are normalized to the geometrical-optics value of the backscattering cross section.

The frequency dependence of the backscattering cross section of a cylinder loaded with two purely reactive loads that yield zero backscattering when ka=6. 5 is displayed in Figure 4. 38(a). Three different types of load reactances are compared: (1) A short circuited TEM parallel plate line with $Z_0/a\delta = 120\pi$ ohms, $\ell_1/a = 0.197$, and $\ell_2/a = 0.402$., (2) A short circuited TEM parallel plate line with $Z_0/a\delta = 240\pi$ ohms, $\ell_1/a = 0.159$, and $\ell_2/a = 0.440$., (3) A constant reactance with $X_1/a\delta = 1267.$ and $X_2/a\delta = -220.5$. The bandwidths for the three types of loading are: (1) UHBW 3%, LHBW 3%, (2) UHBW 5%, LHBW 4%, and (3) UHBW 18%, LHBW 12%. The values of the load reactance for the two cases of short circuited TEM lines are shown in Figure 4. 38(b). Comparing these reactances with the desired reactance function displayed in Figure 4. 20 explains the differences in bandwidth for the three different types of loading. Comparing the curves for constant reactance loading and those for constant impedance loading (i. e., with non-zero resistances) shows that in most cases the purely reactive loading has a significantly narrower bandwidth than general impedance loading.

It has been seen that the reactances necessary for zero backscattering generally have a negative slope as a function of frequency

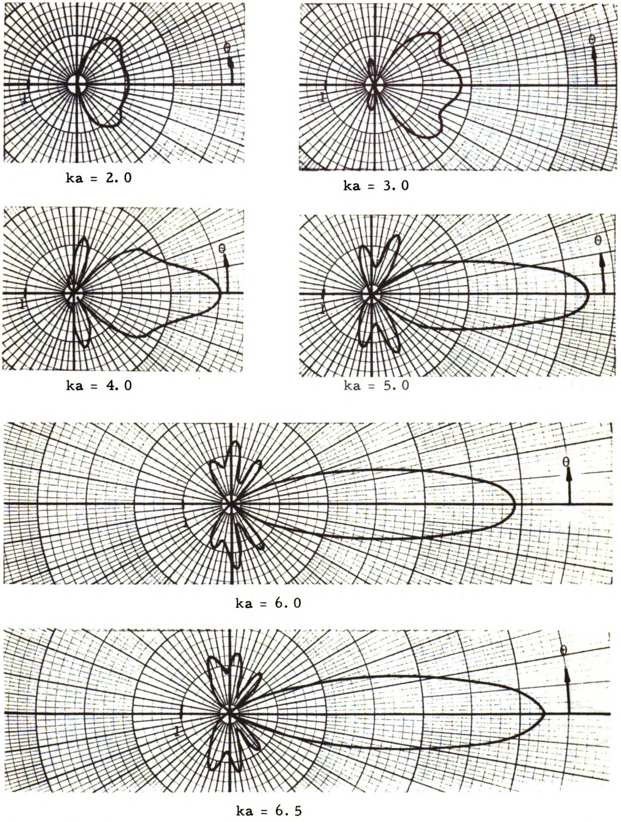


Figure 4. 36. Normalized bistatic scattering cross section patterns, $\sigma(\theta)/\pi a$, for a thick cylinder loaded with impedances $Z_1/a\delta = Z_2/a\delta = 2332 + j2612\Omega$ at $\theta_1 = 170°$ and $\theta_2 = 190°$ with $\delta_1 = \delta_2 = 0.05$ radians.

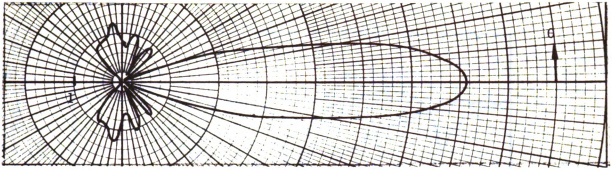


ka = 7.0

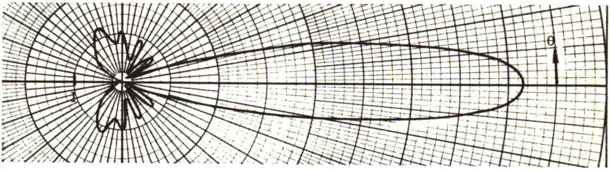


ka = 8.0

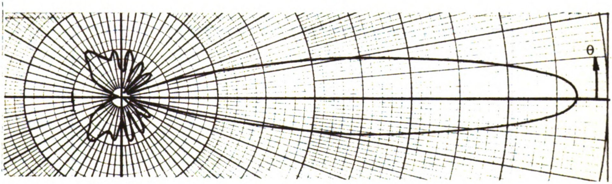


ka = 9.0

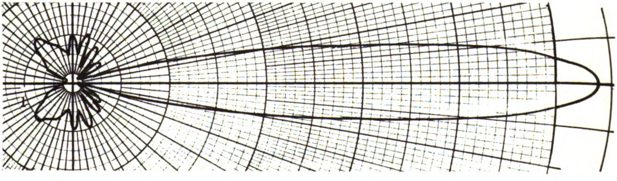


ka = 10.0

Figure 4.37. Normalized bistatic scattering cross section patterns, $\sigma(\theta)/\pi a$, for a thick cylinder loaded with impedances $Z_1/a\delta = Z_2/a\delta = 2332 + j2612\Omega$ at $\theta_1 = 170°$ and $\theta_2 = 190°$ with $\delta_1 = \delta_2 = 0.05$ radians.

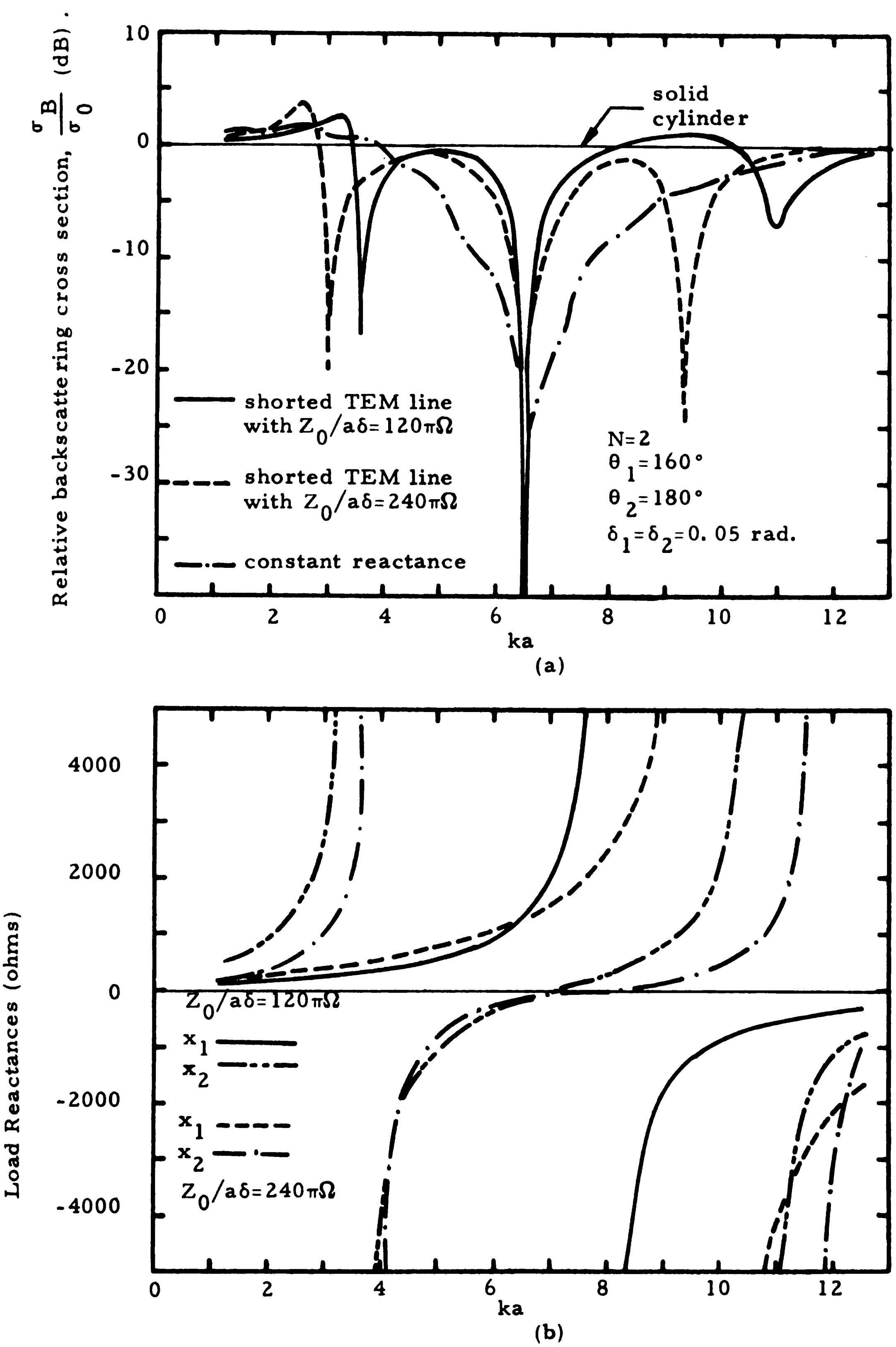


Figure 4. 38. Relative backscattering cross section and load reactance as a function of cylinder size.

while a short circuited TEM line has a $\tan k\ell$ dependence, which has a positive slope. Furthermore, in many cases large reactances are required which force the short circuited line to be operated near antiresonance (i.e., $k\ell \sim \pi/2$). In this region $\tan k\ell$ is a rapidly changing function of frequency which is undesirable from the viewpoint of bandwidth. Increasing the characteristic impedance of the line moves the operating region away from the antiresonance point thus in most cases increasing the bandwidth.[13]

Examing Figure 4.27 suggests a broad band reduction of approximately -5dB in the backscattering might be attained with very large purely reactive loading. This is confirmed for the case of a constant reactance of $X_1/a\delta$ = 20,000 ohms in Figure 4.39(b). The practical problem with this scheme is in realizing a very large reactance which is constant with respect to frequency.

The loading technique developed in Section 3.4 for zero scattering in one direction at several different frequencies suggests a method which might lead to broadband scattering modifications.

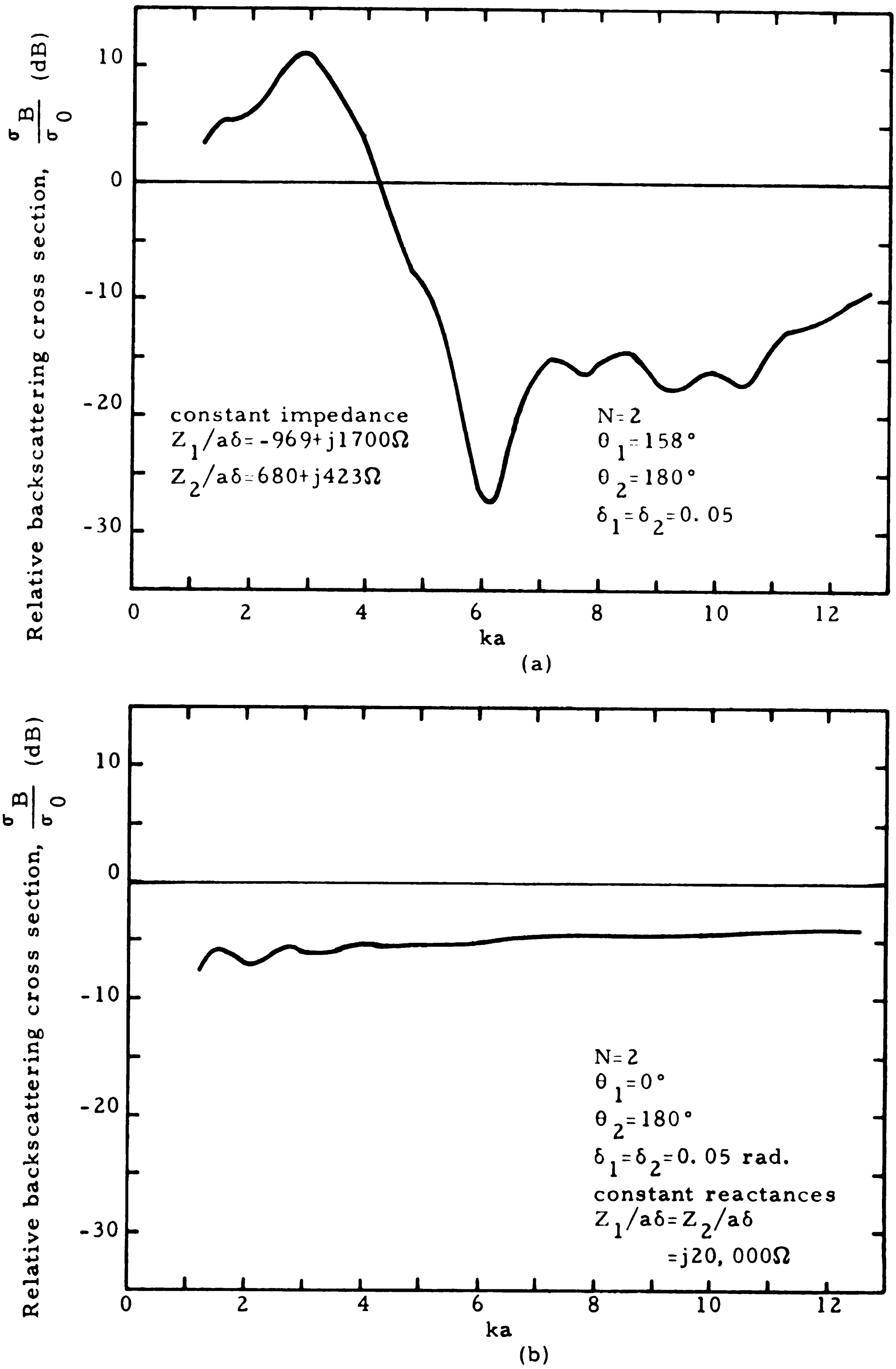


Figure 4.39. Relative backscattering cross section as a function of cylinder size ka for cylinders.
(a) Broad-band loading. (b) Large constant purely reactive loading.

# CHAPTER V

# EXPERIMENT AND COMPARISON TO THEORY

To confirm the preceding theoretical predictions a series of backscattering measurements were performed on a cylinder with one purely reactive loaded slot.

## 5. 1. Experimental Model and Experiment

The experimental model [See Figure 5. 1(a)] consisted of a cylindrical brass tube, 7/8-inch OD, 3/4-inch ID, and 36 inches long, with a 1/8-inch wide longitudinal slot cut in its surface. The slot impedance is implemented by installing a curved parallel plane TEM line interior to the cylinder. The inner wall of the slotted cylinder forms one of the conductors of the line, with the outer surface of a brass cylinder of OD 1/2-inch, installed coaxial with the slotted cylinder forming the other conductor. One end of the line opens at the slot in the cylinder's surface while the other end is short circuited. The short location is adjustable so that the length of the line can be varied, which in turn varies the slot impedance.

The experiment is conducted inside an anechoic chamber at frequencies ranging from 8. 4 to 9. 4 GHz. The experimental arrangement and block diagram of the test instrumentation are shown in Figure 5. 1(a) and (b), respectively. The source separation method[34] is used to measure the backscattering cross section of the cylinder.

The horn antenna does not illuminate the cylinder with a plane wave. The amplitude and phase of the incident wave vary along the axis of the cylinder. It was found that by placing the cylinder about ten wave lengths in front of the horn the consequences of the nonuniform illumination and the end effects (arising from the finite length of the scattering model) were small, while the detection system provided the desired sensitivity.


a) Experimental model of slotted cylinder

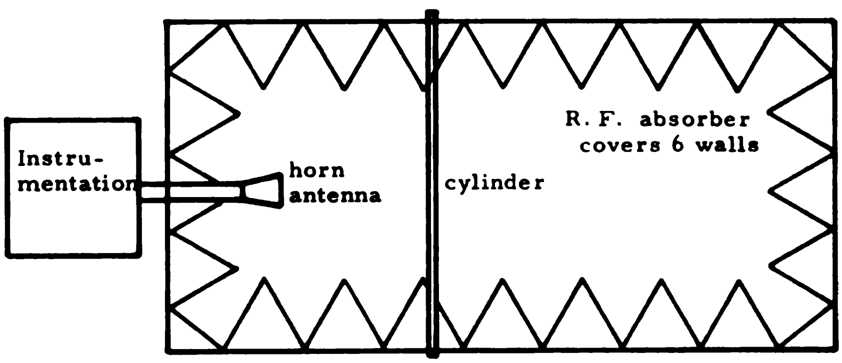


b) Anechoic Chamber

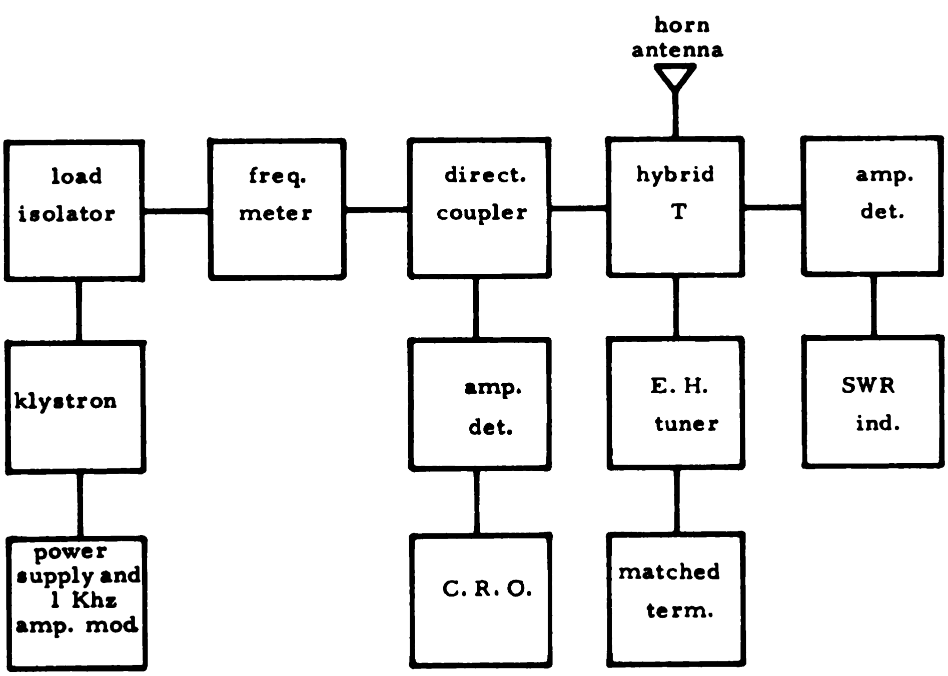


c) Block diagram of instrumentation

Figure 5. 1. Scattering Model and Experimental Arrangement.

## 5.2. Comparison of Theory with Experiment

The first comparison is made with data which depends on the slot orientation but only indirectly on the value of the load impedance. Figure 5.2 compares experimental data and theoretical calculations for the maximum and minimum backscattering cross section, which can be achieved by one purely reactive load, as a function of slot location. The experimental points were determined by setting the position of the slot, then determining the maximum and minimum possible backscattering by varying the short position. The theoretical results were calculated from Equation (31) with the reactances for maximum and minimum backscattering calculated from Equation (39). The agreement between experimental and theoretical results is excellent.

In order to compare results directly involving values of the load reactance, a mathematical model must be developed for the impedance backing the slot in the experimental scattering model. The load impedance of the slot is modeled as a short circuited TEM parallel plane line [See Section 4.6] in series with a lumped reactive impedance which accounts for end effects and the right angle bend at the input end of the line [See Figure 5.3(b)]. The length of the parallel plane line is taken to be the mean length of the curved line

$$\ell = \frac{a'+b}{2}\phi = 0.79375\phi \text{ cm.}$$

where a' is the inner radius of the outer cylinder, b is the outer radius of the inner cylinder, and $\phi$ is the angular displacement of the adjustable short [See Figure 5.3(a)]. The separation of the plates of the line is

$$d = a' - b = 0.13175 \text{ cm.}$$

The approximate model of the impedance backing the slot in the experimental scattering model is

$$Z_1 = jX_E + j1.197 \tan(0.007937k\phi) \text{ ohm-meters.}$$

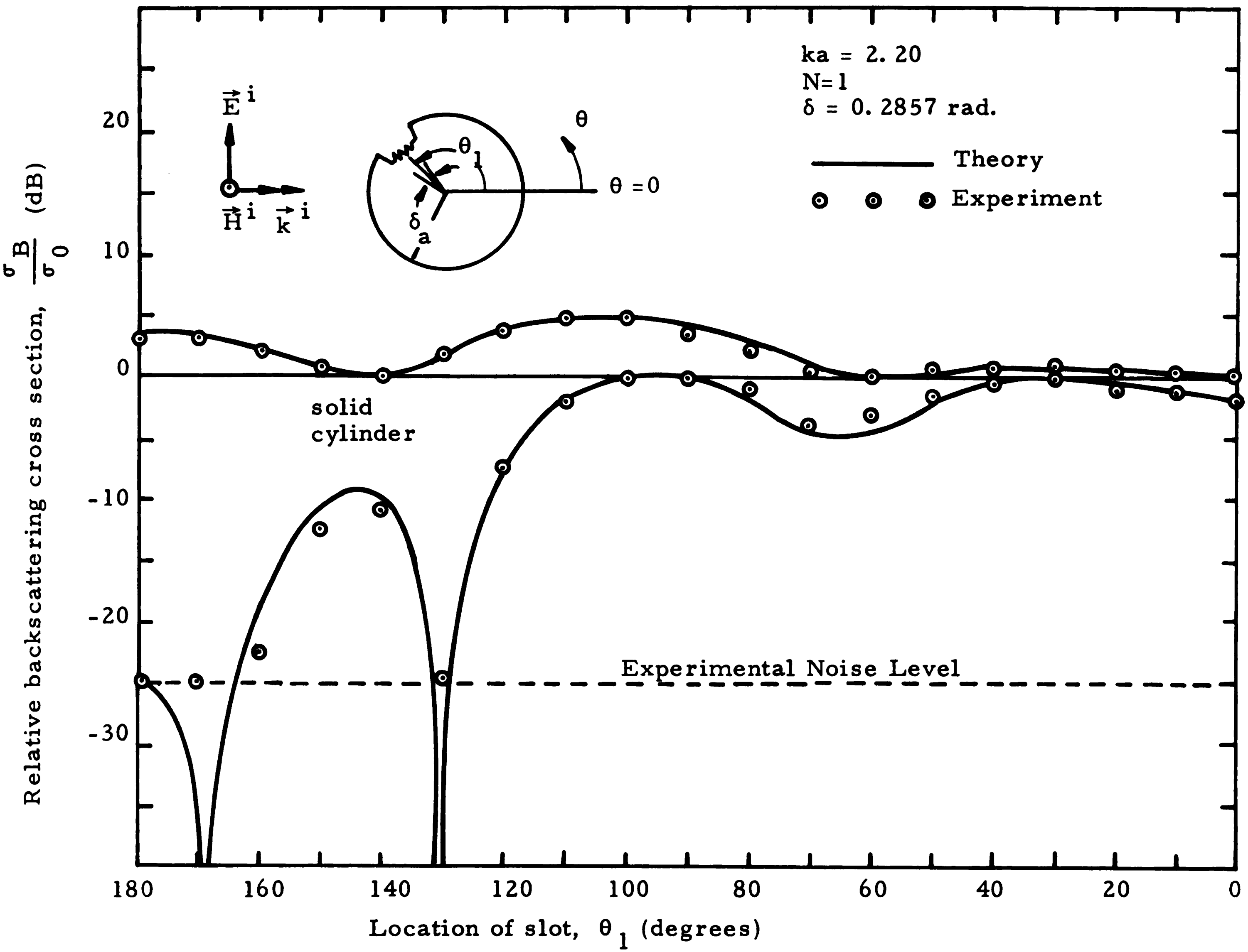


Figure 5.2. Optimum minimum and maximum backscattering cross section as a function of slot position.

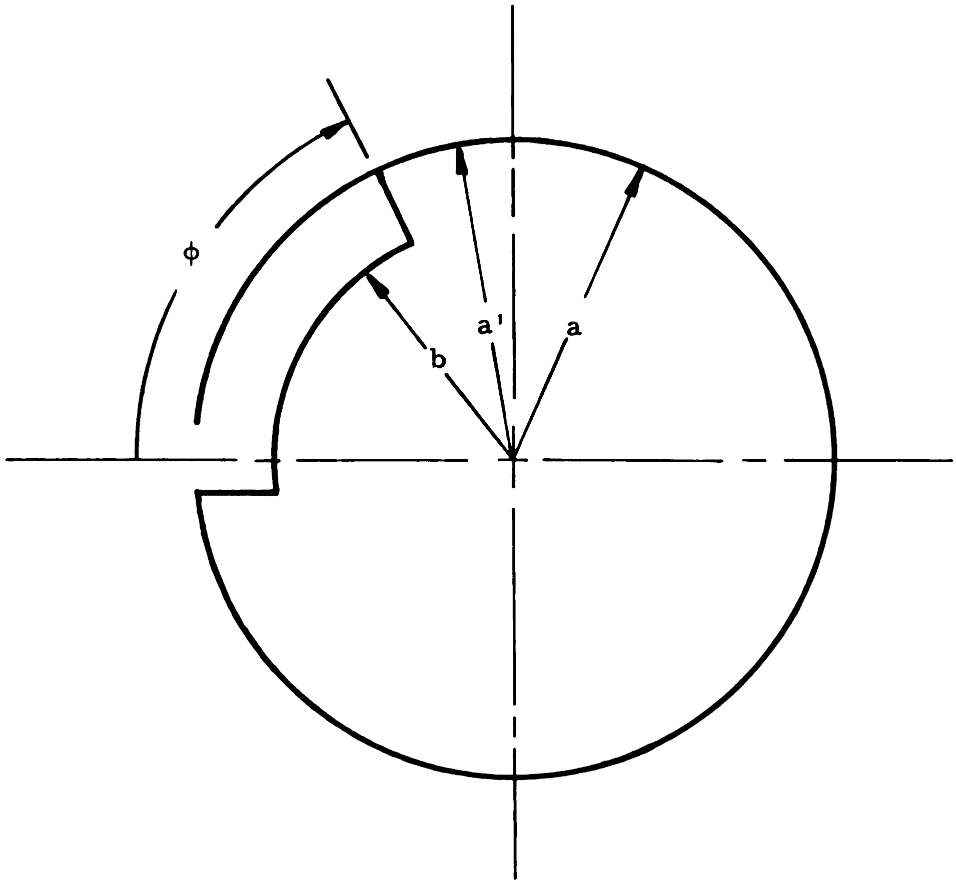


(a)

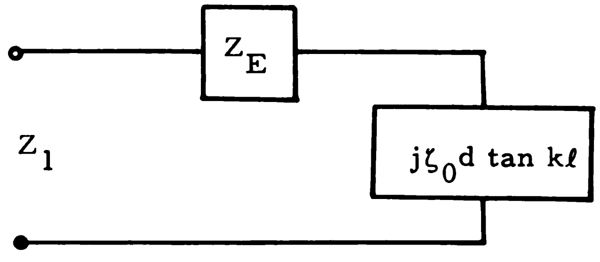


(b)

Figure 5. 3. Cylinder with curved parallel plane line short circuited at $\phi$. (a) Cross-section view. (b) Equivalent circuit for cavity load.

Figure 5.4 compares theoretical and experimental results of backscattering as a function of the angular length of the cavity. The experimental points are obtained by setting $\theta_1 = 180°$ and observing the backscattering while varying the position of the short, $\phi$. The theoretical calculations involve first calculating the slot impedance for a given $\phi$ using the above expression, then calculating the backscattering cross section from Equation (31). The lumped end effect reactance $X_E$ was obtained by matching the position of the first minimum point of the theoretical and experimental results which required a 12 degree shift. This corresponds to an inductive reactance of 0.427 ohm meters. The agreement between the theoretical and experimental results is again excellent. This indicates that not only is the theory valid, but the approximate model for the curved parallel plane line is reasonable.

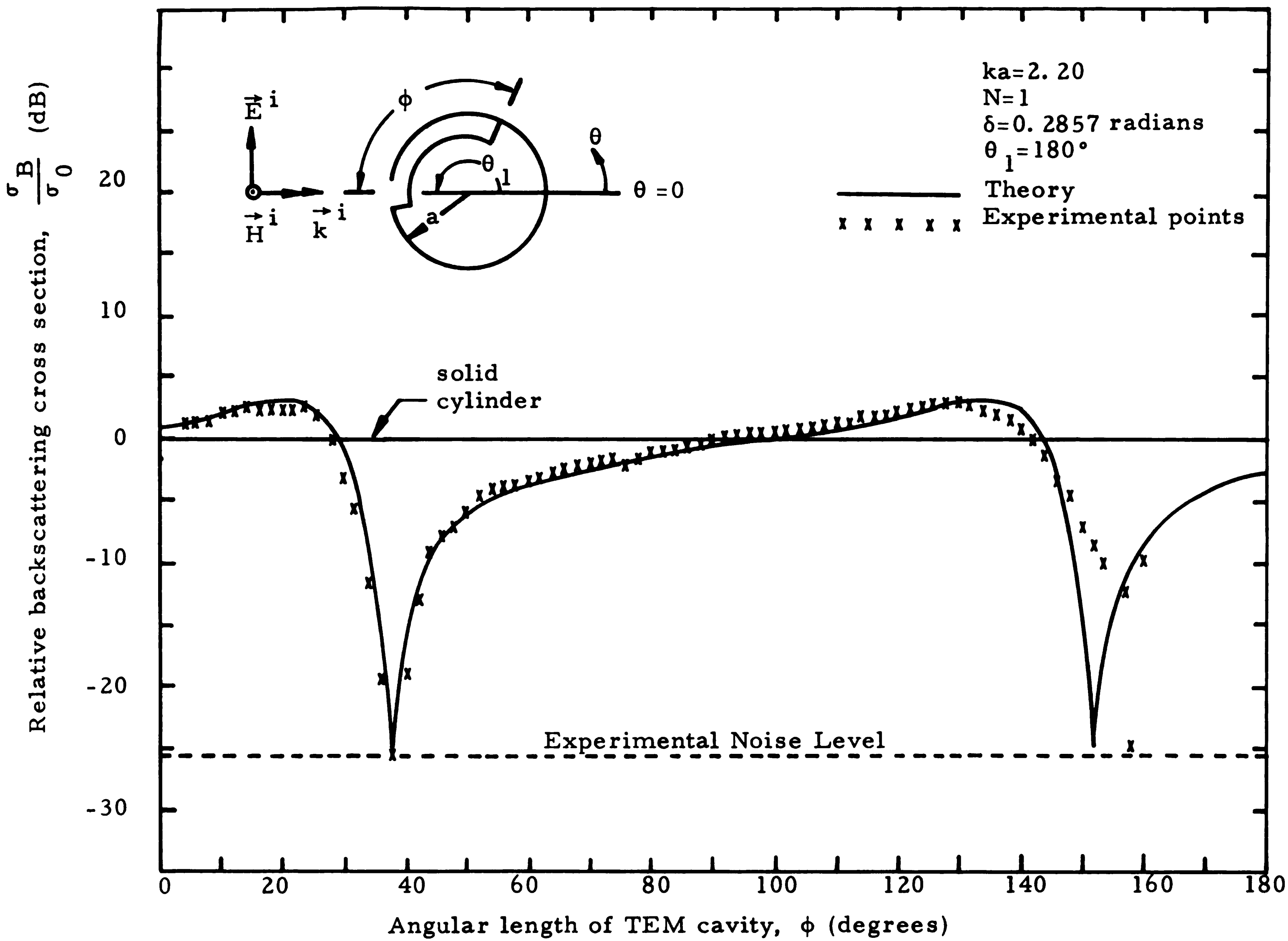


Figure 5.4. Relative backscattering cross section as a function of the length of TEM cavity backing slot.

# CHAPTER VI

# CONCLUSIONS

In the preceding chapters the scattering behavior of a conducting cylinder loaded with N impedance backed longitudinal slots and illuminated with a normally incident plane electromagnetic wave polarized with its $\vec{E}$-field vector perpendicular to the cylinder axis has been considered. The slots were assumed to be electrically narrow but finite and with constant electric fields across them. Under this assumption the analysis was exact.

It has been shown that the field scattered by a cylinder loaded with N slots can be:

1. reduced to zero in N directions when the load impedances are complex and can take on all positive and negative values,
2. reduced to zero in N/2 directions when the loading impedances are purely reactive,
3. reduced to zero in one direction at N different frequencies.

Synthesis procedures have been developed for finding load impedances that produce the above results. For Case (1) the procedure is straightforward, involving only the solution of a system of linear algebraic equations. On the other hand, the constraint equations involved in the procedures for Cases (2) and (3) are nonlinear. This complicates the procedures, and in fact, solutions to these equations do not always exist.

It was found the position of the slots on the cylinder surface is a critical factor in whether or not solutions exist to the last two procedures. The case of a cylinder loaded with two purely reactive slots has been numerically examined in detail. A set of slot positions has been found such that solutions exist for zero backscattering over the entire range of cylinder size considered (i. e., $1 \leq ka \leq 13$). These numerical results seem to indicate that the best positions for the slots are in the center of the illuminated region of the cylinder. For these slot positions, purely reactive loadings which significantly reduce the scattered field in the desired directions can usually be found even when no solution exists for zero scattering in these directions.

The positions of the slots were also found to be important factors in determining the form of the bistatic scattering cross section patterns and null widths for all types of loading impedances. Two different slot configurations having the same number of slots and both being constrained to have zero scattering in the same directions, may have grossly different bistatic scattering patterns and null widths.

The frequency dependence of the fields scattered by the loaded cylinders was considered for three types of load impedances.

1. a short-circuited TEM line.
2. a short-circuited TEM line in series with a constant resistance.
3. a constant impedance (i. e., constant with respect to frequency).

Considerably wider bandwidths are, in general, obtained with load impedances which have resistive parts rather than purely reactive load impedances. Bandwidths of nearly 1:1 are demonstrated.

An experiment has been performed which confirms the theory.

The basic advantage of multiple impedance loading, over loading by a single impedance, is that it gives additional degrees of freedom which can be used to control the scattering of an object over both space and frequency domains.

# APPENDIX A

## DERIVATION OF FOURIER COEFFICIENTS

In this appendix the Fourier Coefficients (17) and (18) for the problem of radiation from a cylinder with N driven slots are derived.

The z component of the $\vec{H}^r$-field is given in terms of the unknown coefficients $A_n$ and $B_n$.

$$H_z^r = \sum_{n=0}^{\infty} [A_n \cos(n\theta) + B_n \sin(n\theta)] \, H_n^{(2)'}(kr) \tag{16}$$

The coefficients are determined from the boundary condition at the cylinder surface

$$E_\theta^r (r=a^+) = \begin{cases} \dfrac{V_m}{a\delta_m} & \text{for } |\theta - \theta_m| < \dfrac{\delta_m}{2} \\ & m = 1, 2, \ldots, N \\ 0 & \text{elsewhere} \end{cases} \tag{6}$$

The $E_\theta^r$ component of the field can be determined from Equation (16) by using Maxwell's equation for a source free region

$$\nabla X \vec{H}^r = j\omega\epsilon \, \vec{E}^r$$

This gives

$$E_\theta^r = \frac{j}{\omega\epsilon_0} \frac{\partial}{\partial r} H_z^r$$

$$= j\,\zeta_0 \sum_{n=0}^{\infty} [A_n \cos(n\theta) + B_n \sin(n\theta)] \, H_n^{(2)'}(kr) \tag{A-1}$$

where the prime denotes a derivative with respect to kr.

Using (A-1), boundary condition (6) can be expressed in terms of the unknown Fourier coefficients

$$E_\theta^r(r=a^+) = j\zeta_0 \sum_{n=0}^{\infty} [A_n \cos(n\theta) + B_n \sin(n\theta)]\, H_n^{(2)'}(ka)$$

$$= \begin{cases} \dfrac{V_m}{a\delta_m} & \text{for } |\theta - \theta_m| < \dfrac{\delta_m}{2} \\ & m=1, 2, \ldots, N \\ 0 & \text{elsewhere} \end{cases} \qquad \text{(A-2)}$$

The coefficient $A_n$ can be found by multiplying (A-2) by cos ($p\theta$), integrating with respect to $\theta$ over the domain $[-\pi, \pi]$, and using the orthogonality property of the sine and cosine functions. For the case $n \neq 0$ this gives

$$j\zeta_0 A_n H_n^{(2)'}(ka)\,\pi = \sum_{m=1}^{N} \int_{\theta_m-\delta_m/2}^{\theta_m+\delta_m/2} \frac{V_m}{a\delta_m} \cos(n\theta)\, d\theta$$

$$= \frac{2}{a} \sum_{m=1}^{N} V_m \frac{\sin\left(\frac{n\delta_m}{2}\right)}{\left(\frac{n\delta_m}{2}\right)} \cos(n\theta_m)$$

so

$$A_n = \frac{2}{j2\pi a\zeta_0} \frac{1}{H_n^{(2)'}(ka)} \sum_{m=1}^{N} V_m \frac{\sin\left(\frac{n\delta_m}{2}\right)}{\left(\frac{n\delta_m}{2}\right)} \cos(n\theta_m)\,. \qquad \text{(A-3)}$$

For the case n=0

$$j\zeta_0 A_0 H_0^{(2)'}(ka)\, 2\pi = \sum_{m=1}^{N} \int_{\theta_m-\delta_m/2}^{\theta_m+\delta_m/2} \frac{V_m}{a\delta_m}\, d\theta$$

$$= \frac{1}{a} \sum_{m=1}^{N} V_m$$

so

$$A_0 = \frac{1}{j2\pi a\zeta_0} \frac{1}{H_n^{(2)'}(ka)} \sum_{m=1}^{N} V_m \tag{A-4}$$

with the Neumann factor

$$\epsilon_{0n} = \begin{cases} 1 & \text{for } n=0 \\ 2 & \text{otherwise,} \end{cases}$$

Equations (A-3) and (A-4) can be combined into the final expression for the coefficient

$$A_n = \frac{\epsilon_{0n}}{j2\pi a\zeta_0} \frac{1}{H_n^{(2)'}(ka)} \sum_{m=1}^{N} V_m \frac{\sin\left(\frac{n\delta_m}{2}\right)}{\left(\frac{n\delta_m}{2}\right)} \cos(n\theta_m) \tag{17}$$

Similarly coefficient $B_n$ is also found from Equation (A-2) by multiplying it by $\sin(p\theta)$ and integrating over the same domain. The result of this derivation is Equation (18).

## APPENDIX B

## PURELY REACTIVE IMPEDANCE LOADS FOR ZERO SCATTERING IN ONE DIRECTION FROM A TWO-SLOT CYLINDER

In this appendix an equation is derived whose solutions are the purely reactive load impedances that cause the field scattered from a cylinder loaded with these loads to be zero in a direction $\theta_0$. The constraint equation that forces the scattered field to be zero in the direction $\theta_0$ is [See Equation (38)]

$$C_{11}(\theta_0)\, V_1 + C_{12}(\theta_0)\, V_2 + C_{10}(\theta_0) = 0 \tag{B-1}$$

Instead of using the nonlinear constraint Equation (37) to force the load impedances to be purely reactive, a different procedure will be used which directly determines an equation for the load reactances. It can be shown that both procedures yield identical results.

Matrix Equation (26) for the case N=2 is

$$\begin{bmatrix} y_{11} + Y_1 & y_{12} \\ y_{21} & y_{22} + Y_2 \end{bmatrix} \begin{bmatrix} V_1 \\ V_2 \end{bmatrix} = \begin{bmatrix} K_{10} \\ K_{20} \end{bmatrix} . \tag{B-2}$$

Equation (B-2) may be used to eliminate the slot voltages from Equation (B-1). This results in a constraint equation which directly involves the load admittances.

$$AY_1 + BY_1Y_2 + CY_2 + D = 0 \tag{B-3}$$

where

$$A = C_{10}y_{22} + C_{12}K_{20}$$

$$B = C_{10}$$

$$C = C_{10}y_{11} + C_{11}K_{10}$$

$$D = \begin{vmatrix} C_{11} & C_{12} & C_{10} \\ y_{11} & y_{12} & -K_{10} \\ y_{21} & y_{22} & -K_{20} \end{vmatrix}$$

The real part of the load admittances are now set equal to zero so that

$$Y_1 = j\beta_1$$

$$Y_2 = j\beta_2$$

where $\beta_1$ and $\beta_2$ are the load susceptances. This step is equivalent to enforcing constraint Equation (37). The complex coefficients of Equation (B-3) are written

$$A = A_r + jA_i$$

$$B = B_r + jB_i$$

$$C = C_r + jC_i$$

$$D = D_r + jD_i$$

where the subscripts r and i refer to the real and imaginary parts of the coefficients, respectively.

With these definitions, complex constraint Equation (B-3) can be separated into real and imaginary parts. This results in two real equations

$$-A_i\beta_1 - B_r\beta_1\beta_2 - C_i\beta_2 + D_r = 0 \tag{B-4}$$

$$A_r\beta_1 - B_i\beta_1\beta_2 + C_r\beta_2 + D_i = 0 \tag{B-5}$$

Solving these equations for $\beta_1$ and $\beta_2$ gives

$$\beta_1 = \frac{D_r - C_i \beta_2}{A_i + B_r \beta_2} \tag{B-6}$$

and

$$\beta_2 = \frac{-G \pm \sqrt{G^2 - 4F(A_r D_r + A_i D_i)}}{2F} \tag{B-7}$$

where

$$F = B_r C_r + B_i C_i$$

$$G = A_i C_r - A_r C_i + B_r D_i - B_i D_r$$

The solutions to Equation (B-6) and (B-7) are the susceptances that give zero scattering in directions $\theta = \theta_0$. There are two possible sets of susceptances to achieve the same purpose. The purely reactive load impedances that result in zero scattering in direction $\theta = \theta_0$ are $Z_1 = -j/\beta_1$ and $Z_2 = -j/\beta_2$.

Equations (B-6) and (B-7) have suitable form for programming on a digital computer.

# APPENDIX C

## ZERO SCATTERING IN ONE DIRECTION AT TWO DIFFERENT FREQUENCIES

In this appendix an equation is derived whose solutions are load impedances which result in zero scattering in one direction $\theta = \theta_0$ at two different frequencies, $\omega_1$ and $\omega_2$. Equation (41) for the case N=2 gives

$$\begin{vmatrix} y_{11} + Y_1 & y_{12} & -K_{10} \\ y_{21} & y_{22} + Y_2 & -K_{20} \\ C_{11} & C_{12} & C_{10} \end{vmatrix}_{\substack{\omega = \omega_1 \\ \theta = \theta_0}} = 0$$

$$\begin{vmatrix} y_{11} + Y_1 & y_{12} & -K_{10} \\ y_{21} & y_{22} + Y_2 & -K_{20} \\ C_{21} & C_{22} & C_{20} \end{vmatrix}_{\substack{\omega = \omega_2 \\ \theta = \theta_0}} = 0$$

Evaluating these determinants leads to

$$A_1 Y_1 + B_1 Y_1 Y_2 + C_1 Y_2 + D_1 = 0 \qquad \text{(C-1)}$$

$$A_2 Y_1 + B_2 Y_1 Y_2 + C_2 Y_2 + D_2 = 0 \qquad \text{(C-2)}$$

where

$$A_1 = [C_{10} y_{22} + C_{12} K_{20}]_{\substack{\omega = \omega_1 \\ \theta = \theta_0}}$$

$$B_1 = C_{10}(\omega = \omega_1, \ \theta = \theta_0)$$

$$C_1 = [C_{10}y_{11} + C_{11}K_{10}]_{\substack{\omega = \omega_1 \\ \theta = \theta_0}}$$

$$D_1 = \begin{vmatrix} C_{11} & C_{12} & C_{10} \\ y_{11} & y_{12} & -K_{10} \\ y_{21} & y_{22} & -K_{20} \end{vmatrix}_{\substack{\omega = \omega_1 \\ \theta = \theta_0}}$$

$$A_2 = [C_{20}y_{22} + C_{22}K_{20}]_{\substack{\omega = \omega_2 \\ \theta = \theta_0}}$$

$$B_2 = C_{20}(\omega = \omega_2, \ \theta = \theta_0)$$

$$C_2 = [C_{20}y_{11} + C_{21}K_{10}]_{\substack{\omega = \omega_2 \\ \theta = \theta_0}}$$

$$D_2 = \begin{vmatrix} C_{21} & C_{22} & C_{20} \\ y_{11} & y_{12} & -K_{10} \\ y_{21} & y_{22} & -K_{20} \end{vmatrix}_{\substack{\omega = \omega_2 \\ \theta = \theta_0}}$$

Equations (C-1) and (C-2) are easily manipulated into the form

$$Y_1 + LY_2 + M = 0 \tag{C-3}$$

$$Y_2^2 + NY_2 + P = 0 \tag{C-4}$$

where

$$L = \frac{C_1B_2 - C_2B_1}{A_1B_2 - A_2B_1}$$

$$M = \frac{D_1B_2 - D_2B_1}{A_1B_2 - A_2B_1}$$

$$N = \frac{A_2L + B_2M - C_2}{B_2L}$$

$$P = \frac{A_2M - D}{B_2L} \quad .$$

Define

$$Y_1 = G_1 + j\beta_1$$

$$Y_2 = G_2 + j\beta_2$$

and

$$L = L_r + jL_i$$

$$M = M_r + jM_i$$

$$N = N_r + jN_i$$

$$P = P_r + jP_i$$

where the subscripts r and i refer to the real and imaginary parts of the coefficients, respectively. Separating Equations (C-3) and (C-4) into real and imaginary parts and performing some alegebra these equations become

$$G_1 = -L_rG_z + L_i\beta_2 - M_r \qquad \text{(C-5)}$$

$$\beta_1 = -L_r\beta_2 - L_iG_2 - M_i$$

$$G_2 = \left(\frac{P_i - N_r\beta_2}{N_i + 2\beta_2}\right) \qquad \text{(C-7)}$$

$$\beta_2^4 + 2N_i\beta_2^3 + \left(\frac{5N_i^2}{4} - \frac{N_r^2}{2} - P_r\right)\beta_2^2 + \left(\frac{N_i^3}{4} - N_iP_r + \frac{N_r^2N_i}{4}\right)\beta_2$$

$$+ \left(\frac{N_rN_iP_i}{4} - \frac{P_i^2}{4} - \frac{N_i^2P_r}{4}\right) = 0 \qquad \text{(C-8)}$$

Equation (C-8) is a quartic equation which may have real or complex roots. The only roots that are solutions to this problem are the real roots. Substituting the real roots of Equation (C-8) into Equations (C-5), (C-6), and (C-7) gives admittances

$$Y_1 = G_1 + j\beta_1$$

$$Y_2 = G_2 + j\beta_2$$

which result in zero scattering in direction $\theta = \theta_0$ at frequencies $\omega = \omega_1$, and $\omega = \omega_2$.

## REFERENCES


1. J. K. Schindler, R. B. Mack, and P. Blacksmith, Jr., "The control of electromagnetic scattering by impedance loading," Proc. IEEE, 53, 993-1004 (August 1965).

2. K. M. Chen, "Minimization of backscattering of a cylinder by double loading," IEEE Trans. Ant. Prop., AP-13, 262-270 (March 1965).

3. K. M. Chen, "Reactive loading of arbitarily illuminated cylinders to minimize microwave backscattering," Radio Sci., 690, 1481 (1965).

4. R. F. Harrington and J. L. Ryerson, "Electromagnetic scattering by loaded wire loops," Radio Sci., 1, 347-352 (March, 1966).

5. K. M. Chen, "Minimization of end-fire radar echo of a long thin body by impedance loading," IEEE Trans. Ant. Prop., AP-14, 318-323 (May 1966).

6. K. M. Chen and M. Vincent, "A new method of minimizing the radar cross section of a sphere," Proc. IEEE, 54, 1629-1630 (November 1966).

7. K. M. Chen, J. L. Lin, and M. Vincent, "Minimization of backscattering of a metallic loop by impedance loading," IEEE Trans. Ant. Prop., AP-15, 492-494 (May 1967).

8. M. Vincent and K. M. Chen, "A new method of minimizing the backscattering of a conducting plate," Proc. IEEE, 55, 1109-1111 (June 1967).

9. J. L. Lin and K. M. Chen, "Minimization of backscattering of a loop by impedance loading - theory and experiment," IEEE Trans. Ant. Prop., AP-16, 299-304 (May 1968).

10. M. C. Vincent and K. M. Chen, "Modification of backscattering of a sphere by attaching loaded wires," IEEE Trans. Ant. Prop., AP-16, 462-468 (July 1968).

11. C. L. Chen, "Modification of the backscattering cross-section of a long metal wire by impedance loading," IEEE 1968 G-AP International Symposium

12. J. E. Clark and J. L. Tauritz, "Cross section control of a thin wire loop by impedance loading techniques," IEEE Trans. Ant. Prop., AP-17, 106-107 (January 1969).

13. D.P. Nyquist, J.R. Short, and K.M. Chen, "Broad-band reduction of backscattering from a thin cylinder," IEEE Trans. Ant. Prop., AP-17, 248-250 (March 1969).

14. O.D. Sledge, "Scattering of a plane electromagnetic wave by a linear array of cylindrical elements," IEEE Trans. Ant. Prop., AP-17, 169-175 (March 1969).

15. J.R. Short and K.M. Chen, "Backscattering from an impedance loaded cylinder," IEEE Trans. Ant. Prop., AP-17, 315-323 (May 1969).

16. R.J. Coe and A. Ishimaru, "Optimum scattering from an array of half-wave dipoles," IEEE Trans. Ant. Prop., AP-18, (March 1970).

17. J.L. Tauritz, "A useful graphical representation in the theory of loaded scatterers," IEEE Trans. Ant. Prop. AP-18, 826-829 (November 1970).

18. V.V. Liepa and T.B.A. Senior, "Modification of the scattering behavior of a sphere by reactive loading," Proc. IEEE, 53, 1004-1011 (August 1965).

19. R.F. Harrington, "Theory of loaded scatters," Proc. IEE (London), III, 617-623 (April 1964).

20. R.F. Harrington, Field Computation By Moment Methods (Macmillan, New York, 1968), Ch. 6.

21. B.J. Strait and K. Hirasawa, "Array design for specified pattern by matrix methods," IEEE Trans. Ant. Prop., AP-17, 237-239 (March 1969).

22. B.J. Strait and A.T. Adams, "Analysis and design of wire antennas with applications to EMC," IEEE Trans. Electromag. Compatibility, EMC-12, 45-54 (May 1970).

23. B.J. Strait and K. Hirasawa, "On long wire antennas with multiple excitations and loading," IEEE Trans. Ant. Prop., AP-18, 699-700 (September 1970).

24. J.A. Stratton, Electromagnetic Theory (McGraw-Hill, New York, 1941), 371-372.

25. R.W.P. King and T.T. Wu, The Scattering and Diffraction of Waves (Harvard University Press, Cambridge, Mass., 1959), Chapter 2.

26. J.J. Bowman, T.B.A. Senior, and P.L.E. Uslenghi, Electromagnetic and Acoustic Scattering by Simple Shapes (North-Holland Publishing Co., Amsterdam, 1969), 103-111.

27. M. Abramowitz and I.A. Stegun, Handbook of Mathematical Functions (Dover, New York, 1965) 364, eq. (9.2.4).

28. M. Abramowitz and I. A. Stegun, Handbook of Mathematical Functions (Dover, New York, 1965), 365, eq. (9. 3. 1).

29. C. H. Papas and R. W. P. King, "Currents on the surface of an infinite cylinder excited by an axial slot," Quart. Appl. Math., 7, 175-182 (July 1949).

30. G. Sinclair, "The patterns of slotted-cylinder antennas," Proc. IRE, 36, 1487-1492 (December 1948).

31. E. L. McMahon, "Circuit realization of impedance loading for cross section reduction," Scientific Report No. 8, AFCRL-70-0514, Air Force Cambridge Research Laboratories, Laurence G. Hanscom Field, Bedofrd, Mass., (September 1970).

32. C. G. Montgomery, R, H. Dicke, and E. M. Purcell, Principles of Microwave Circuits (Dover, New York, 1965), 97.

33. S. Ramo, J. R. Whinnery, and T. Van Duzer, Fields and Waves in Communication Electronics (Wiley, New York, 1965), 33, 375-377.

34. P. Blacksmith, Jr., R. E. Hiatt, and R. B. Mack, "Introduction to radar cross-section measurement," Proc. IEEE, 53, 901-920 (August 1965).

# PART II

# MODIFICATION OF RADIATION FIELDS AND CIRCUIT PROPERTIES OF A LOOP ANTENNA BY MULTI-IMPEDANCE LOADING

# CHAPTER I

# INTRODUCTION

The modification of the radiation and circuit properties of a circular wire loop antenna by lumped impedance loading is investigated in this study.

When a wire antenna is excited, a current is induced on the antenna. This current radiates an electromagnetic field and determines the input impedance of the antenna. Lumped impedances can be installed along the antenna to modify the magnitude and phase of the antenna current which, in turn, modifies the antenna radiation and input impedance. The modified current can assume quite an irregular distribution and hence a fairly accurate theory must be developed.

The problem of determining the current distribution on a circular loop antenna can be formulated in terms of two coupled integral equations.[1] These equations reduce to a single one dimensional integral equation after the "thin wire" approximation is introduced. Fourier series solutions to the thin wire integral equation have been studied by Hallen[2], Storer[3], and Wu[1]. An iterative solution has been considered by Adachi and Mushiake[4, 5]. The theory formulated in this study is based on the work of Hallen, Storer, and Wu.

A point exists in Hallen's series where the terms become very large and for some antenna dimensions infinite. Hallen concluded that the series was divergent and could only be used as an asymptotic series. He suggested that the problem arose from the one dimensional approximation. Storer extended Hallen's result by summing the first five terms of Hallen's series exactly and using an approximate integral technique to sum the remaining terms. The troublesome point in Hallen's series now occurred under an integral which Storer evaluated as a Cauchy principle value. Wu questioned Storer's technique and re-examined Hallen's solution. He pointed out that Hallen's difficulty did not arise from the one dimensional integral equation, but arose from other approximations made. Wu used a less approximate Kernel and modified Hallen's solution eliminating the troublesome point.

All of the above authors assumed a $\delta$-function (or slice) voltage generator in their model of the loop antenna. This leads to an infinite input susceptance and thus a divergent series for the input admittance of the antenna. Wu[1] suggested a possible procedure for calculating the apparent input admittance of a half loop antenna above a conducting ground plane driven by a coaxial line, but unsolved problems still exist in applying this procedure to the loop antenna.

King, Harrison and Tingley[6, 7] have calculated values for the input admittance of, and current distribution on, moderate size loop antennas using Wu's theory. They retain twenty terms in Wu's series. The number of terms retained in the divergent series for the loop susceptance appears to be somewhat arbitrary. For example, the susceptance of a thin loop one half wave length in circumference increases by more than 20% when thirty terms rather than twenty are retained. In this study further reference to this theory will be made as the twenty term theory.

An alternate approach to modeling the voltage driver is taken in this study. The generator is assumed to be of finite size and to exist over a finite gap along the loop. This leads to a convergent series for the admittance of the loop and the number of terms retained in the series is determined by the desired accuracy of the solution. A discussion and justification of the "finite gap" theory is given in Chapter III of this study. It is shown that by introducing the finite gap into the theory, the agreement between the theory and experimental results is improved. Very recently, Ito, Inagaki, and Sekiguchi[8] published a paper on arrays of loop antennas where they also introduced a finite gap generator.

Multiloaded loop antennas have been investigated by Iizuka[9, 10] and Harrington[11]. Iizuka developed his theory by the superposition of Storer's results and found a significant discrepancy between his theory and his measured admittances. Harrington based his results essentially on Hallen's series and did not include Wu's correction. He did not compare his theoretical results with any experimental results. Both authors developed their theories for more than one loading, but restricted their results and discussions to singly loaded loops. Furthermore, most of the existing results are confined to resonant loops of one wave length in circumference.

When a loop is loaded by more than one load the number of variables (i. e., load resistances, load reactances, position of the loads, etc.) becomes overwhelming. To overcome this problem, synthesis procedures are developed in this study to facilitate the design of a multiple-loaded loop antenna.

The major purposes of this study are (1) to develop an improved theory for the loaded loop antenna, and (2) to develop and analyze procedures for the design of a multiple loaded loop antenna that results in desired radiation or circuit characteristics.

In Chapter II an integral equation for the multi-loaded loop excited by a finite gap generator is developed and a Fourier series solution is obtained.

Numerical methods used in evaluating the theory results are discussed in Chapter III. In addition, a comparison of the "finite gap" theory to other existing theories and experimental results is made. A brief discussion of the characteristics of unloaded loop antennas is also presented. Since the "finite gap" theory is more applicable to larger loops than Storer's theory or the twenty term theory, some examples of impedances, currents, and radiation fields of large loop antennas are also presented.

Chapter IV deals with procedures for determining (1) the loadings necessary for a specific modification of the radiation pattern of a loop antenna, (2) the optimum reactive loading to produce maximum gain in a specified direction from a loop loaded with a single impedance, and (3) the set of reactive loadings that leads to a specified input impedance.

Chapter V summarizes the results obtained in this study.

# CHAPTER II

## THEORY OF THE LOADED LOOP ANTENNA

### 2.1. An Integral Equation for the Current on the Loaded Loop Antenna

A transmitting circular loop antenna of radius b and constructed of perfectly conducting wire of radius a is loaded with N impedances as shown in Figure 2.1. The loop is excited by a finite-gap, voltage generator which produces a uniform, impressed electric field in the gap region $|\phi| < \delta_o/2$. The $n^{th}$ load impedance $Z_n$ is lumped into a gap region of angular width $\delta_n$ whose center is located at $\phi = \phi_n$. There are two components of surface current density induced on the loop, $K_\phi(\phi, \psi)$ flowing around the loop in the $\phi$ direction and $K_\psi(\phi, \psi)$ flowing about the wire in the $\psi$ direction. Integral equations for the currents on the loop can be obtained from the boundary condition on the tangential component of the electric field at the loop surface.

The problem is greatly simplified by assuming a thin wire loop whose gap generator and load impedances are restricted to regions small with respect to a wave length, that is

$$a^2 \ll b^2 \qquad \text{and} \qquad ka \ll 1 \tag{1}$$

and

$$\delta_n b \ll \lambda \qquad \text{for all n.} \tag{2}$$

where $k = \omega\sqrt{\mu_o \epsilon_o} = 2\pi/\lambda$ is the propagation constant. Harmonic time dependence of the form $e^{j\omega t}$ is assumed.

Under the thin wire assumption, the $\psi$ component of surface current will be small in comparison to the $\phi$ component of surface current and can be neglected. It is also reasonable to assume the total current flowing in the loop is

$$I_\phi(\phi) = 2\pi a\, K_\phi(\phi) .$$

The integral equation for $I_\phi(\phi)$ can be derived from the boundary condition on the $\phi$ component of the electric field at the loop surface which is

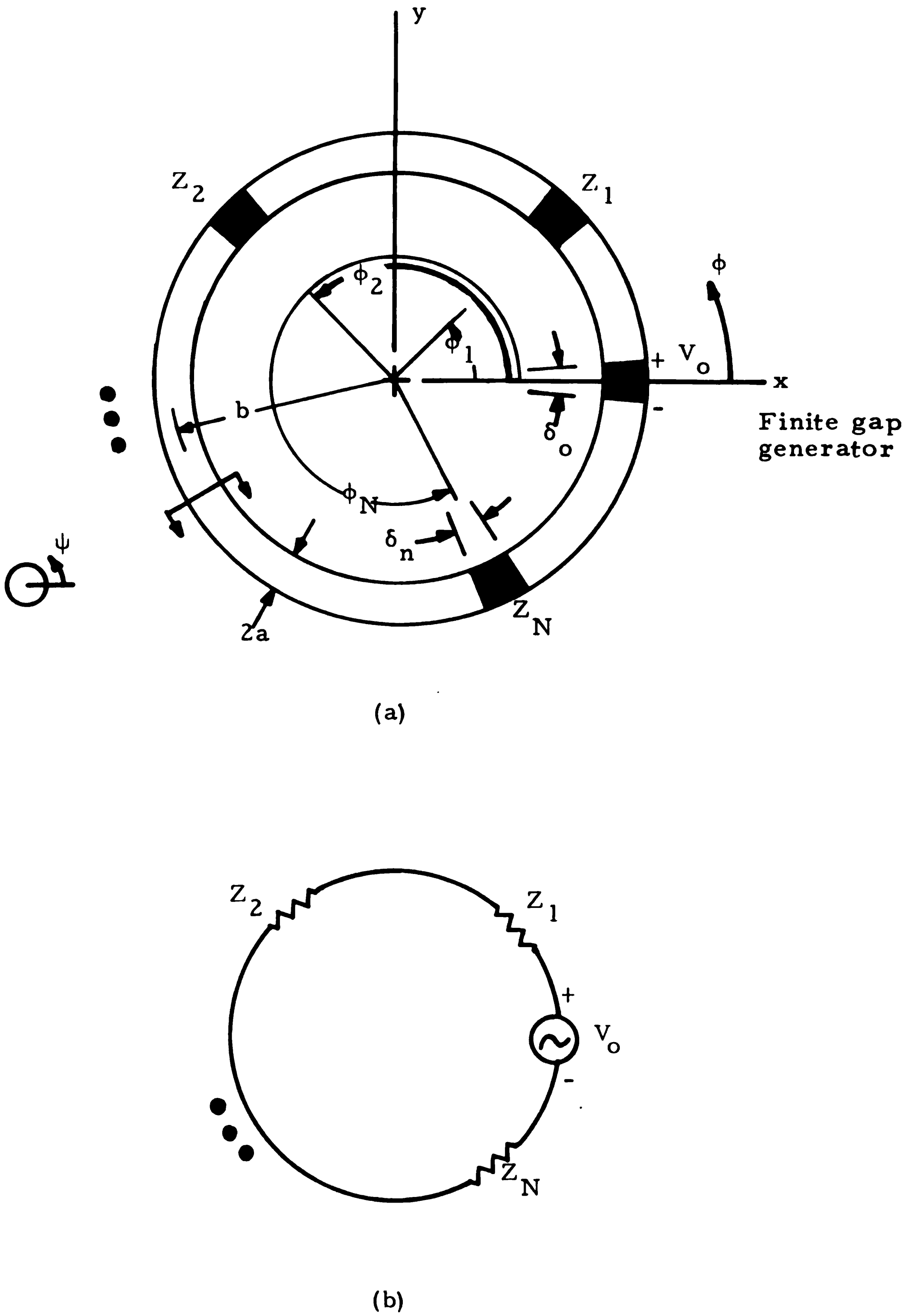


Figure 2.1. Loop antenna loaded with N impedances: (a) Geometry, (b) Schematic.

$$[E_\phi^i - E_\phi^a] = 0 \qquad \text{--- at the surface of the loop} \tag{3}$$

where $E_\phi^i$ is the impressed electric field at the surface of the loop and $E_\phi^a$ is the induced electric field at the surface of the loop maintained by the current and charge on the antenna.

The impressed field is

$$E_\phi^i = \begin{cases} -V_o\, P_o(\phi) & \text{--- for } |\phi| < \delta_o/2 \\ I_\phi(\phi_m)\, Z_m\, P_m(\phi - \phi_m) & \text{--- for } |\phi-\phi_m| < \delta_m/2 \\ & \quad m = 1, 2, \ldots, N^m \\ 0 & \text{--- elsewhere on the loop} \end{cases} \tag{4}$$

where

$$P_n(\phi) = \begin{cases} \dfrac{1}{\delta_n b} & \text{--- for } |\phi| < \delta_n/2 \\ 0 & \text{--- elsewhere} \end{cases} \tag{5}$$

is a unit area pulse function. The distance from the center of the loop to the observation point of the field on the loop surface has been taken to be b everywhere which is consistent with the thin wire assumption.

The induced field is

$$E_\phi^a = -\frac{1}{b}\frac{\partial \Phi}{\partial \phi} - j\omega A_\phi \tag{6}$$

where

$$\Phi(\vec{r}) = \frac{1}{4\pi\epsilon_o} \int_V \rho(\vec{r}\,')\, \frac{e^{-jkR}}{R}\, dV'$$

and

$$A_\phi(\vec{r}) = \frac{\mu_o}{4\pi} \int_V \hat{\phi} \cdot \vec{J}(\vec{r}\,')\, \frac{e^{-jkR}}{R}\, dV'$$

are the scalar potential and the $\phi$ component of the vector potential, respectively. $\rho(\vec{r}\,')$ and $\vec{J}(\vec{r}\,')$ are volume charge and current densities and $R = |\vec{r} - \vec{r}\,'|$ is the distance between the source point $\vec{r}\,'$ and field observation point $\vec{r}$. For the loop

$$\vec{J}(\vec{r}\,')\, dV' \rightarrow \hat{\phi}'\, \frac{I_\phi(\phi')}{2\pi a}\, a d\psi'\, b d\phi'$$

$$\rho(\vec{r}\,')\,dV' \rightarrow \frac{q(\phi')}{2\pi a}\, a d\psi'\; b d\phi'$$

where $q(\phi')$ is the total charge per unit length on the loop and is related to the total current on the loop by the continuity equation

$$\frac{1}{b}\frac{\partial I_\phi(\phi')}{\partial \phi'} = -j\omega q(\phi') .$$

The potentials maintained by the current and charge on the loop are now

$$\Phi(\phi) = -\frac{1}{j\omega\, 4\pi\epsilon_o b}\int_{-\pi}^{\pi}\frac{\partial I_\phi(\phi')}{\partial\phi'}\, W(\phi-\phi')\, d\phi' \tag{7}$$

$$A_\phi(\phi) = \frac{\mu_o}{4\pi}\int_{-\pi}^{\pi} I_\phi(\phi')\, W(\phi-\phi')\cos(\phi-\phi')\, d\phi' \tag{8}$$

where

$$W(\phi-\phi') = \frac{b}{2\pi}\int_{-\pi}^{\pi}\frac{e^{-jkR}}{R}\, d\psi' . \tag{9}$$

Substituting equations (7) and (8) into equation (6) yields

$$E_\phi^a(\phi) = \frac{1}{j\omega 4\pi\epsilon_o b^2}\frac{\partial}{\partial\phi}\int_{-\pi}^{\pi}\frac{\partial I_\phi(\phi')}{\partial\phi'}\, W(\phi-\phi')\, d\phi'$$
$$-\frac{j\omega\mu_o}{4\pi}\int_{-\pi}^{\pi} I_\phi(\phi')\, W(\phi-\phi')\cos(\phi-\phi')\, d\phi' .$$

Integrating the first integral in the above expression by parts and noting that $\frac{\partial}{\partial\phi'} W(\phi-\phi') = -\frac{\partial}{\partial\phi} W(\phi-\phi')$ gives

$$E_\phi^a(\phi) = -\frac{j\zeta_o}{4\pi b}\int_{-\pi}^{\pi} I_\phi(\phi')\left[\frac{1}{kb}\frac{\partial^2}{\partial\phi^2} + kb\cos(\phi-\phi')\right] W(\phi-\phi')\, d\phi' \tag{10}$$

where $\zeta_o = \sqrt{\mu_o/\epsilon_o}$ is the intrinsic impedance of the medium. Substituting equations (4) and (10) into equation (3) results in the following integral equation for the current on the loaded loop antenna.

$$V_o P_o(\phi) = \sum_{m=1}^{N} I_\phi(\phi_m)\, Z_m P_m(\phi-\phi_m) + \frac{j\zeta_o}{4\pi b}\int_{-\pi}^{\pi} I_\phi(\phi')\, M(\phi-\phi')\, d\phi' \tag{11}$$

The kernel is now

$$M(\phi - \phi') = \left[ kb \cos(\phi - \phi') + \frac{1}{kb} \frac{\partial^2}{\partial \phi^2} \right] W(\phi - \phi') \tag{12}$$

where

$$W(\phi - \phi') = \frac{1}{2\pi} \int_{-\pi}^{\pi} \frac{e^{-jkbR_1}}{R_1} d\psi' \tag{13}$$

with

$$\begin{aligned} R_1 &= R/b \\ &\doteq \frac{\sqrt{4b^2 \sin^2[(\phi-\phi')/2] + 4a^2 \sin^2(\psi'/2)}}{b} \\ &= \sqrt{4 \sin^2[(\phi-\phi')/2] + A^2/b^2} \end{aligned} \tag{14}$$

where

$$A = 2a \sin(\psi'/2) .$$

The approximate expression for R given above is consistent with the thin wire assumption and retains the essential characteristic of the singularity in the integrand of $W(\phi - \phi')$.

## 2.2. Fourier Series Solution for the Current on a Loaded Loop Antenna

A solution of integral equation (11) can be obtained in the form of a Fourier series. The current $I_\phi(\phi')$, the kernel $W(\phi - \phi')$, and the pulse function $P_m(\phi - \phi_m)$ are expanded in Fourier series.

$$I_\phi(\phi') = \sum_{n=-\infty}^{\infty} I_n e^{-jn\phi'} \tag{15}$$

$$W(\phi - \phi') = \sum_{n=-\infty}^{\infty} K_n e^{-jn(\phi-\phi')} \tag{16}$$

$$P_m(\phi - \phi_m) = \sum_{n=-\infty}^{\infty} B_{nm} e^{-jn(\phi-\phi_m)} \tag{17}$$

where $I_n$, $K_n$, and $B_{nm}$ are unknown Fourier coefficients which are defined by the following integrals.

$$I_n = \frac{1}{2\pi} \int_{-\pi}^{\pi} I_\phi(\phi') \, e^{jn\phi'} \, d\phi' \tag{18}$$

$$\begin{aligned} K_n &= \frac{1}{2\pi} \int_{-\pi}^{\pi} W(\phi - \phi') \, e^{jn(\phi-\phi')} \, d\phi \\ &= K_{-n} \end{aligned} \tag{19}$$

$$B_{nm} = \frac{1}{2\pi} \int_{-\pi}^{\pi} P_m(\phi - \phi_m) \, e^{j(\phi-\phi_m)} \, d\phi \tag{20}$$

$B_{nm}$ is easily evaluated by substituting equation (5) into equation (20) and performing the integration. The result is

$$B_{nm} = \frac{1}{2\pi b} \, \frac{\sin\left(\frac{n\,\delta_m}{2}\right)}{\left(\frac{n\,\delta_m}{2}\right)} \tag{21}$$

A Fourier series expansion of the kernel $M(\phi - \phi')$ is obtained by substituting equation (16) into equation (12) and is

$$M(\phi - \phi') = \sum_{n=-\infty}^{\infty} a_n \, e^{-jn(\phi-\phi')} \tag{22}$$

where

$$a_n = \frac{kb}{2} (K_{n+1} + K_{n-1}) - \frac{n^2}{kb} K_n \tag{23}$$

Substituting equations (15), (17), and (22) into integral equation (11) gives

$$V_o \sum_{n=-\infty}^{\infty} B_{no} \, e^{-jn\phi} - \sum_{m=1}^{N} I_\phi(\phi_m) \, Z_m \sum_{n=-\infty}^{\infty} B_{nm} \, e^{-jn(\phi-\phi_m)}$$

$$= \frac{j\,\zeta_o}{4\pi b} \int_{-\pi}^{\pi} \sum_{n=-\infty}^{\infty} I_n \, e^{-jn\phi'} \sum_{\ell=-\infty}^{\infty} a_\ell \, e^{-j\ell(\phi-\phi')} \, d\phi'$$

$$= \frac{j\zeta_o}{2b} \sum_{n=-\infty}^{\infty} I_n a_n e^{-jn\phi}$$

The following expression for $I_n$ is derived from the previous equation by using the orthogonality property of the $e^{jn\phi}$ functions.

$$I_n = \frac{2b}{j\zeta_o a_n} \left[ V_o B_{no} - \sum_{m=1}^{N} I_\phi(\phi_m) Z_m B_{nm} e^{jn\phi_m} \right] \tag{24}$$

The series determining the current on the loaded loop antenna is given by equations (15), (21), and (24) and is

$$I_\phi(\phi) = \frac{-j}{\zeta_o \pi} \left\{ V_o \left[ \frac{1}{a_o} + 2 \sum_{n=1}^{\infty} \frac{\sin\left(\frac{n\delta_o}{2}\right)}{\left(\frac{n\delta_o}{2}\right)} \frac{\cos(n\phi)}{a_n} \right] \right.$$

$$\left. - \sum_{m=1}^{N} I_\phi(\phi_m) Z_m \left[ \frac{1}{a_o} + 2 \sum_{n=1}^{\infty} \frac{\sin\left(\frac{n\delta_m}{2}\right)}{\left(\frac{n\delta_m}{2}\right)} \frac{\cos\left(n(\phi - \phi_m)\right)}{a_n} \right] \right\} \tag{25}$$

The values of the current at the positions of the loads must now be determined. Load voltages are defined as

$$V_m = I_\phi(\phi_m) Z_m \tag{26}$$

where $V_m$ is the voltage drop across the $m^{th}$ load impedance $Z_m$. It is also convenient to define

$$y(\phi - \phi_m) = \frac{-j}{\zeta_o \pi} \left[ \frac{1}{a_o} + 2 \sum_{n=1}^{\infty} \frac{\sin\left(\frac{n\delta_m}{2}\right)}{\left(\frac{n\delta_m}{2}\right)} \frac{\cos\left(n(\phi - \phi_m)\right)}{a_n} \right] \tag{27}$$

which has the same dimension as admittance but is actually the current distribution on an unloaded loop antenna driven by a generator of unit voltage located at $\phi = \phi_n$. For the case of the voltage generator located at $\phi = \phi_o = 0^o$ the notation $y(\phi)$ will be used and it is implied that $\delta = \delta_o$. Evaluating equation (25) at the N positions of the load impedances and noting that $I_\phi(\phi_m) = V_m Y_m$ where $Y_m = 1/Z_m$ and is the $m^{th}$ load admittance gives N simultaneous equations:

$$V_n Y_n = V_o\, y(\phi_n) - \sum_{m=1}^{N} V_m\, y(\phi_n - \phi_m)$$

$$n = 1, 2, \ldots, N \tag{28}$$

With the notation

$$y_{nm} = y(\phi_n - \phi_m), \qquad y_n = y(\phi_n) \tag{29}$$

the previous set of simultaneous equations can be written in matrix form as

$$\begin{bmatrix} y_{11}+Y_1 & y_{12} & \ldots & y_{1N} \\ y_{21} & y_{22}+Y_2 & & y_{2N} \\ \cdot & & & \\ \cdot & & & \\ \cdot & & & \\ y_{N1} & y_{N2} & & y_{NN}+Y_N \end{bmatrix} \begin{bmatrix} V_1 \\ V_2 \\ \cdot \\ \cdot \\ \cdot \\ V_N \end{bmatrix} = V_o \begin{bmatrix} y_1 \\ y_2 \\ \cdot \\ \cdot \\ \cdot \\ y_N \end{bmatrix} \tag{30}$$

which can easily be solved for the load voltages.

The current on the loaded loop antenna is now completely determined and given by

$$I_\phi(\phi) = V_o\, y(\phi) - \sum_{m=1}^{N} V_m\, y(\phi - \phi_m) \tag{31}$$

The corresponding input admittance is

$$Y_{in} = \frac{I_\phi(0)}{V_o} = y_o - \sum_{m=1}^{N} \overline{V}_m\, y_m \tag{32}$$

where

$$\overline{V}_m = V_m / V_o$$

is the normalized load voltage.

The above results can be interpreted in terms of a superposition picture which will be useful later. Equation (31) shows that the current on the loaded loop antenna is the superposition of N + 1 currents. The first current (corresponding to the first term on the right hand side of equation (31)) is equivalent to the current on an unloaded loop driven at $\phi = 0^{\circ}$ by $V_o$, the second current is equivalent to the current on an unloaded loop driven at $\phi = \phi_1$, by $-V_1$, etc. The load voltages $V_1, V_2, \ldots, V_N$ are determined by matrix equation (31).

The input impedance and current distribution of the loaded loop antenna depend on the coefficient

$$a_n = \frac{kb}{2}(K_{n+1} + K_{n-1}) - \frac{n^2}{kb}K_n \tag{23}$$

where $K_n$ has been defined as [see equations (13) and (19)]

$$K_n = \frac{1}{(2\pi)^2}\int_{-\pi}^{\pi}\left(\int_{-\pi}^{\pi}\frac{e^{-jkbR_1}}{R_1}\,d\psi'\right)e^{jn(\phi-\phi')}\,d\phi \tag{33}$$

and

$$R_1 = \sqrt{4\sin^2\left((\phi-\phi')/2\right) + 4(a^2/b^2)\sin^2(\psi'/2)}$$

Wu[1, 11, 12] has evaluated this integral under the assumption $a^2 << b^2$ and obtained

$$K_o = \frac{1}{\pi}\ln\left(\frac{8b}{a}\right) - \frac{1}{2}\int_o^{2kb}[\Omega_o(x) + j\,J_o(x)]\,dx \tag{34}$$

$$K_n = \frac{1}{\pi}[\overline{K}_o(\tfrac{na}{b})\,\overline{I}_o(\tfrac{na}{b}) + C_n] - \frac{1}{2}\int_o^{2kb}[\Omega_{2n}(x) + j\,J_{2n}(x)]\,dx \tag{35}$$

where

$$C_n = \ln(4n) + \gamma - 2\sum_{m=0}^{n-1}\frac{1}{2m+1} \tag{36}$$

and $\gamma = 0.5772\ldots$ is Euler's constant, $\overline{I}_o(x)$ and $\overline{K}_o(x)$ are the modified Bessel functions of the first and second kinds of order 0, $J_n(x)$ is the Bessel function of the first kind and order n, and $\Omega_n(x)$ is the Lommel-Weber function* [13, 14] defined by

$$\Omega_n(x) = \frac{1}{\pi}\int_o^{\pi}\sin(x\sin\theta - n\theta)\,d\theta\,. \tag{37}$$

---

*Some authors define the negative of this function as the Weber function denoted $E_n(x)$, that is $E_n(x) = -\Omega_n(x)$.

2.3. Radiation Fields of a Loaded Loop Antenna

The electromagnetic fields radiated by a loaded loop antenna can be obtained by integrating term by term the Fourier series expansion of the current on the loop. The electromagnetic fields in terms of the vector potential are given by

$$\vec{E}(\vec{r}) = -j\omega\vec{A} + \frac{\nabla(\nabla\cdot\vec{A})}{j\omega\mu_o\epsilon_o} \tag{38}$$

$$\vec{H}(\vec{r}) = \frac{1}{\mu_o}\nabla \times \vec{A} \tag{39}$$

where

$$\vec{A}(\vec{r}) = \frac{\mu_o}{4\pi}\int_V \vec{J}(\vec{r}\,')\,\frac{e^{-jkR}}{R}\,dV' \tag{40}$$

and $R = |\vec{r} - \vec{r}\,'|$ .

Consider the loaded loop antenna which lies in the $\theta = 90^\circ$ plane with its center at the origin of a spherical coordinate system as shown in Figure 2.2. Dropping terms of higher order than $1/r$ and making the following standard radiation zone approximation

$$R \doteq \begin{cases} r - \hat{r}\cdot\vec{r}\,' & \text{--- for the phase term} \\ r & \text{--- for the amplitude term} \end{cases}$$

equations (33), (34), and (35) become

$$\vec{E}(\vec{r}) \doteq -j\omega\left(\hat{\theta}\,A_\theta(\vec{r}) + \hat{\phi}\,A_\phi(\vec{r})\right) \tag{41}$$

$$\vec{H}(\vec{r}) \doteq -jk\left(-\hat{\theta}\,A_\phi(\vec{r}) + \hat{\phi}\,A_\theta(\vec{r})\right) \tag{42}$$

$$\vec{A}(\vec{r}) = \frac{\mu_o}{4\pi}\frac{e^{-jkr}}{r}\int_0^{2\pi} I_\phi(\phi')\,\hat{\phi}'\,e^{jk\hat{r}\cdot\vec{r}\,'}\,b\,d\phi' \tag{43}$$

which is valid in the radiation zone where $r \gg b$.

The integral that results from substituting equation (31), the current on the loaded loop, into equation (43) can be integrated exactly in terms of Bessel functions of the first kind. A similar integral for the unloaded loop has been evaluated[15, 16] and the result for the loaded loop can be obtained by superposition in accordance with equation (31). The resulting radiation fields of the loaded loop antenna are

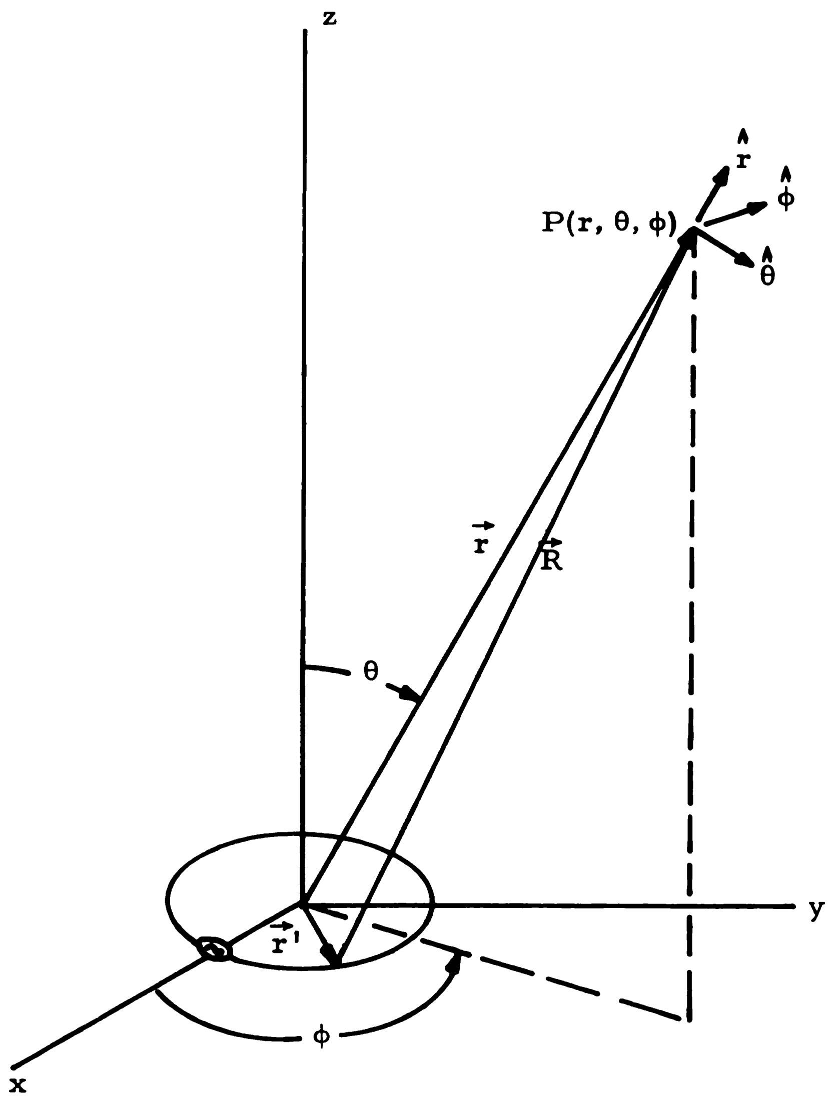


Figure 2. 2. Coordinate system for the fields radiated by a loop antenna.

$$\vec{E}(\vec{r}) = \hat{\theta} E_\theta + \hat{\phi} E_\phi \tag{44}$$

$$\vec{H}(\vec{r}) = -\hat{\theta} E_\phi/\zeta_o + \hat{\phi} E_\theta/\zeta_o \tag{45}$$

where

$$E_\theta = \frac{jkb}{\pi} \frac{e^{-jkr}}{r} V_o \left[ F_{\theta o} - \sum_{m=1}^{N} \bar{V}_m F_{\theta m} \right] \tag{46}$$

$$E_\phi = \frac{jkb}{\pi} \frac{e^{-jkr}}{r} V_o \left[ F_{\phi o} - \sum_{m=1}^{N} \bar{V}_m F_{\phi m} \right] \tag{47}$$

and

$$F_{\theta m} = \cos\theta \sum_{n=1}^{\infty} \frac{(j)^n}{a_n} \frac{\sin\left(\frac{n\delta_m}{2}\right)}{\left(\frac{n\delta_m}{2}\right)} \frac{1}{2} [ J_{n-1}(kb \sin\theta) + J_{n+1}(kb \sin\theta] \sin\left(n(\phi - \phi_m)\right)$$

$$= \cos\theta \sum_{n=1}^{\infty} \frac{(j)^n}{a_n} \frac{\sin\left(\frac{n\delta_m}{2}\right)}{\left(\frac{n\delta_m}{2}\right)} n \frac{J_n(kb \sin\theta)}{kb \sin\theta} \sin\left(n(\phi - \phi_m)\right) \tag{48}$$

$$F_{\phi m} = -\frac{J_1(kb \sin\theta)}{2a_o} + \sum_{n=1}^{\infty} \frac{(j)^n}{a_n} \frac{\sin\left(\frac{n\delta_m}{2}\right)}{\left(\frac{n\delta_m}{2}\right)} \frac{1}{2} [ J_{n-1}(kb \sin\theta) - J_{n+1}(kb \sin\theta)] \cos\left(n(\phi - \phi_n)\right)$$

$$= \frac{J_o'(kb \sin\theta)}{2a_o} + \sum_{n=1}^{\infty} \frac{(j)^n}{a_n} \frac{\sin\left(\frac{n\delta_m}{2}\right)}{\left(\frac{n\delta_m}{2}\right)} J_n'(kb \sin\theta) \cos\left(n(\phi - \phi_n)\right) \tag{49}$$

where $J_n(z)$ is the Bessel function of the first kind and $J_n'(z) = \frac{\partial}{\partial z} J_n(z)$. Examination of equations (44) through (49) indicates that the radiation fields are outward traveling spherical waves. It also indicates $E_\theta$ and $E_\phi$ are in phase implying that the radiation is linearly polarized.

A parameter which is useful in describing antenna radiation is the gain of the antenna. The gain of an antenna is defined by

$$G(\theta, \phi) = 4\pi \frac{\text{power density per unit solid angle in direction } \theta, \phi}{\text{total input power to antenna}} . \tag{50}$$

The gain of an antenna differs from its directivity by a factor which takes into account the efficiency of the antenna.

For the loaded loop antenna the gain is given by

$$G(\theta, \phi) = \frac{4(kb)^2}{\zeta_o \pi G_{in}} \left\{ \left| F_{\theta o} - \sum_{m=1}^{N} \overline{V}_m F_{\theta m} \right|^2 + \left| F_{\phi o} - \sum_{n=1}^{N} \overline{V}_m F_{\phi m} \right|^2 \right\} . \tag{51}$$

where $G_{in}$ is the input conductance of the loop.

## CHAPTER III

## IMPEDANCES, CURRENTS, AND RADIATION FIELDS OF A LOOP ANTENNA EXCITED BY A FINITE GAP GENERATOR

This chapter deals with the numerical method used in calculating the results of the loaded loop antenna with the finite gap excitation which was developed in the previous chapter. Theoretical results based on the finite gap excitation and theoretical results based on the $\delta$-function generator are compared with existing experimental results. Finally, some examples of impedances, currents, and gain patterns of large loop antennas excited by finite gap generators are presented.

### 3.1. Numerical Method

Numerical results based on series expansions for the radiation fields, current distributions, and input admittances of loop antennas have been evaluated on a CDC 6500 computer system. These series depend on coefficients $a_n$ which are functions of the kb and a/b. These coefficients also depend on the $K_n$ integrals [ see equation (23)] which were evaluated using Wu's expression as given in equations (34), (35), and (36). A standard M. S. U. computer library subroutine[17] was used to generate the Bessel functions of the first kind. The modified Bessel functions were calculated by polynomial approximations[18] while a series expansion[13, 14] was used to evaluate the Lommel-Weber functions.

Examples of the first four coefficients are shown in Figure 3.1 as functions of kb with $\Omega = 2\ln(2\pi b/a) = 12$. Increasing the value of $\Omega$ (i. e., constructing the loop with thinner wire) tends to sharpen the peaks of the $a_n$ while decreasing $\Omega$ tends to flatten the peaks.

The series determining the radiation fields [equations (48) and (49)] are rapidly convergent if kb is not too large. In this study twenty terms were retained to insure accurate results for $kb \le 10$.

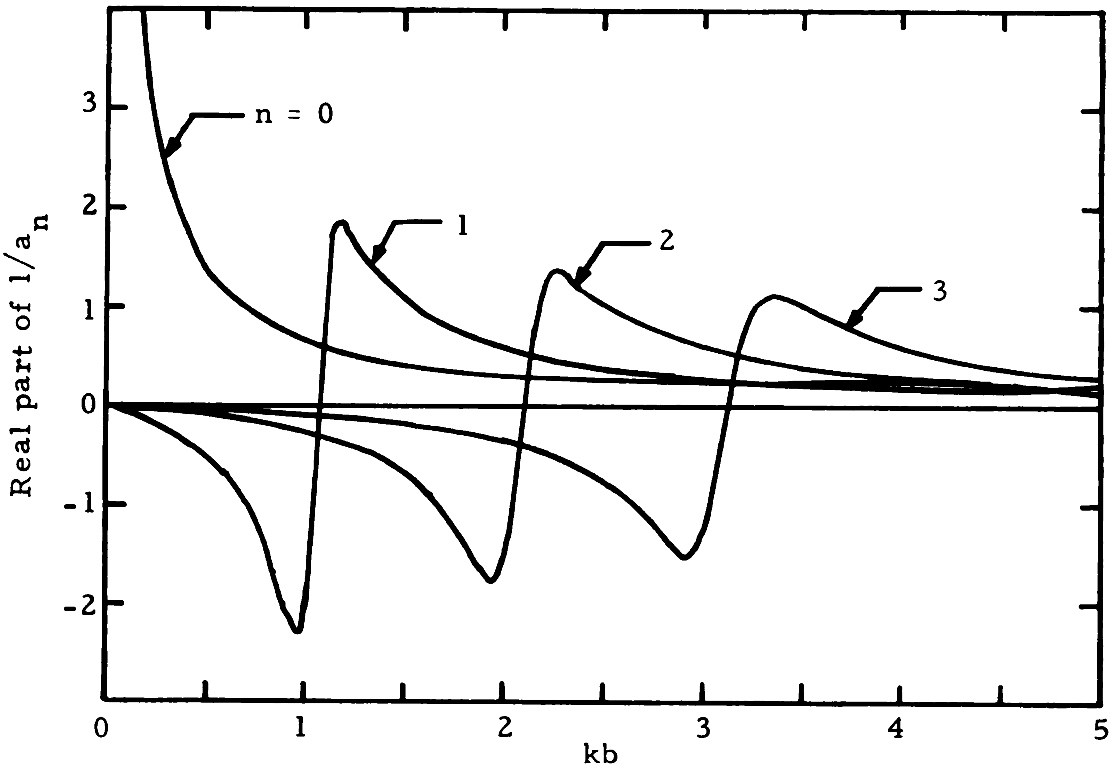


(a)

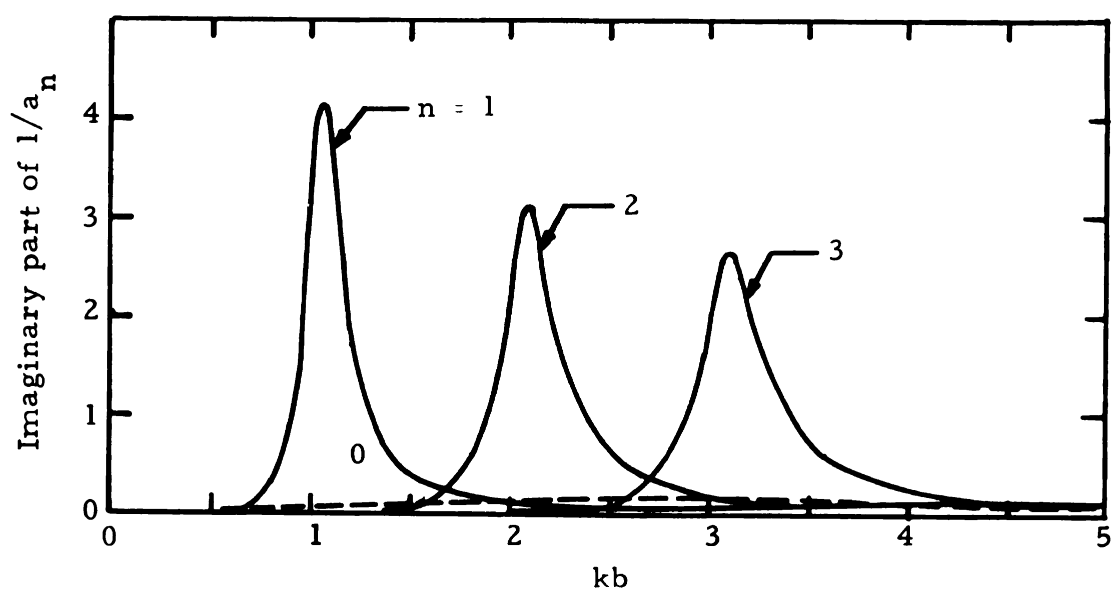


(b)

Figure 3.1. Real and imaginary parts of $1/a_0$, $1/a_1$, $1/a_2$, $1/a_3$ for $\Omega = 12$. (a) Real parts. (b) Imaginary parts.

The series determining the input admittance is given by expressions (27), (29), and (32). The real part of this series which corresponds to the input conductance converges very rapidly independent of the gap width. For example, with kb = 2.5 three digit accuracy can be obtained for the conductance rataining only four terms in the series. On the other hand, the imaginary part of this series which corresponds to the input susceptance is somewhat more troublesome. Consider briefly the convergence properties of this series. The input admittance of the unloaded loop is found from eq. (32) to be

$$Y_{in} = y_o = \frac{-j}{\zeta_o \pi}\left[\frac{1}{a_o} + 2\sum_{n=1}^{\infty} \frac{\sin\left(\frac{n\delta_o}{2}\right)}{\left(\frac{n\delta_o}{2}\right)} \frac{1}{a_n}\right] \tag{52}$$

For large n with n >> kb

$$a_n \sim -\frac{n^2}{kb} K_n$$

and when n >> b/a the dominant term in $K_n$ is the term involving the product of the modified Bessel functions. Retaining the first term in an asymptotic expansion for this product[19] results in the following expression:

$$K_n \sim \frac{1}{\pi} \overline{K}_o\left(\frac{na}{b}\right) \overline{I}_o\left(\frac{na}{b}\right) \sim \frac{1}{2\pi} \frac{b}{na}$$

Hence

$$\frac{1}{a_n} \sim 2\pi kb \left(\frac{a}{b}\right) \frac{1}{n}$$

and the $n^{th}$ term in the admittance series has the following asymptotic form for large n

$$-j \frac{4}{\zeta_o} ka \frac{\sin\left(\frac{n\delta_o}{2}\right)}{\left(\frac{n\delta_o}{2}\right)} \frac{1}{n} \; . \tag{53}$$

When $\delta_o > 0$ the series converges,[20] but when $\delta_o = 0$ (which is the case of the $\delta$-function generator), the series diverges. Physically this implies an infinite stray capacitance existing at a gap with an infinitesimal gap width. It is interesting to note that (53) depends only on the wire size ka and the term $\frac{\sin(n\delta_o/2)}{(n\delta_o/2)}$, which arose from expanding the loop excitation in a Fourier series, and does not depend on the loop size kb. For small n the terms are also a function of kb. The above observations imply that the detailed behavior of the susceptance is determined strongly by the manner of excitation of the loop at the driving point. A comparison of the input susceptances obtained from equation (52) with $\delta_o = 0.0$ and $\delta_o = 0.1$ rad. as a function of the number of terms retained in the series is made in Table 3.1.

The actual computation of the input admittance $Y_{in}$, the current distribution $I_\phi(\phi)$, and the self and mutual short circuit admittances of the loading points $y_{nm}$ was accomplished by summing 1001 terms of their respective series. The first 61 coefficients were calculated exactly. The following approximate expression was used in calculating the remaining coefficients.

$$K_n \doteq \frac{1}{\pi} \overline{K}_o\left(\frac{na}{b}\right) \overline{I}_o\left(\frac{na}{b}\right) + \frac{1}{2\pi}\left(\frac{kb}{n}\right)^2 \tag{54}$$

The last term in the above expression arises from integrating the first term in a series representation of the Lommel-Weber function.[13] This method of calculation assures at least two digit accuracy. Only slightly over one second of computer time was needed to generate the 1001 coefficients and sum them.

## 3.2. Effect of Finite Gap Generator

The gap size has no effect on the conductance of small and moderate size loops and only a slight effect on large loops in the range of kb = 10.0. Physically this is to be expected since the conductance is proportional to the total power radiated by the loop and should not be significantly affected by the gap size.

The effect of the gap size on the susceptance is shown in Figures 3.2 and 3.3. Decreasing the gap size tends to make the loop susceptance more capacitive. Figure 3.2 shows that the susceptance of thick loops is more sensitive to gap size than thinner loops. It can be seen that the effect of the gap increases with increasing loop size. For very small loops the susceptance is nearly independent of gap width. This can be explained by the fact that the current is essentially uniform

| Number of terms in partial sum | Susceptance, millimhos | |
|---|---|---|
| | $\delta_o = 0.0$ | $\delta_o = 0.1$ rad. |
| 2 | -0.868 | -0.868 |
| 4 | -1.36 | -1.36 |
| 6 | -0.666 | -0.673 |
| 8 | -0.366 | -0.378 |
| 10 | -0.182 | -0.199 |
| 12 | -0.0527 | -0.0762 |
| 14 | 0.0451 | 0.0153 |
| 16 | 0.123 | 0.0865 |
| 18 | 0.187 | 0.144 |
| 20 | 0.242 | 0.191 |
| 22 | 0.289 | 0.230 |
| 24 | 0.331 | 0.264 |
| 26 | 0.368 | 0.292 |
| 28 | 0.401 | 0.317 |
| 30 | 0.432 | 0.338 |
| 40 | 0.553 | 0.408 |
| 50 | 0.643 | 0.441 |
| 60 | 0.715 | 0.452 |
| 70 | 0.775 | 0.450 |
| 80 | 0.827 | 0.443 |
| 90 | 0.874 | 0.433 |
| 100 | 0.915 | 0.425 |
| 200 | 1.19 | 0.428 |
| 300 | 1.36 | 0.425 |
| 400 | 1.48 | 0.423 |
| 500 | 1.57 | 0.423 |
| 1000 | 1.86 | 0.424 |

Table 3.1. Input susceptance of circular loop antenna as a function of terms retained in series solution with $kb = 2.5$ and $\Omega = 12.0$.

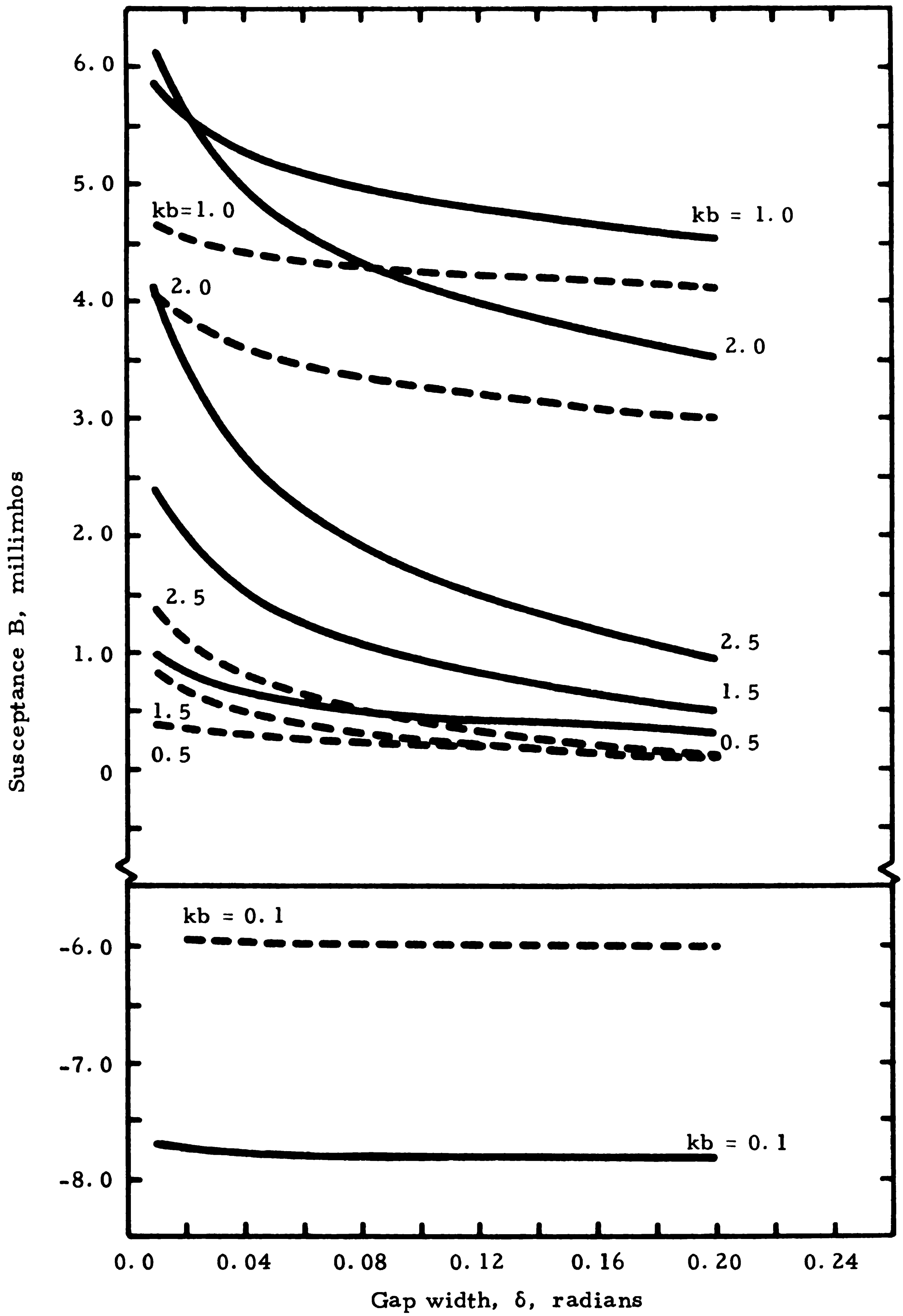


Figure 3.2. Input susceptance of loop antenna as a function of gap width for $\Omega = 10$ (———) and $\Omega = 12$ (- - - - -).

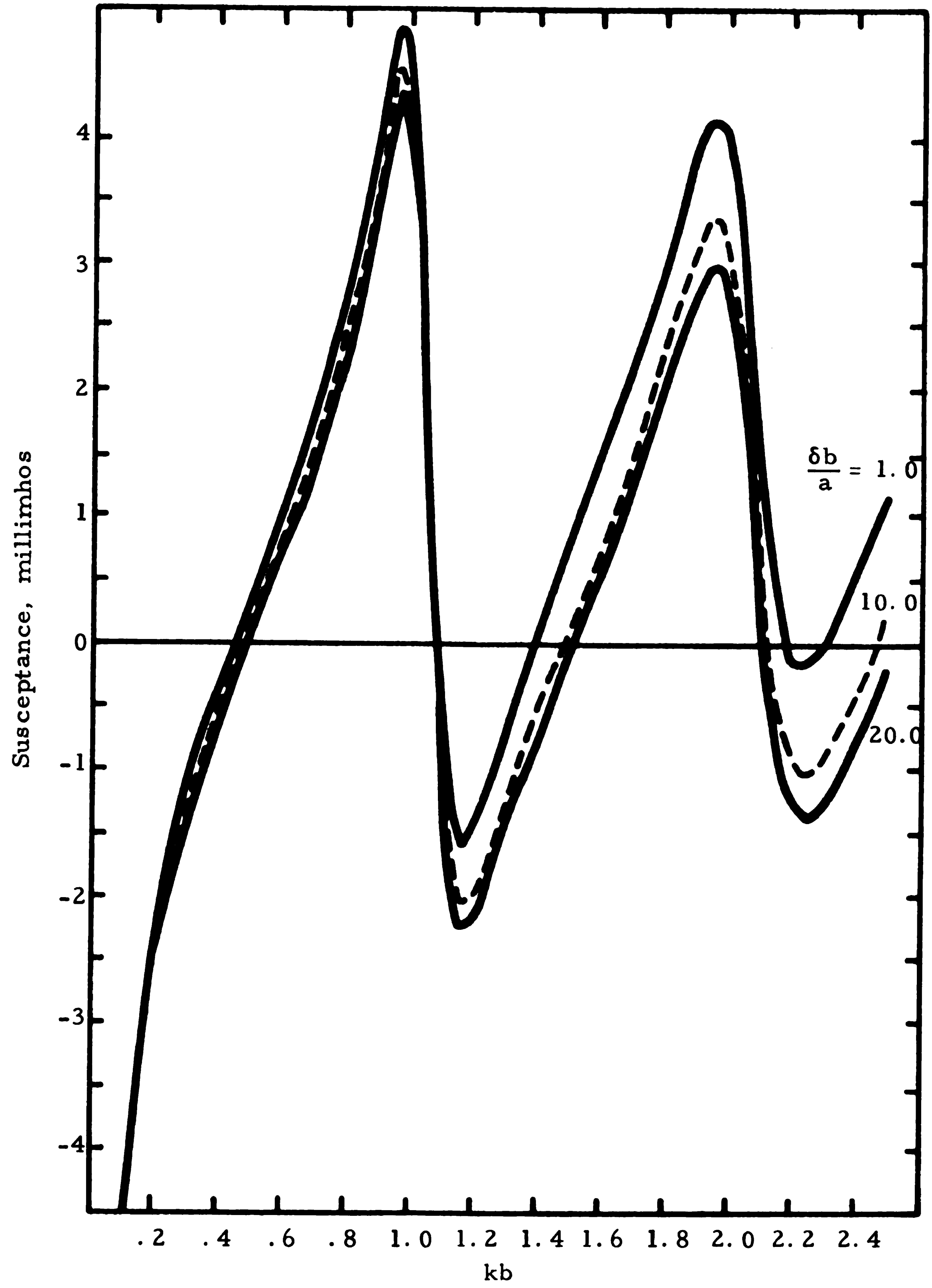


Figure 3.3. Input susceptance of loop antenna as a function of kb for $\delta b/a = 1.0$, 10.0, and 20.0 with $\Omega = 12$ (i.e., $a/b \doteq 0.0155$).

on small loops and hence there is no charge buildup on the loop. Thus, changing the gap width does not change the distribution of current and charge and hence does not change the input susceptance of the loop.

## 3.3. Comparison of "Finite Gap" Theory with Experimental Results

Theoretical analysis of wire antennas usually makes use of an idealized generator, whether it be a δ-function generator or a finite gap generator, that eliminates the transmission line which is usually present in practice. The theoretical admittance of the antenna is thus an intrinsic quantity of the antenna and idealized generator. On the other hand, the measured admittance of an antenna is the apparent admittance the antenna presents to a transmission line when connected as a terminating load. The theoretical admittance neglects:

a. Electromagnetic coupling between the antenna and transmission line near the junction between them.

b. Changes in the characteristic impedance of the transmission line near the junction due to the fact that the line is not infinitely long.

and, in addition, for the case of a two wire transmission line driving the antenna:

c. The absence of the antenna in the gap between the two conductors of the transmission line.

For the case of a dipole antenna driven by a two wire line, King[21] (this paper references other related works) has derived a terminal-zone correction to relate the ideal, theoretical admittance to the apparent admittance of the antenna. Likewise, correction terms have been found for a monopole over a ground plane driven by a coaxial line.[22, 23, 24] No such terminal correction terms have been determined for the loop antenna.

It is noted that the terminal zone corrections for the dipole depend mainly on the transmission line geometry and not on the length of the dipole and that the dominant term in the correction is a lumped shunt susceptance. It has been seen in the last two sections that the high order terms in the series determining the admittance of the loop depend on the gap size and the loop wire size but not on the size of the loop, and that changing the gap width affected the loop admittance in the same was as a lumped susceptance shunting the loop would. In view of the similar characteristics of the terminal zone corrections and the finite gap generator, it is proposed that "effective" gap widths be defined which result in theoretical loop admittances which correspond to apparent measured admittances. For the case of the loop driven by a two wire line the effective gap width is taken to be the distance between the centers of the two wires of the line. For the case of a half loop over a ground plane driven by a coaxial line the effective gap width is taken to be the inside diameter of the outer conductor of the coaxial line. The justification for these effective gap widths is that they yield theoretical admittances that compare very well to measured admittances.

Experimental measurements of the admittance of loop antennas driven by a two wire line has been reported by Kennedy.[25] A comparison of her measured conductances with theoretical results calculated from equation (52) is shown in Figure 3.4. The $\delta$-function theories and the finite gap theory give essentially identical conductances. Figure 3.5 compares measured susceptances, twenty term, $\delta$-function theory susceptances, and susceptances resulting from the finite gap theory with two different gap widths. In the region $4.0 < \pi kb < 6.0$ the susceptances of the twenty term, $\delta$-function theory fall between those of the two finite gap theories and are not shown. A detailed description of the experiment is found in the above reference, but it is worth noting that the experiment was performed at a constant frequency of 750 MHz with the loop size being changed from $\pi kb = 1.48$ with $\Omega = 2\ln(\frac{2\pi b}{a}) = 8.16$ to $\pi kb = 9.38$ with $\Omega = 11.84$. A comparison of Kennedy's data and Storer's $\delta$-function theory can be found in the literature.[3, 25] It is found that the finite gap theory gives susceptances that are in better agreement to the experimental data than Storer's theory.

Iizuka[9] has reported measurements of the admittances of half of a circular loop antenna imaged into a conducting ground plane and driven by a coaxial line. A comparison of the finite gap theory, the twenty term, $\delta$-function theory, and Iizuka's measured admittances is shown in Figure 3.6. The experiment was performed at 600 MHz and

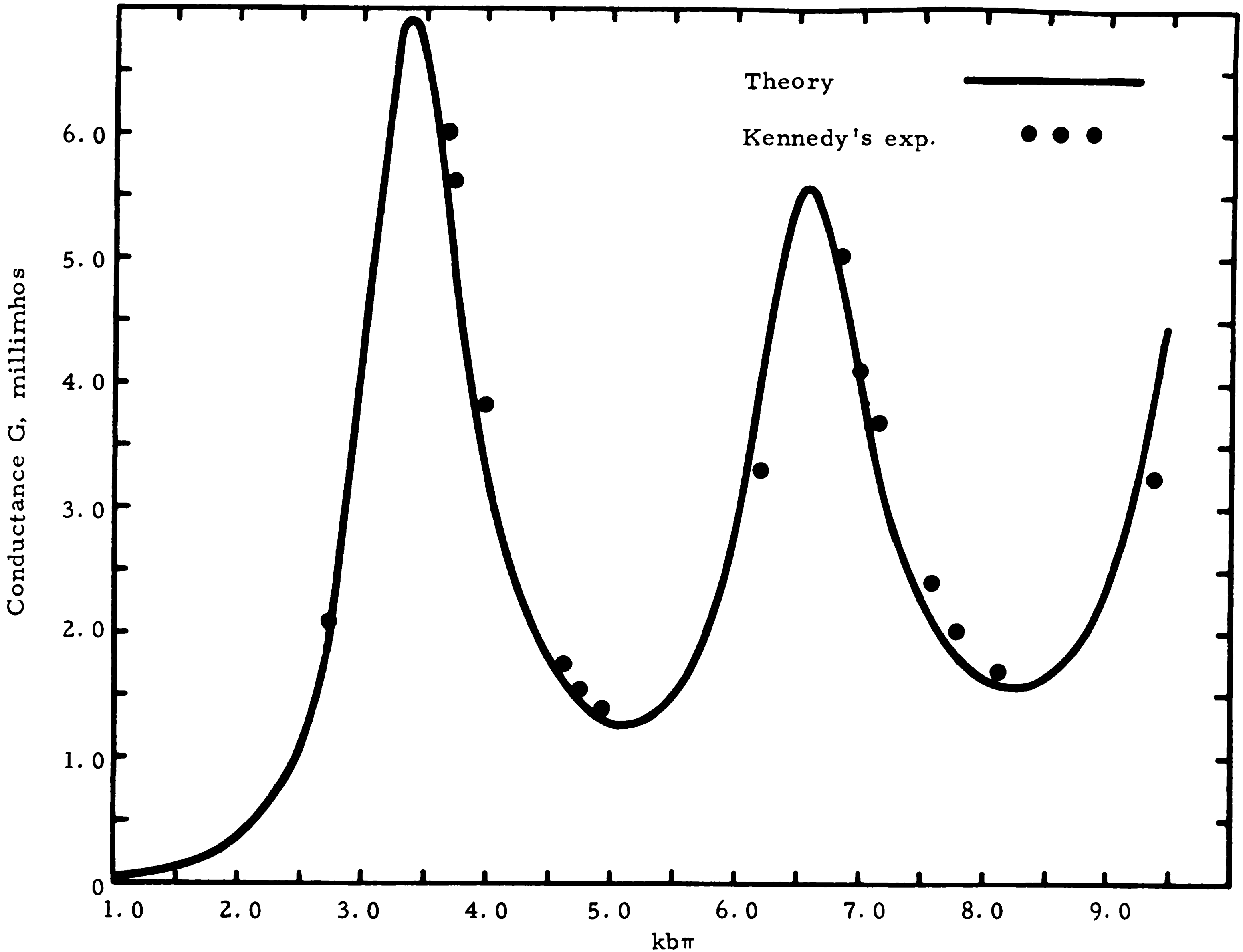


Figure 3.4. Comparison of finite gap theory and experimental conductances of a loop driven by a two wire line.

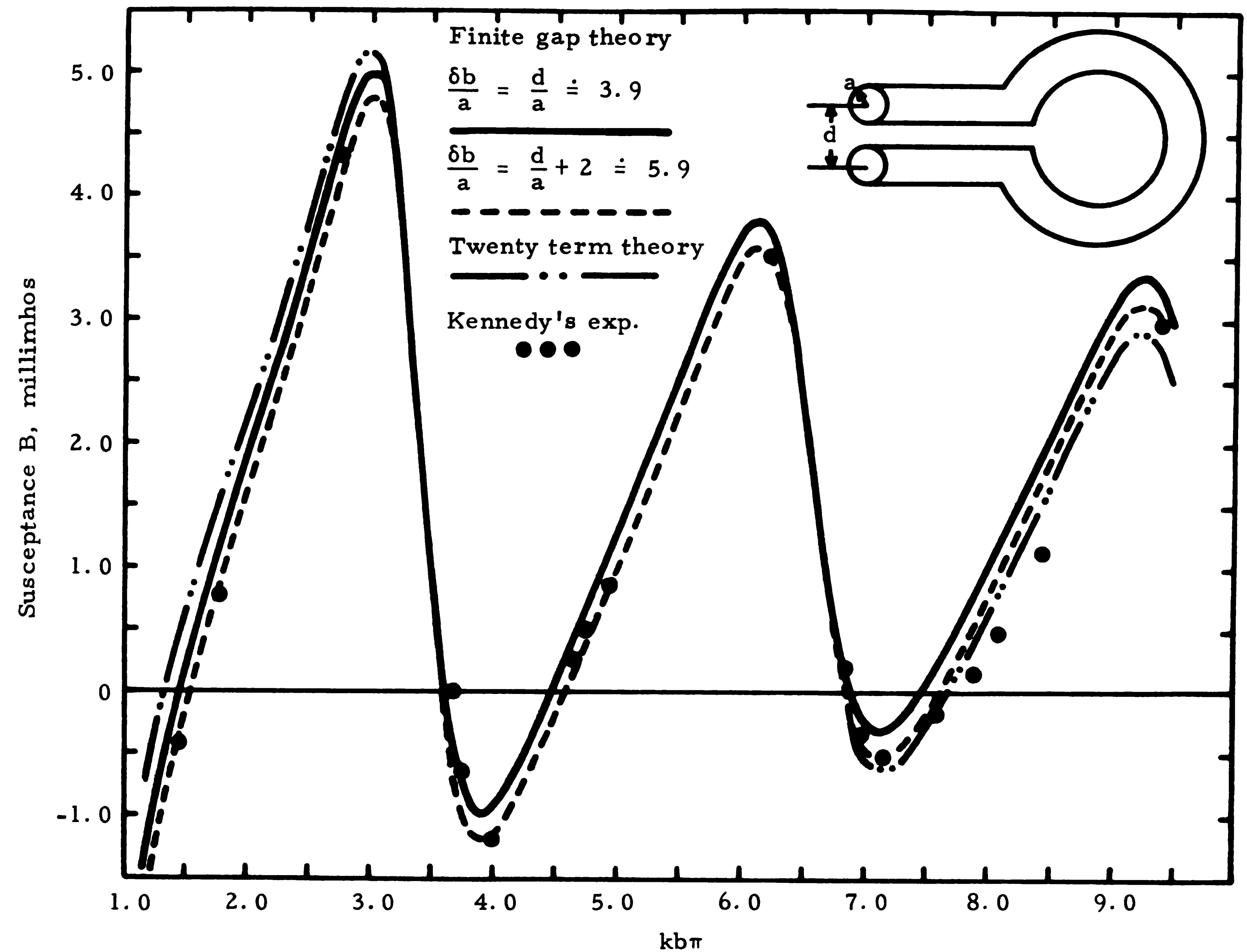


Figure 3.5. Comparison of finite gap theory and experimental susceptances of a loop driven by a two wire line.

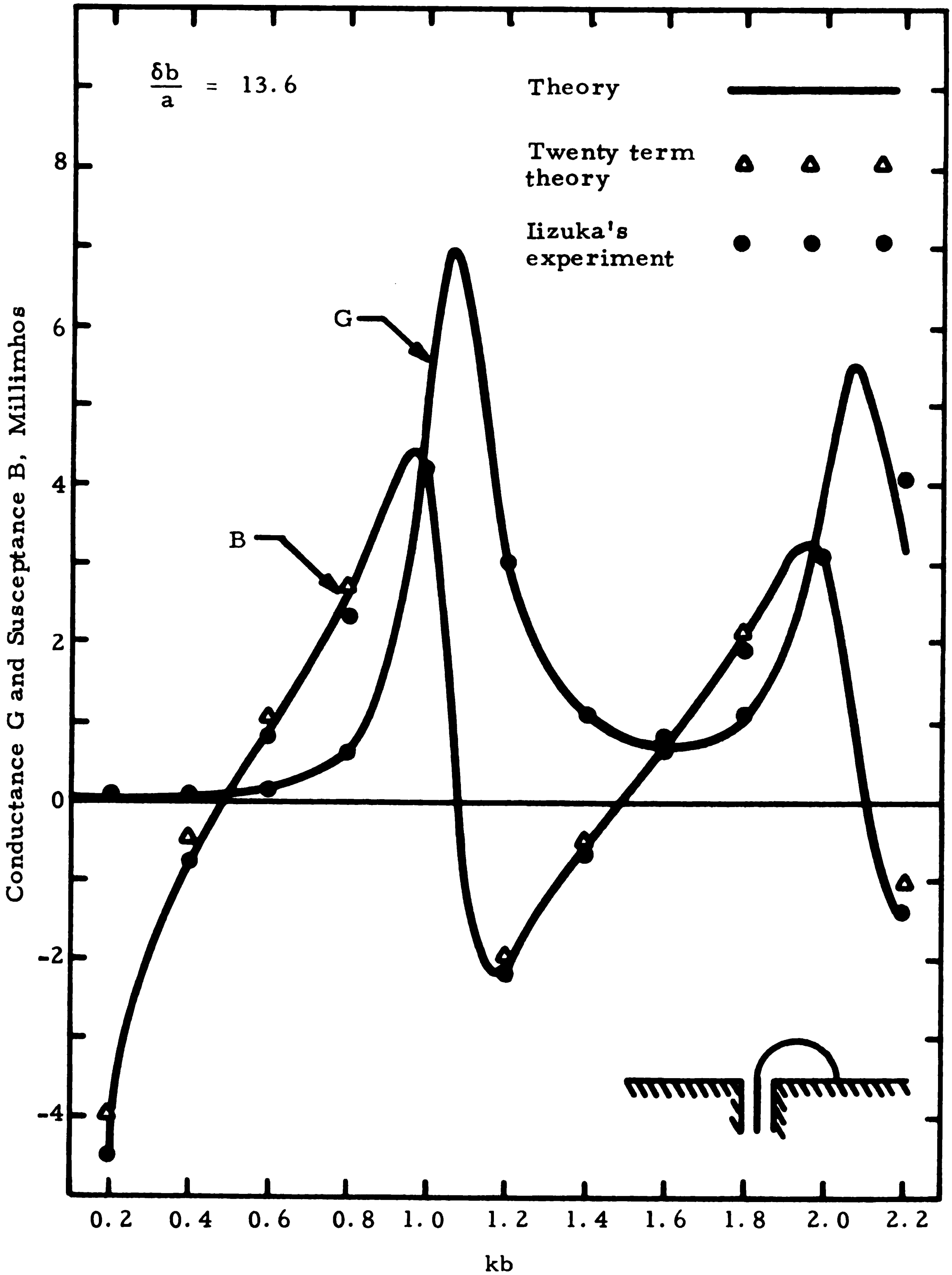


Figure 3.6. Comparison of finite gap theory and experimental admittances of a loop driven by a coaxial line.

once again the physical size of the loop was changed to effect changes in kb. $\Omega = 2\ln(2\pi b/a)$ takes on values which range from approximately 8 through 14 while kb changes from 0.2 to 2.2. The gap width is taken to be the inside diameter of the outer conductor of the coaxial line which results in $\delta_o b/a = 13.6$. Excellent agreement between theory and measured admittances is obtained. Increasing the gap width to $\delta_o b/a = 27.2$ reduces the susceptance by approximately 0.2 millimhos over the range of kb considered. Reducing the gap width to $\delta_o b/a = 6.8$ increases the theoretical susceptance by roughly 0.15 millimhos. Thus it appears a gap width equal to the inside diameter of the outer conductor of the coaxial line is optimum.

Values for the susceptance calculated by the twenty term theory are denoted by an "◘" in Figure 3.6. At kb = 1.0 and 2.0 the twenty term susceptance and the finite gap susceptance are essentially identical and no ◘ is indicated. It is seen the twenty term theory does not compare to the measured susceptances as well as the finite gap theory. At kb = 0.2 the twenty term susceptance is approximately 0.6 millimhos more capacitive than the measured value while at kb = 2.2 the twenty term value is approximately 0.4 millimhos more inductive than the measured value. This can be explained as follows. A numerical study of the twenty term, $\delta$-function theory and the finite gap theory over the range of parameters considered in this experiment has shown that truncating the $\delta$-function series at twenty terms yields approximately the same susceptance as using the finite gap theory with $\delta_o = 0.15$ radians. However, in Iizuka's experiment $\delta_o b/a$ was held constant while b was varied, hence $\delta_o$ varied as kb was changed. In the experiment with kb = 0.2, $\delta_o \doteq 1.07$ radians while at kb = 2.2, $\delta_o \doteq 0.1$ radians. It is concluded that the inaccuracy in the twenty term, $\delta$-function theory is introduced by not taking into account change in the excitation of the loop.

Iizuka[9] has also reported admittances of a loop loaded at $\phi = 180^o$ with a lumped impedance $Z_1 = \infty$. The load impedance is implemented by simply removing a short segment of the loop at $\phi = 180^o$. The theoretical gap width for the load, $\delta_1$, was taken to be identical to the physical gap width used in the experiment which was $.012\lambda$ at 600 MHz.

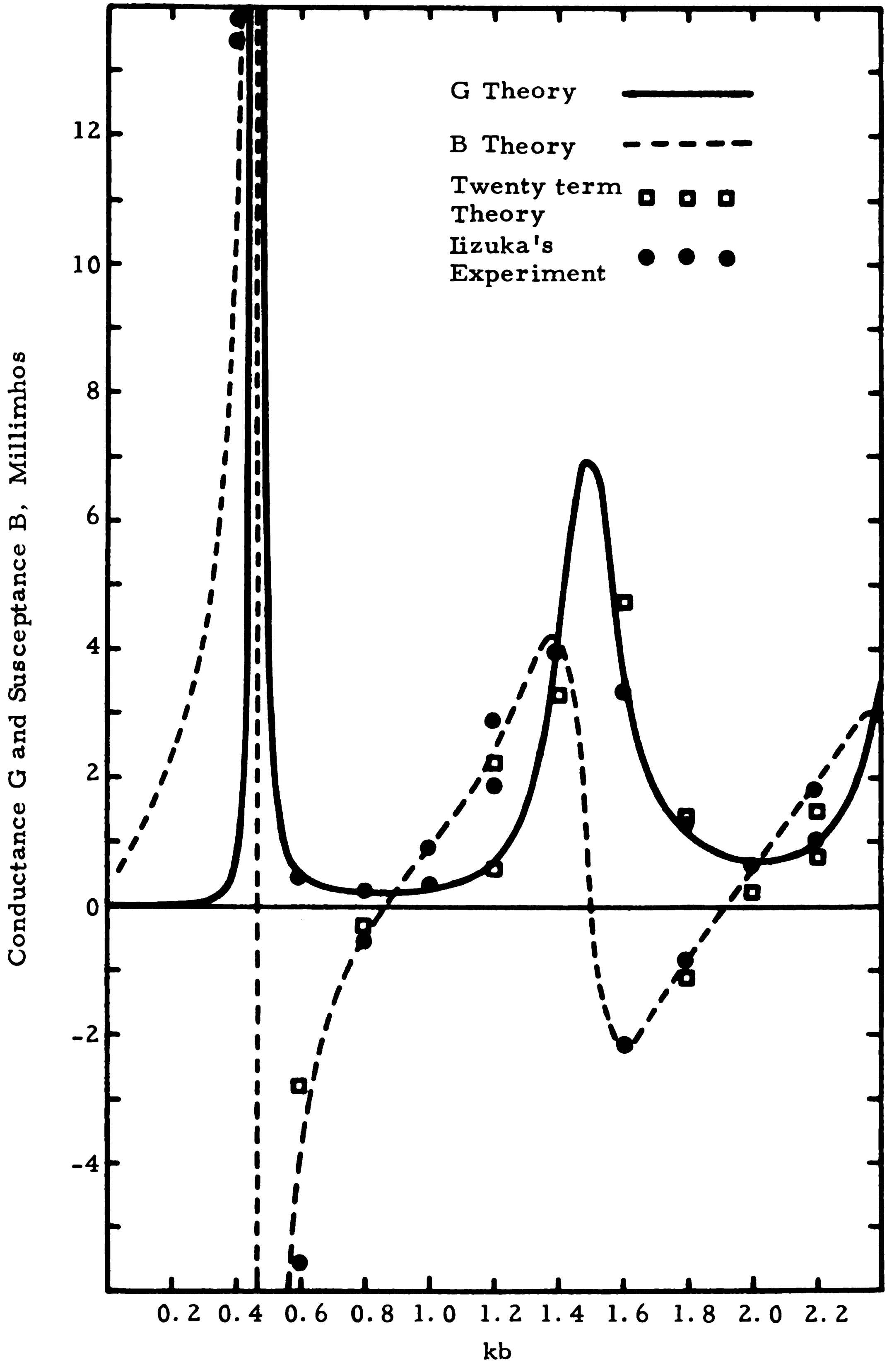


Figure 3.7. Comparison of finite gap theory with $\delta_0 b/a = 13.6$ and experimental admittances of a loop loaded at $\phi = 180^\circ$ with $Z_1 = \infty$ (i.e., a gap).

Calculations made using equations (30) and (32) are compared with Iizuka's measured admittances in Figure 3.7. Once again, excellent agreement between the finite gap theory and the measured admittances is obtained. Again, it is found that the twenty term admittances do not agree with the measured admittances as well as the finite gap theory does. Iizuka found a fairly large discrepancy between his theory and his measured values (which are used in Figure 3.7) and it may be concluded that the finite gap theory is a significant improvement in the theory of the loaded loop antenna.

### 3.4. Input Impedances, Currents and Radiation Fields of Loop Antennas

The electrical properties of small loop antennas with $kb \le 0.1$ are well known. The radiation resistance of a small loop is[26]

$$R \doteq \frac{\pi \zeta_o}{6} (kb)^4 \tag{55}$$

and the input reactance is inductive with an inductance of

$$L \doteq \mu_o b \left( \ln \left( \frac{8b}{a} \right) - 2 \right) \tag{56}$$

The current on a small loop is uniformly distributed and the radiation fields have the form,

$$\vec{E} \sim \hat{\phi} \frac{e^{-jkr}}{r} \sin\theta \ . \tag{57}$$

The input impedances of and the current distributions on loops of moderate size up to $kb = 2.5$ have been tabulated by Storer[3] and King[6, 7]. Radiation patterns in the plane of the loop for loops of size $kb = 1, 2,$ and 3 have been calculated by Sherman[27] under the assumption of a $\cos(kb\phi)$ current distribution. Rao[28] has reported the radiation patterns of loops of size $kb = 1.5, 2.0,$ and 2.5 with both measured results and theoretical results calculated by using the first 5 terms of Storer's series solution.

The input admittances of loop antennas of size $0 \le kb \le 10$ and $\Omega = 2\ln(2\pi b/a) = 12$ and 18 are displayed in Figure 3.8. The corresponding input impedance for the case $\Omega = 12$ is shown in Figure 3.9.

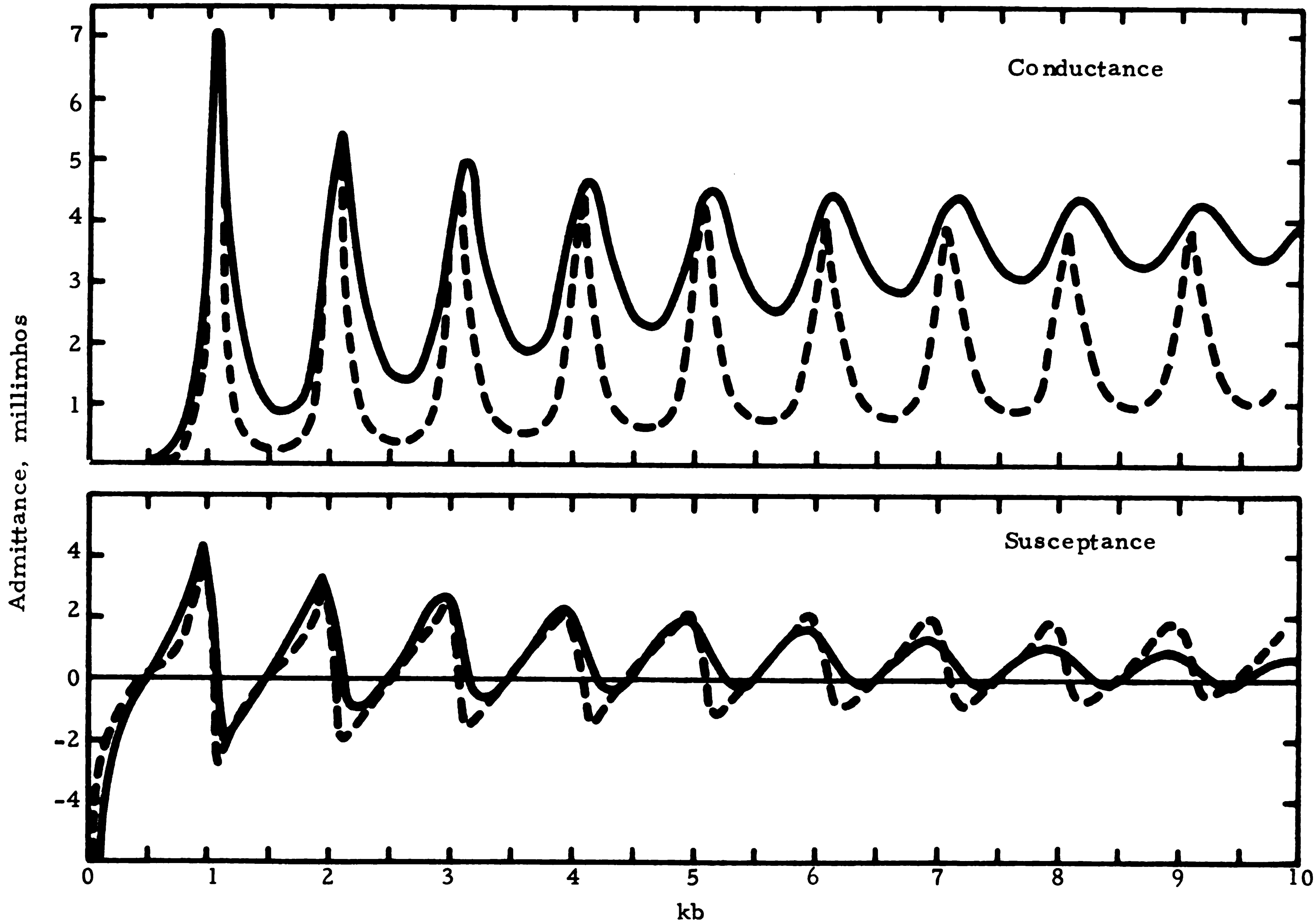


Figure 3.8. Admittance of circular loop antenna driven by a finite gap generator $\delta_o b/a = 12.1$ and ($\Omega = 12$ ———), ($\Omega = 18$ - - - - -).

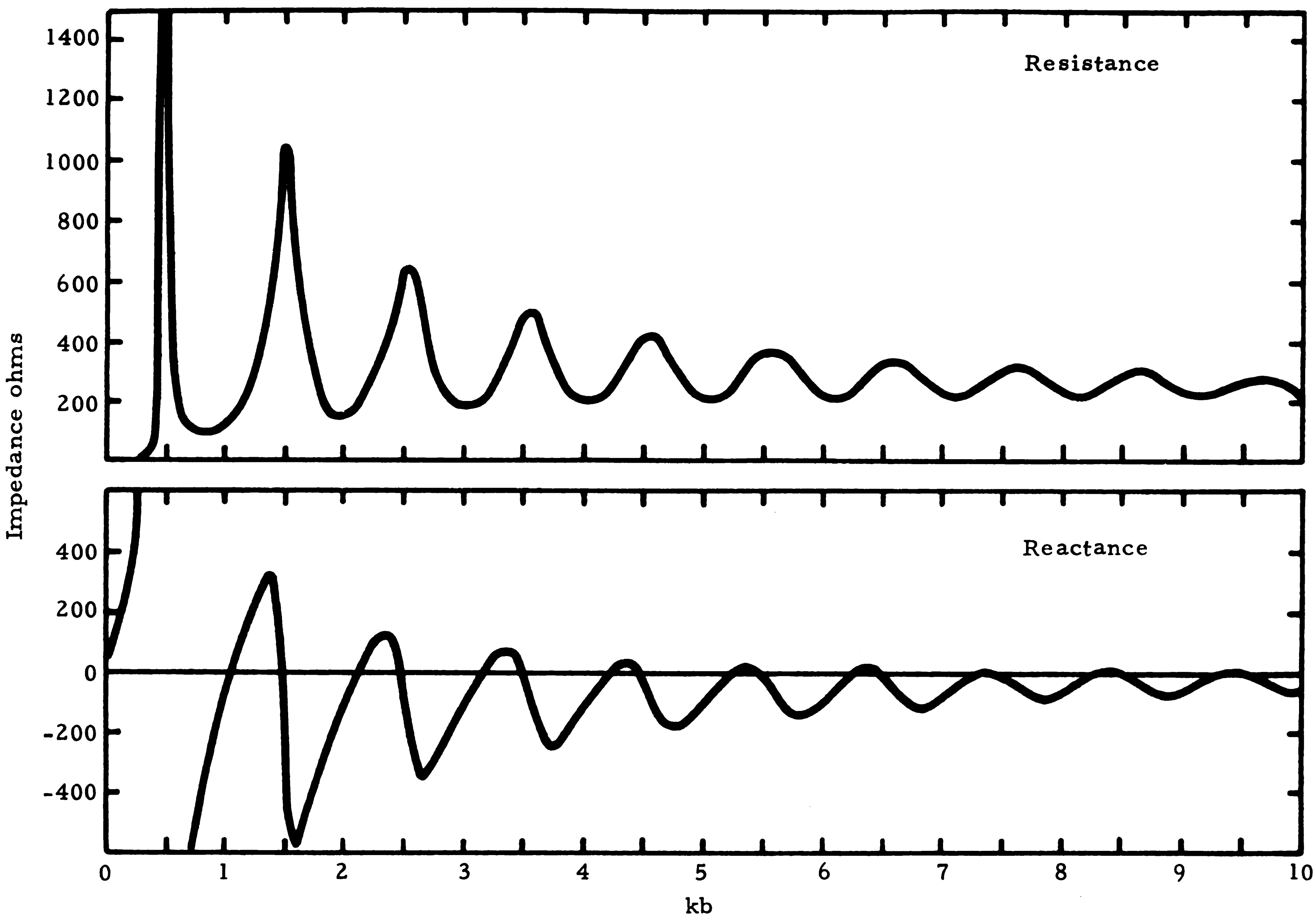


Figure 3.9. Impedance of circular loop antenna driven by a finite gap generator $\delta_o b/a = 12.1$ and $\Omega = 12$.

These impedances and admittances were $\delta_o b/a = 12.1$ which is the effective gap width for a 300 ohm, two wire line.

The current distributions on large loops of size $kb = 5.0$ and 10.0 are displayed in Figures 3.10 and 3.11. It can be seen that the current distribution differs greatly from a cosinusoidal distribution. The current distributions for gap widths of $\delta_o b/a = 6$ and 12 are shown in Figure 3.10. The current distribution for $\delta_o b/a = 6$ is plotted over the range $0^o < \phi < 8^o$ which is the only region where it significantly differs from the other distribution. A numerical study over a range of loop sizes of $0 < kb \leq 5$ showed that the gap width only affected the current distribution in and very near the gap region itself.

Loop antenna gain patterns for loop sizes of $kb = 1$, 1.5, 5, and 10 are shown in Figures 3.12, 3.13, 3.14, and 3.15. The figures display the patterns in: (a) the $\phi = 0^o$ plane; (b) the $\phi = 90^o$ plane, and (c) the $\theta = 90^o$ plane which is the plane of the loop sometimes called the $\vec{E}$-plane of the loop. The $\vec{E}$-field is polarized in the $\phi$ direction in the $\phi = 0^o$ and $\theta = 90^o$ planes and has both a $\theta$ and $\phi$ component in the $\phi = 90^o$ plane. The ratio of $|E_\theta|$ to the magnitude of the total field is also shown in part (b) of each figure.

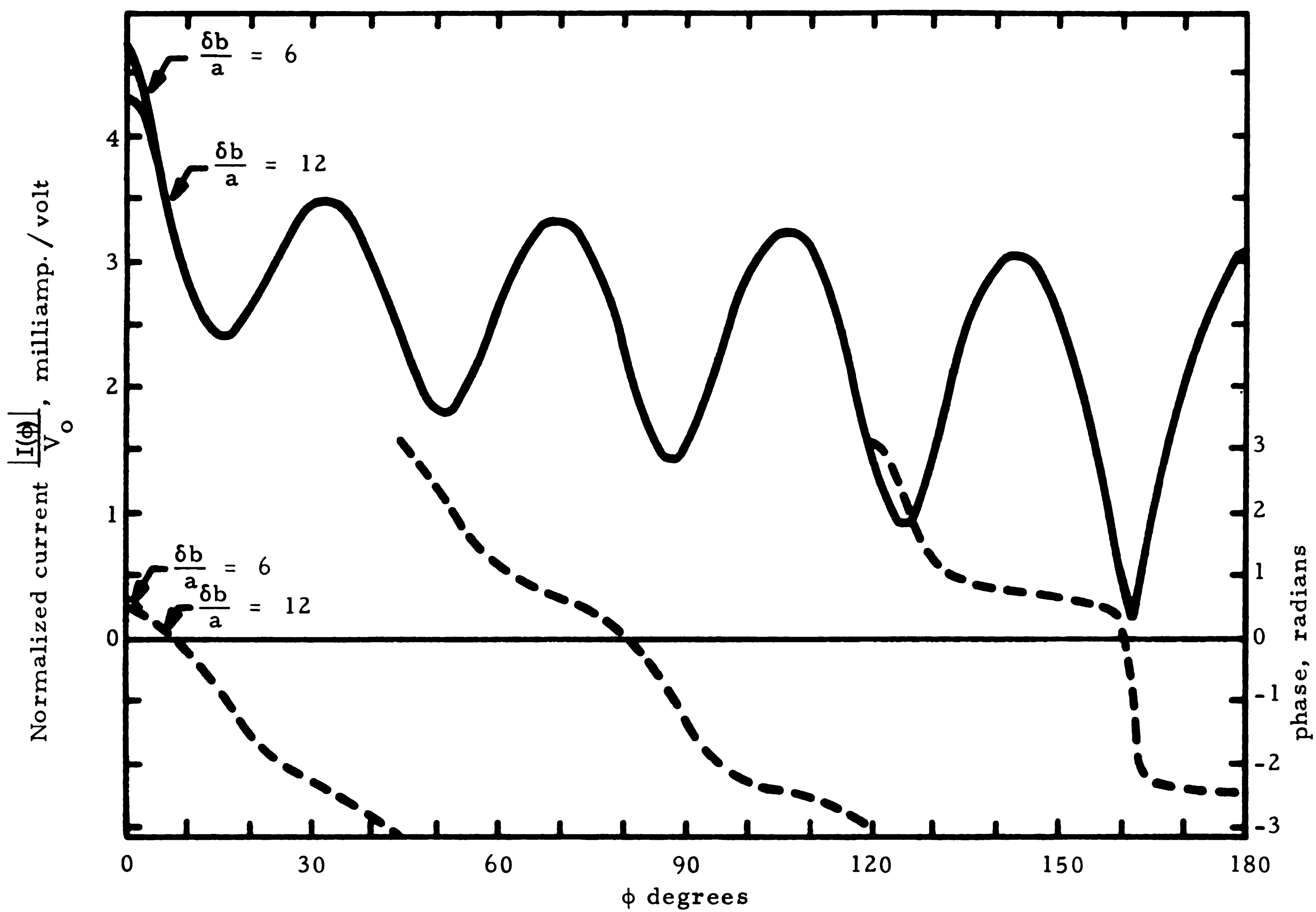


Figure 3.10. Magnitude and phase of the current distribution on a loop antenna with kb = 5.0, $\Omega = 12$, $\delta b/a = 12$, (——— magnitude), (- - - - - phase).

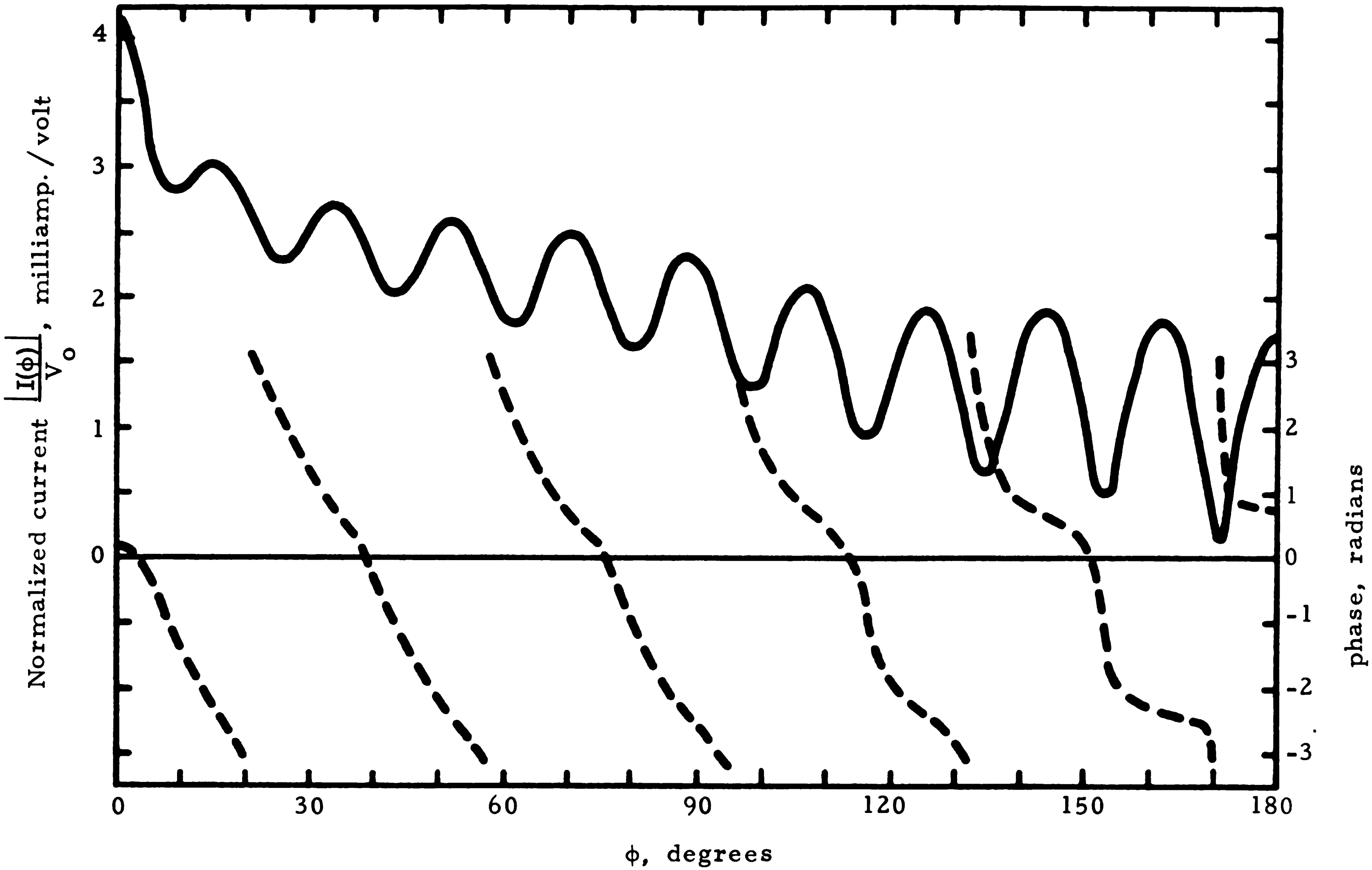


Figure 3.11. Magnitude and phase of the current distribution on a loop antenna with kb = 10.0, $\Omega = 12$, $\delta b/a = 12$, (——— magnitude) (- - - - - phase).

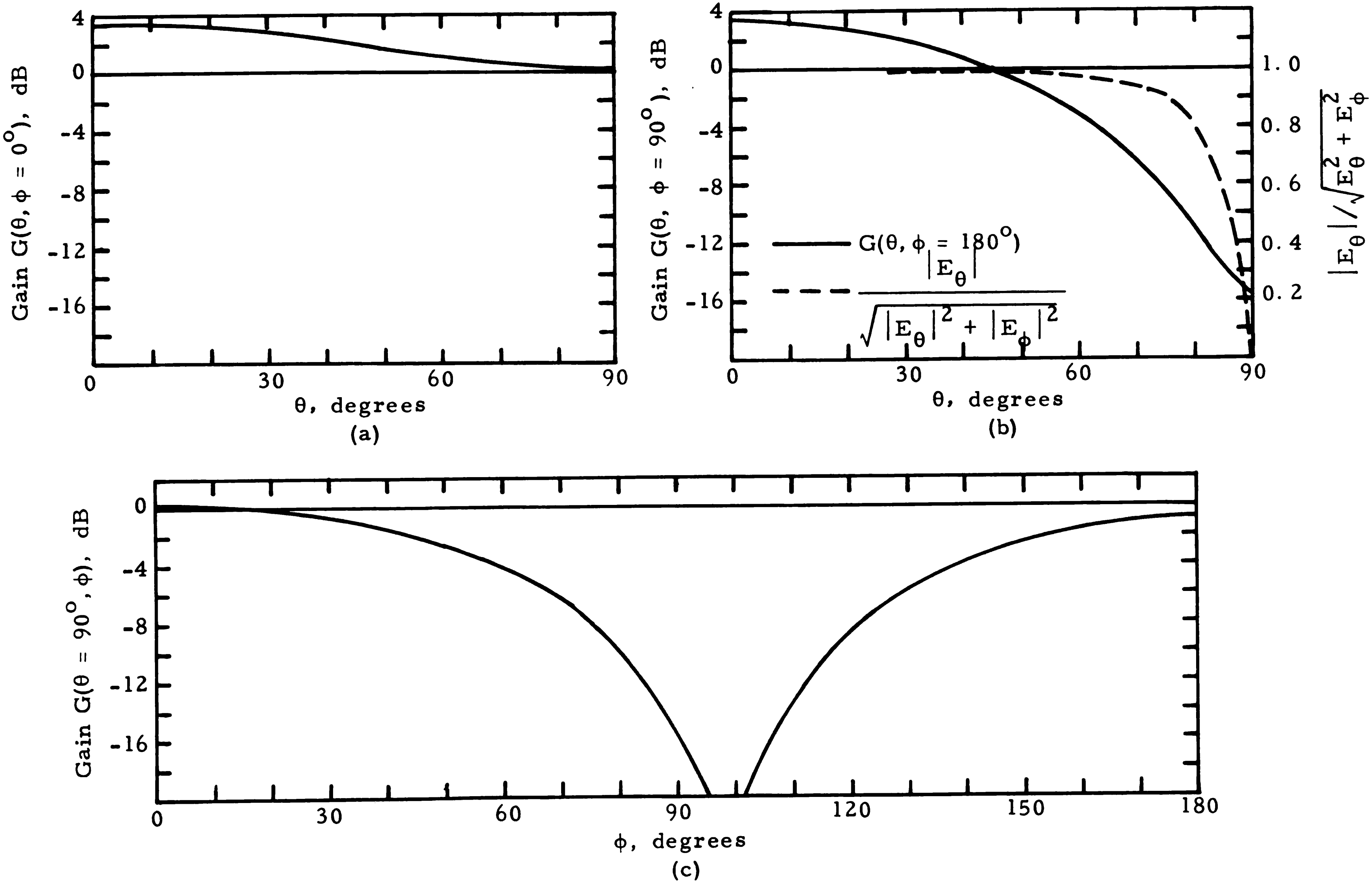


Figure 3.12. Gain patterns of a loop antenna with kb = 1.0, $\Omega$ = 12, and $\delta b/a$ = 12. (a) $\phi = 0^o$ plane, (b) $\phi = 90^o$ plane, and (c) $\theta = 90^o$ plane.

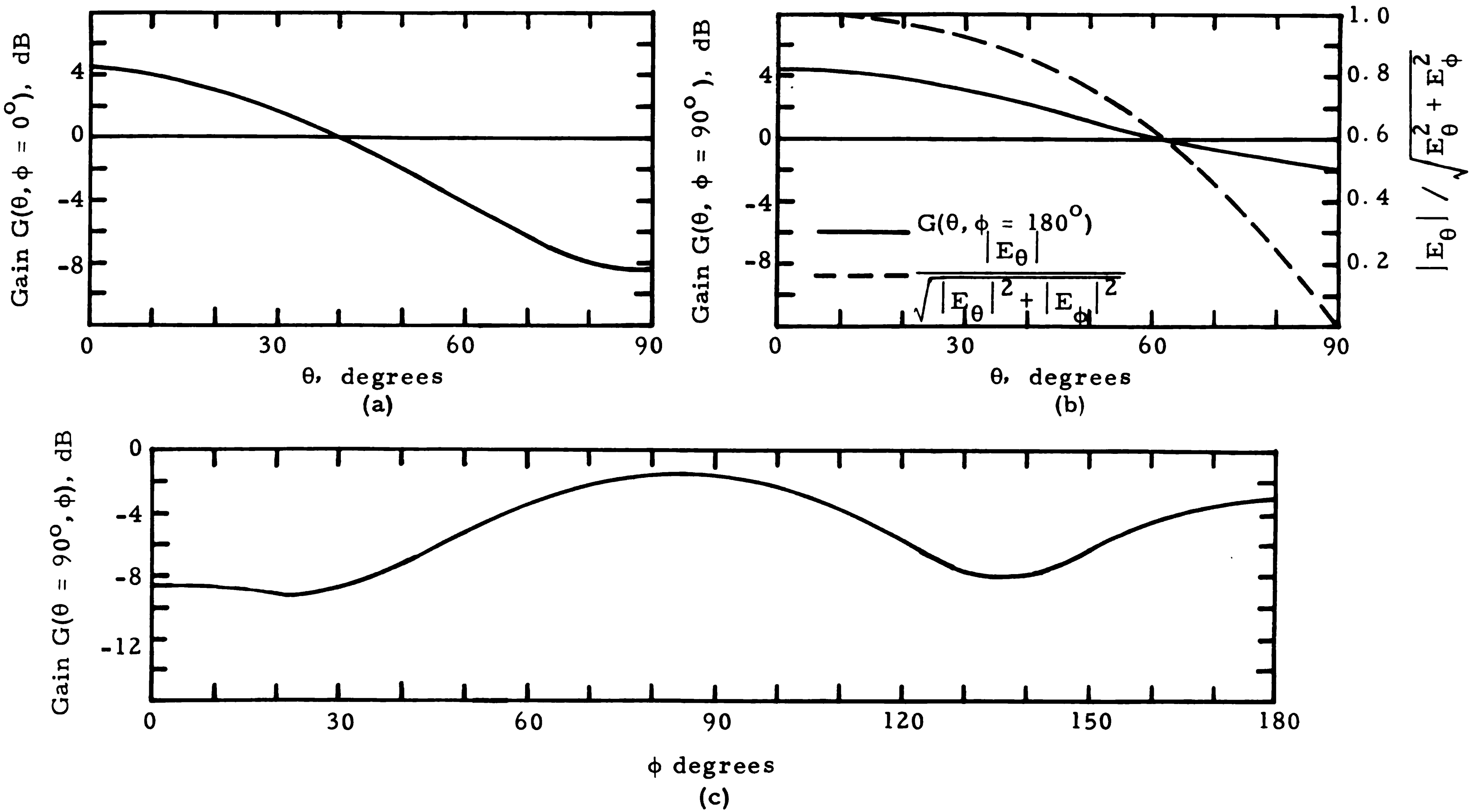


Figure 3.13. Gain patterns of a loop antenna with kb = 1.5, $\Omega$ = 12, and $\delta b/a$ = 12. (a) $\phi = 0^{o}$ plane, (b) $\phi = 90^{o}$ plane, and (c) $\theta = 90^{o}$ plane.

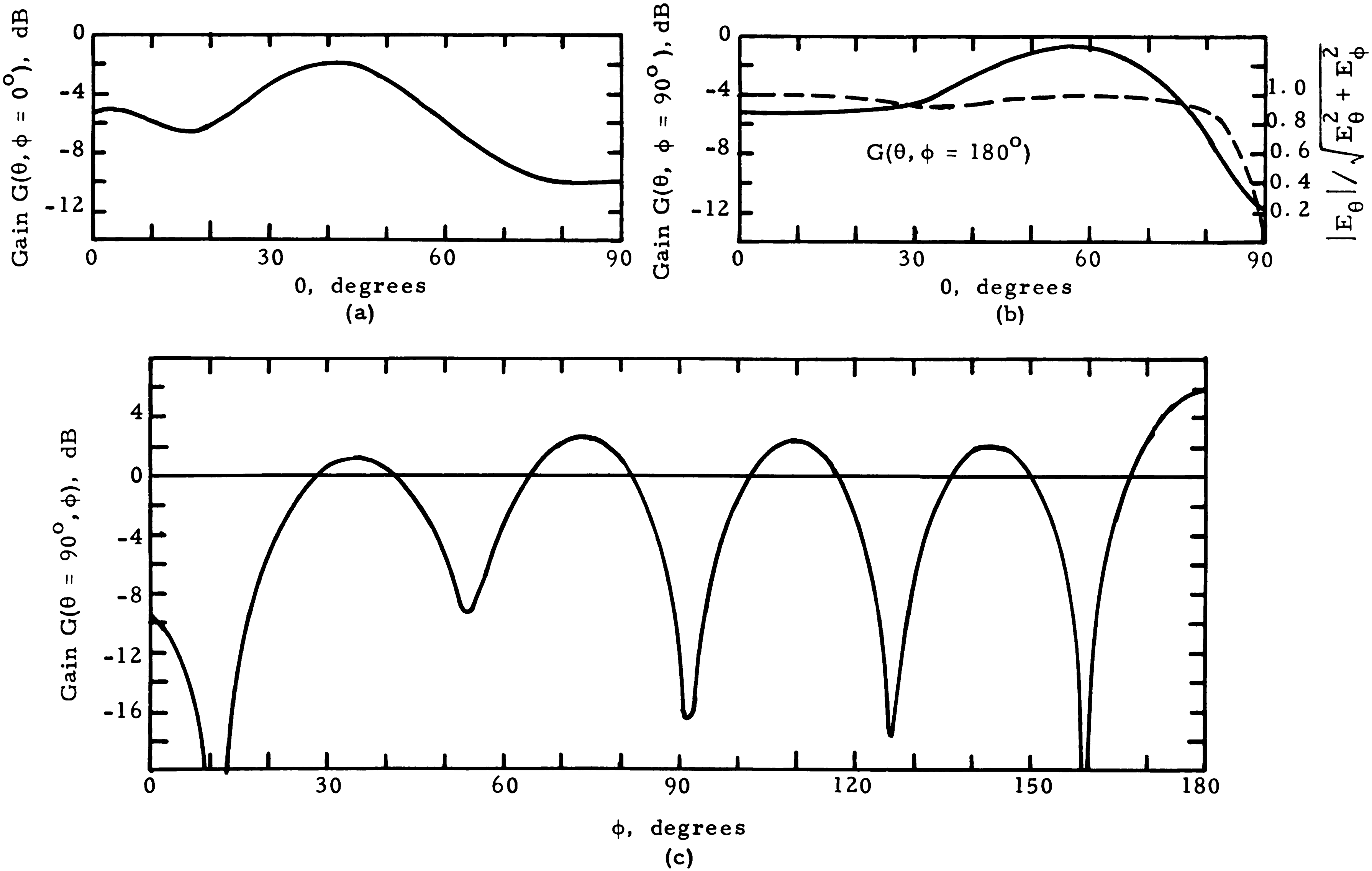


Figure 3.14. Gain patterns of loop antenna with kb = 5.0, $\Omega$ = 12, and $\delta_o b/2$ = 12. (a) $\phi = 0^\circ$ plane, (b) $\phi = 90^\circ$ plane, and (c) $\theta = 90^\circ$ plane.

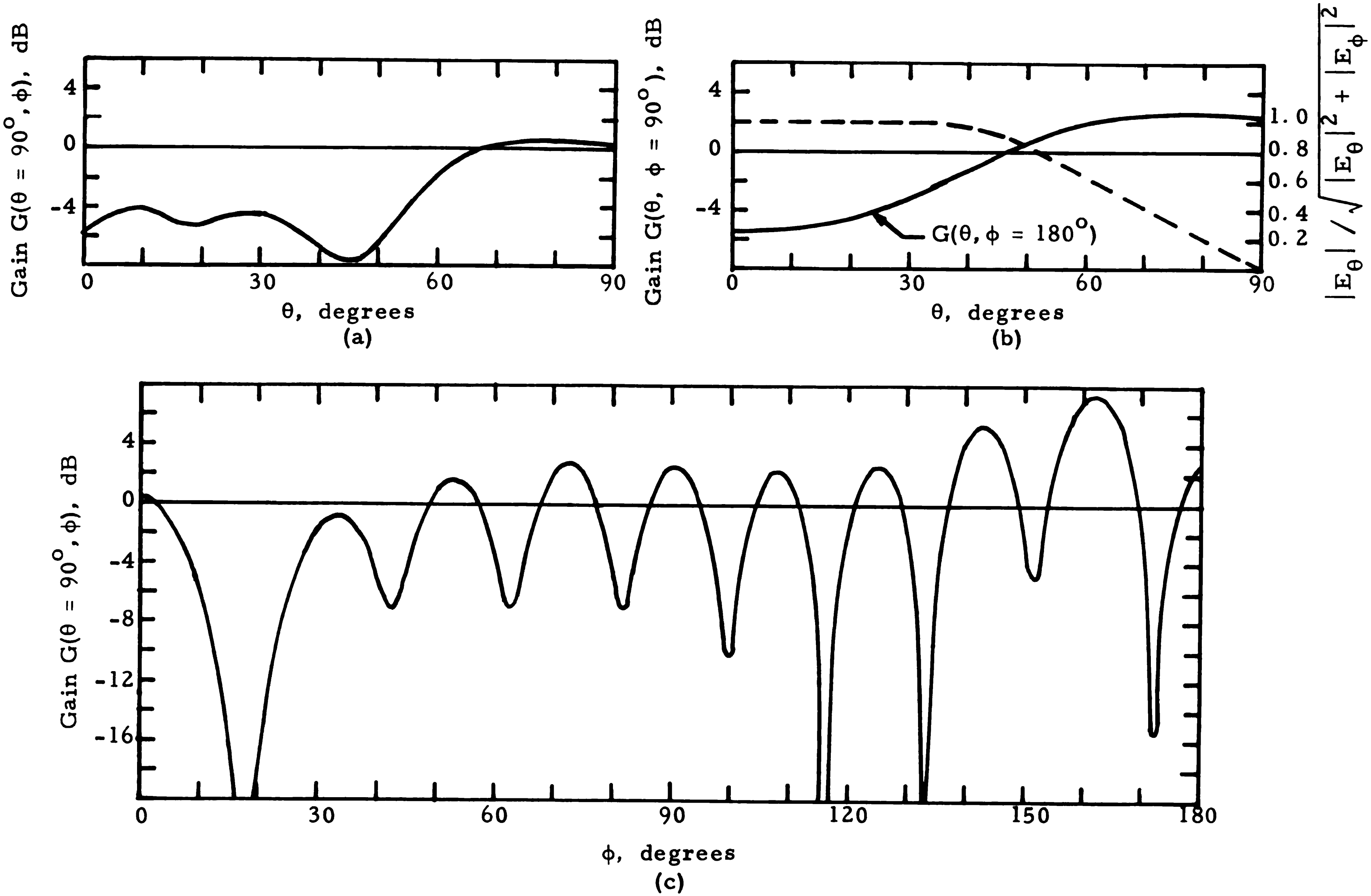


Figure 3.15: Gain patterns of loop antenna with $kb = 10.0$, $\Omega = 12$, and $\delta_o b/2 = 12$. (a) $\phi = 0^o$ plane, (b) $\phi = 90^o$ plane, and (c) $\theta = 90^o$ plane.

# CHAPTER IV

# MODIFICATION OF RADIATION FIELDS AND INPUT IMPEDANCES OF LOOP ANTENNAS BY MULTI-IMPEDANCE LOADING

Several procedures are developed in this chapter that determine the loadings necessary to realize specific modifications of the radiation and circuit properties of loaded loop antennas.

## 4.1. A Loop Loaded with a Single Impedance

A simple, approximate formula is developed in this section that shows the essential characteristics of radiation patterns of loops of size $kb \leq 1.0$ loaded with a single impedance.

Examining Figure 3.1 and equations (48) and (49) indicates that the radiation fields of loops of size $kb \leq 1.0$ can be approximated fairly well by the first three terms of their series solutions. With this series truncation and approximating the Bessel functions by

$$J_o(x) \doteq 1 - \left(\frac{x}{2}\right)^2$$

$$J_n(x) \doteq \frac{1}{n!}\left(\frac{x}{2}\right)^n$$

and using the relations

$$J_o'(x) = -J_1(x)$$

$$J_n'(x) = \frac{1}{2}\Big(J_{n-1}(x) - J_{n+1}(x)\Big)$$

equations (48) and (49) become

$$F_{\theta m} \doteq \frac{j}{2a_1} \cos\theta \sin(\phi - \phi_m) - \frac{kb}{4a_2} \sin\theta \cos\theta \sin\Big(2(\phi - \phi_m)\Big) \tag{58}$$

$$F_{\phi m} = -\frac{kb}{4a_o}\sin\theta + \frac{j}{2a_1}\left(1-\frac{3}{8}(kb)^2\sin^2\theta\right)\cos(\phi-\phi_m)$$
$$-\frac{kb}{4a_2}\sin\theta\cos\left(2(\phi-\phi_m)\right) \tag{59}$$

When a loop is loaded with a single impedance the load is usually located at $\phi_1 = 180^o$. This retains the symmetry of the loop, and for kb ≤ 1 it is the point at which maximum current occurs with the exception of points near the driving point. With the restriction N = 1 and $\phi_1 = 180^o$

$$F_\theta = F_{\theta o} - \overline{V}_1 F_{\theta 1}$$
$$= \frac{j}{2a_1}[1+\overline{V}_1]\cos\theta\sin\phi$$
$$-\frac{kb}{4a_2}[1-\overline{V}_1]\cos\theta\sin\theta\sin(2\phi) \tag{60}$$

and

$$F_\phi = F_{\phi o} - \overline{V}_1 F_{\phi 1}$$
$$\doteq \frac{kb}{4a_o}[1-\overline{V}_1]\sin\theta + \frac{j}{2a_1}[1+\overline{V}_1]\left(1-\frac{3}{8}(kb)^2\sin^2\theta\right)\cos\phi$$
$$-\frac{kb}{4a_2}[1-\overline{V}_1]\sin\theta\cos(2\phi) \tag{61}$$

where

$$\overline{V}_1 = \frac{y_1}{y_{11}+Y_1} = \frac{y_1 Z_1}{1+y_{11}Z_1} \tag{62}$$

is found from equation (30).

Consider two cases, a small loop kb = 0.1 and a resonant loop kb = 1.0. First, when kb = 0.1 and Ω = 12

$$\left(\frac{1}{a_o}\right) \doteq 7.4 + j9.1\times10^{-4} \doteq 7.4$$

$$\left(\frac{1}{a_1}\right) \doteq -0.075 + j1.8\times10^{-5} \doteq -0.075$$

$$(\frac{1}{a_2}) \doteq -0.022 + j\,2.4 \times 10^{-9} \doteq -0.022$$

$$y_1 \doteq 7.4 \times 10^{-7} - j\,6.3 \times 10^{-3} \text{ mhos}$$

$$y_{11} \doteq 8.0 \times 10^{-7} - j\,6.0 \times 10^{-3} \text{ mhos}$$

and equations (60) and (61) become

$$F_\theta \doteq -j\,0.037[1+\overline{V}_1] \cos\theta \sin\phi + 0.0005[1-\overline{V}_1] \cos\theta \sin\theta \sin(2\phi)$$

$$\doteq j\,0.037[1+\overline{V}_1] \cos\theta \sin\phi \tag{63}$$

$$F_\phi \doteq -0.18[1-\overline{V}_1] \sin\theta - j\,0.037[1+\overline{V}_1] \cos\phi \tag{64}$$

For the case of small loops the terms arising from $(1/a_2)$ are always small in comparison with the terms arising from $(1/a_o)$ and quantity $[1 + \overline{V}_1]$ appears in both terms. Thus, the $(1/a_2)$ terms are dropped in equations (63) and (64). This shows that the approximation of dropping higher order terms is very accurate for very small loops.

The radiation fields of the small loaded loop ($\phi_1 = 180^o$) take on two limiting cases. First, when $\overline{V}_1 \doteq 0$ or $|1 + \overline{V}_1| \doteq 0$

$$F_\theta \doteq 0$$

$$F_\phi \sim \sin\theta$$

which is the pattern of the unloaded loop. This gives an omidirectional pattern in the x-y plane and a $\sin\theta$ pattern in the x-z plane. $\overline{V}_1 = 0$ implies $Z_1 = 0$ and $1 + \overline{V}_1 = 0$ implies $Z_1 \doteq -0.01 - j\,81$ ohms. The second limiting case arises when $|1 - \overline{V}_1| \doteq 0$. The fields then become

$$F_\theta \sim \cos\theta \sin\phi$$

$$F_\phi \sim \cos\phi$$

This gives a $\cos\phi$ pattern in the x-y plane and an omidirectional pattern in the x-z plane which is just a rotation of the first limiting case. $|1 - \overline{V}_1| \doteq 0$ arises when $|Z_1| \to \infty$ or when $Z_1 \doteq -0.67 + j\,3300$ ohms.

Now consider the second case with $kb = 1.0$ and $\Omega = 12$.

$$\left(\frac{1}{a_o}\right) \doteq 0.67 + j\,0.061 \doteq 0.67$$

$$\left(\frac{1}{a_1}\right) \doteq -2.1 + j\,3.0$$

$$\left(\frac{1}{a_2}\right) \doteq -0.29 + j\,0.0032 \doteq -0.29$$

$$y_1 \doteq -5.0 \times 10^{-3} - j\,3.7 \times 10^{-3}$$

$$y_{11} \doteq 5.1 \times 10^{-3} + j\,4.1 \times 10^{-3}$$

With these coefficients

$$F_\theta \doteq -(1.5 + j1.1)[1 + \overline{V}_1] \cos\theta \sin\phi + 0.075[1 - \overline{V}_1] \cos\theta \sin\theta \sin(2\phi) \qquad (65)$$

$$\begin{aligned} F_\phi &\doteq -0.17[1 - \overline{V}_1] \sin\theta - (1.5 + j1.1)[1 + \overline{V}_1]\left(1 - \frac{3}{8}\sin^2\theta\right) \cos\phi \\ &\qquad + 0.075[1 - \overline{V}_1] \sin\theta \cos(2\phi) \\ &= -0.17[1 - \overline{V}_1] \;\; 1 - 0.44\cos(2\phi) \;\; \sin\theta \\ &\qquad - (1.2 - j\,0.89)[1 + \overline{V}_1]\Big(1 + 0.23\cos(2\theta)\Big) \cos\phi \end{aligned} \qquad (66)$$

In the x-y plane ($\theta = 90^\circ$)

$$F_\theta = 0$$

$$F_\phi = -0.17[1 - \overline{V}_1]\Big(1 - 0.44\cos(2\phi)\Big) - (0.93 + j69)[1 + \overline{V}_1] \cos\phi$$

and in the x-z plane ($\phi = 0^\circ,\ 180^\circ$)

$$F_\theta = 0$$

$$F_\phi = -0.095[1 - \overline{V}_1] \sin\theta \mp (1.2 + j0.89)[1 + \overline{V}_1]\Big(1 + 0.23\cos(2\theta)\Big) \quad \text{for } \theta = \begin{cases} 0^\circ \\ 180^\circ \end{cases}.$$

Once again it is seen that there are two limiting cases of the loaded radiation pattern.

None of the equations developed in this section are used in actual calculations.

## 4.2. Maximum and Minimum Gain of a Loop Loaded with a Single Impedance

Many times it is of interest to determine the maximum and minimum gain or directivity of an antenna, in a given direction. For the case of the loaded antenna it is also of interest to determine the optimum loadings that result in the maximum or minimum gain. If no restrictions are placed on the load impedances, it is found that many times the optimum load impedances have large negative real parts. To eliminate this in this discussion, the load resistance is assumed to have a fixed value and only the reactive part of the load is optimized. For simplicity, the additional restriction is made that the direction in which the gain is to be optimized is in the plane $\theta = 90^{\circ}$.

The gain of a loop loaded with one impedance is found from equation (51) to be

$$G(\theta=90^{\circ}, \phi) = \frac{8(kb)^2}{\zeta_o \pi} \frac{|F_{\phi}|^2}{Y_{in} + Y_{in}^*} \tag{67}$$

where the * sign denotes the complex conjugate of the quantity, and

$$F_{\phi} = F_{\phi o} - \overline{V}_1 F_{\phi 1}$$

$$Y_{in} = y_o - \overline{V}_1 y_1$$

and from equation (30)

$$\overline{V}_1 = \frac{y_1}{y_{11} + G_1 + jB_1}$$

where $G_1$ is the fixed load conductance and $B_1$ is the load susceptance to be optimized. After some algebra it is found

$$G(\theta=90^{\circ}, \phi) = \frac{8(kb)^2}{\zeta_o \pi} \frac{A + CB_1 + DB_1^2}{H + IB_1 + JB_1^2} \tag{68}$$

where

$$A = |F_{\phi o}|^2 |y_{11}+G_1|^2 - 2 \text{ Real } [F_{\phi o}^* F_{\phi 1} y_1 (y_{11}^* + G_1)] + |F_{\phi 1}|^2 |y_1|^2$$

$$C = 2 \text{ Imag } [y_{11}] \; |F_{\phi o}|^2 - 2 \text{ Imag } [F_{\phi o}^* F_{\phi 1} y_1]$$

$D = |F_{\phi o}|^2$

$H = 2 \text{ Real } [y_o] \; |y_{11} + G_1|^2 - 2 \text{ Real } [y_1^2 (y_{11}^* + G_1)]$

$I = 4 \text{ Real } [y_o] \text{ Imag } [y_{11}] - 2 \text{ Imag } [y_1^2]$

$J = 2 \text{ Real } [y_o]$

are real constants and "Real" and "Imag" are operators which retain only the real and imaginary part of a complex quantity, rexpectively. Differentiating equation (68) with respect to $B_1$ and setting this result equal to zero gives

$$(DI - JC) B_1^2 + 2 (DH - JA) B_1 + (CH - IA) = 0 \tag{69}$$

which can easily be solved for $B_1$.

Several examples of the special case of a purely reactive loading (i.e., $R_1 = 0$) are now considered. Figure (4.1) displays the maximum and minimum gain and corresponding optimum load reactances of a loop with kb = 1 loaded at $\phi_1 = 180^o$ as a function of the position where the gain is maximized. The unloaded loop gain is also displayed. Figures (4.2) and (4.3) display the maximum and minimum gains in the directions $\phi = 90^o$ and $\phi = 180^o$ and corresponding optimum reactances as a function of loop size kb. Corresponding gain patterns for kb = 1.0 and kb = 5.0 are given in Figures (4.4) and (4.5).

It was found that by introducing a resistance into the load impedance, the ability to modify the radiation is increased in many cases.

## 4.3. Modification and Design of Radiation Patterns of Loops by Multi-Impedance Loading

A method of determining the load impedances necessary to produce specific modifications in the radiation pattern of a loaded loop antenna is developed in this section. The idea is simply to specify the radiation pattern in N directions which determines a set of N simultaneous linear, algebraic equations in terms of the N unknown, normalized load voltages. This set of equations may be solved, and the load impedances are determined from the normalized load voltages.

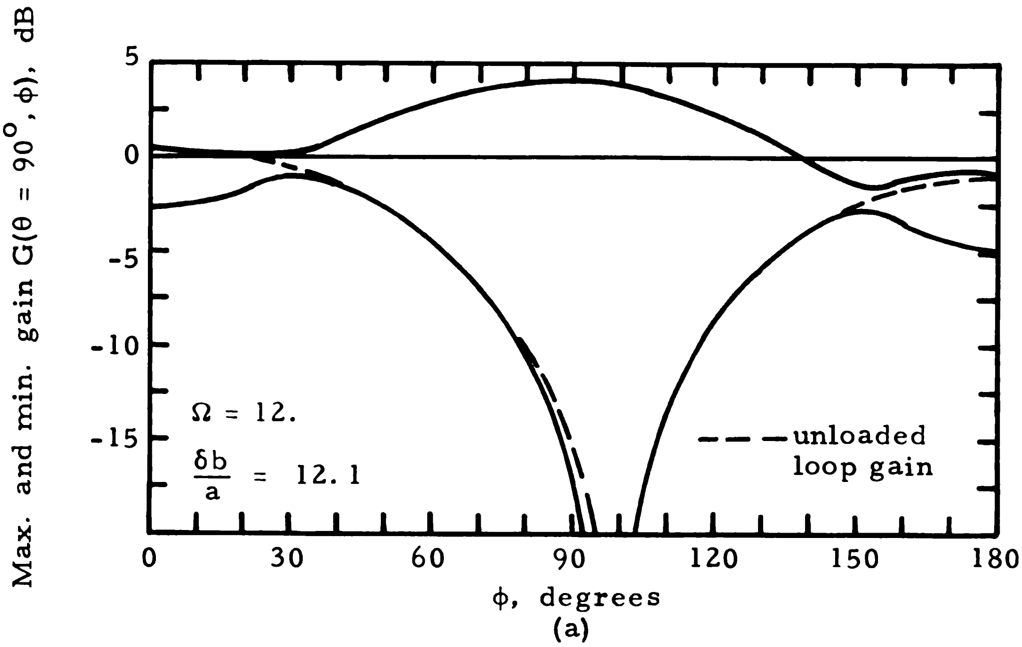


(a)

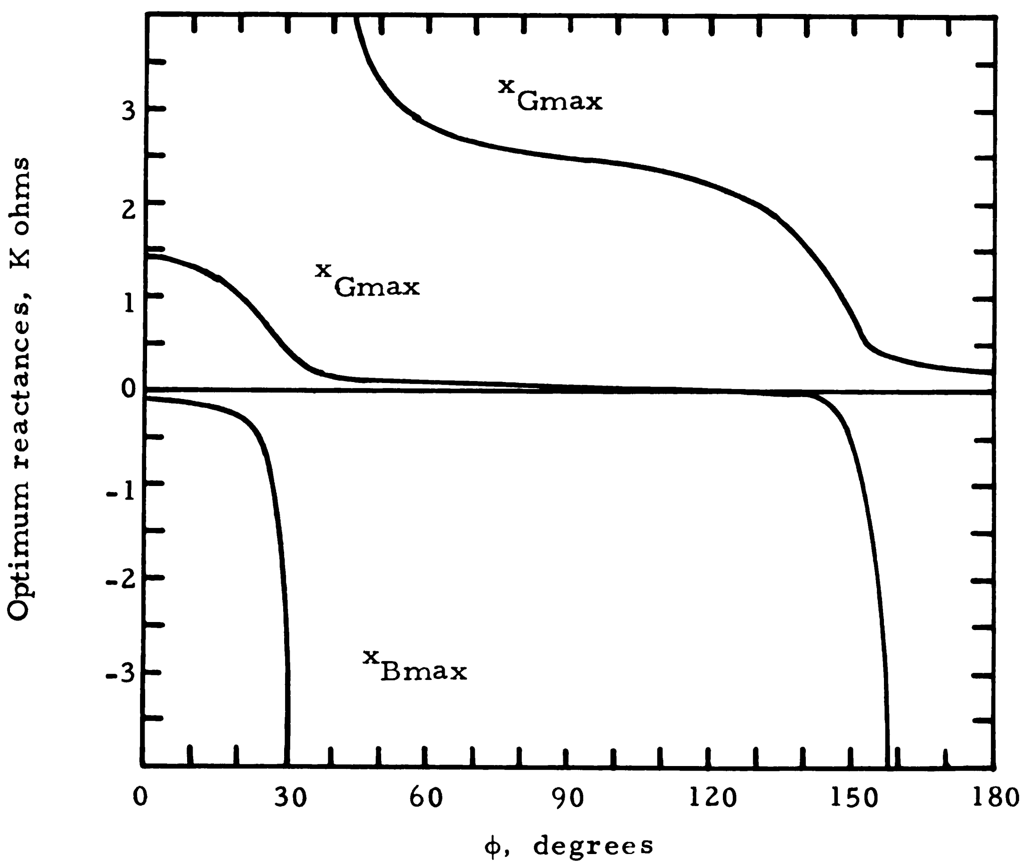


(b)

Figure 4. 1. (a) Maximum and Minimum gain of a loop antenna kb = 1. 0 loaded at $\phi_1 = 180^o$ with a purely reactive load.
(b) Optimum load reactances for maximum and minimum gain.

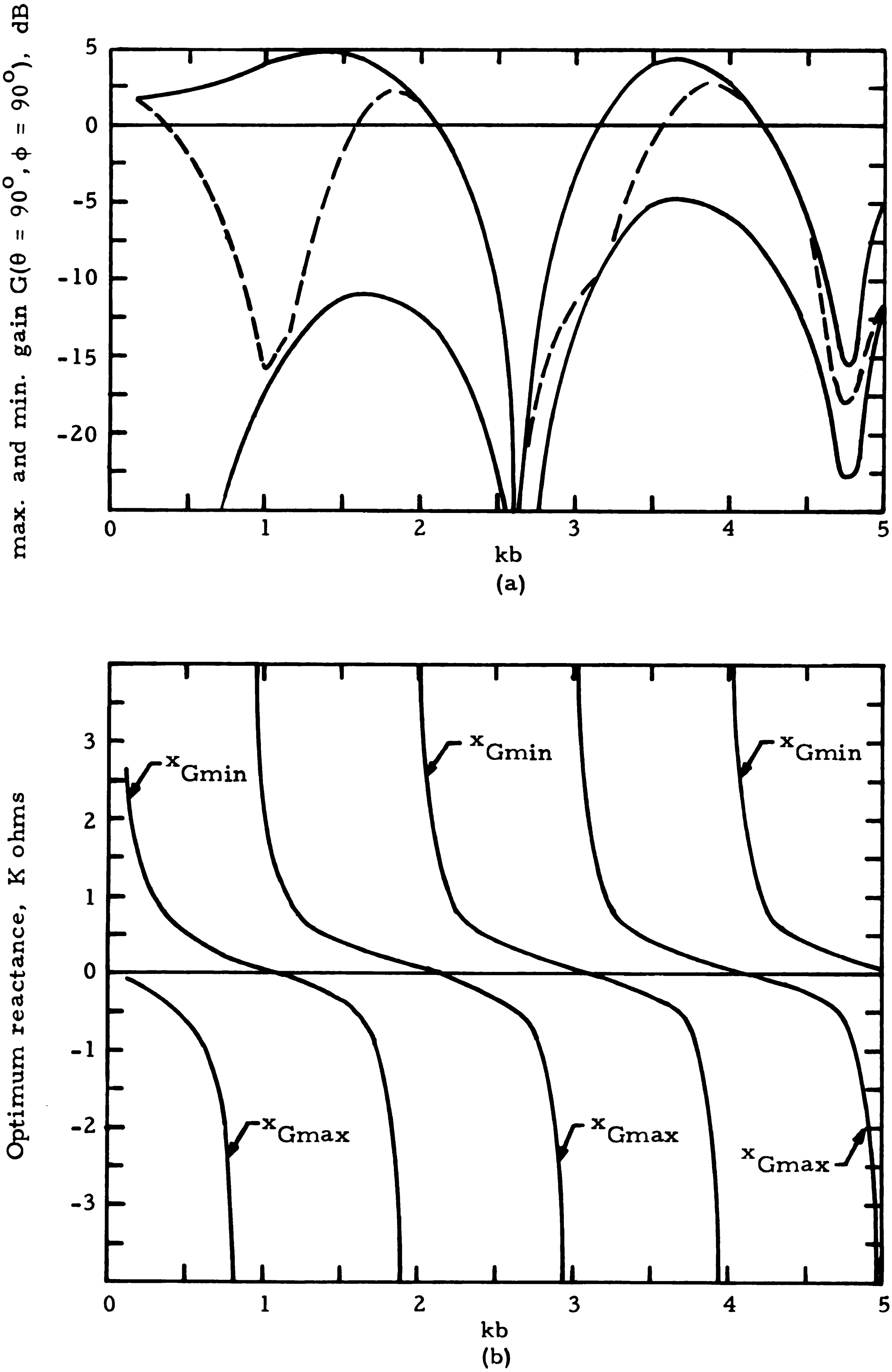


Figure 4. 2. (a) Maximum and Minimum gain in direction $\theta = 90^{\circ}$, $\phi = 90^{\circ}$ of a loop antenna loaded at $\phi_o = 180^{\circ}$ with a purely reactive load as a function of kb. (b) Optimum load reactances for max. and min. gain in direction

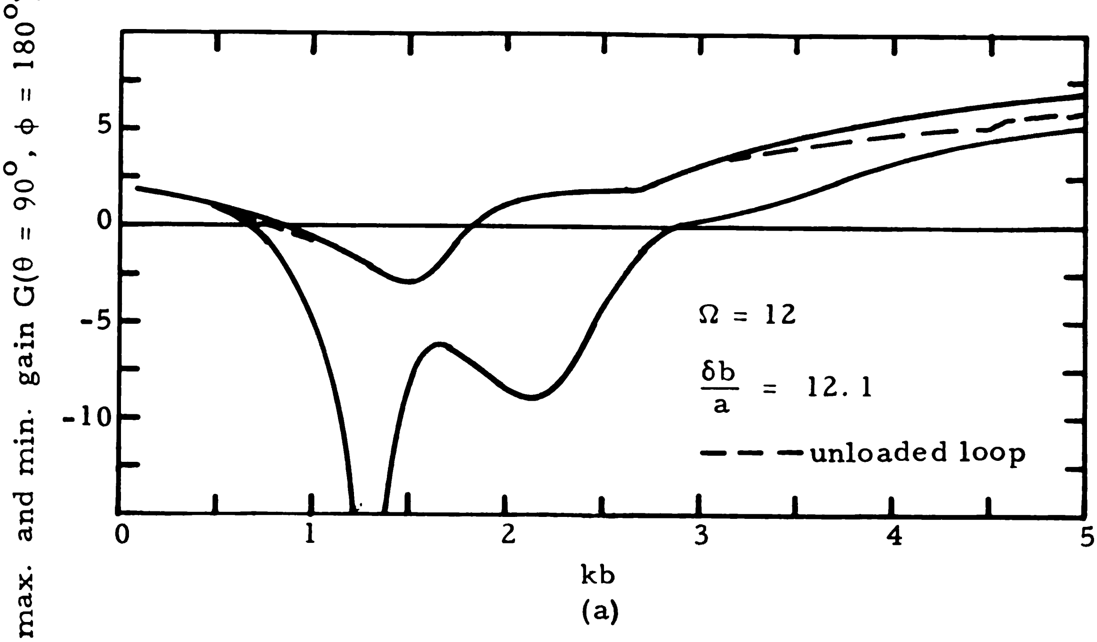


(a)

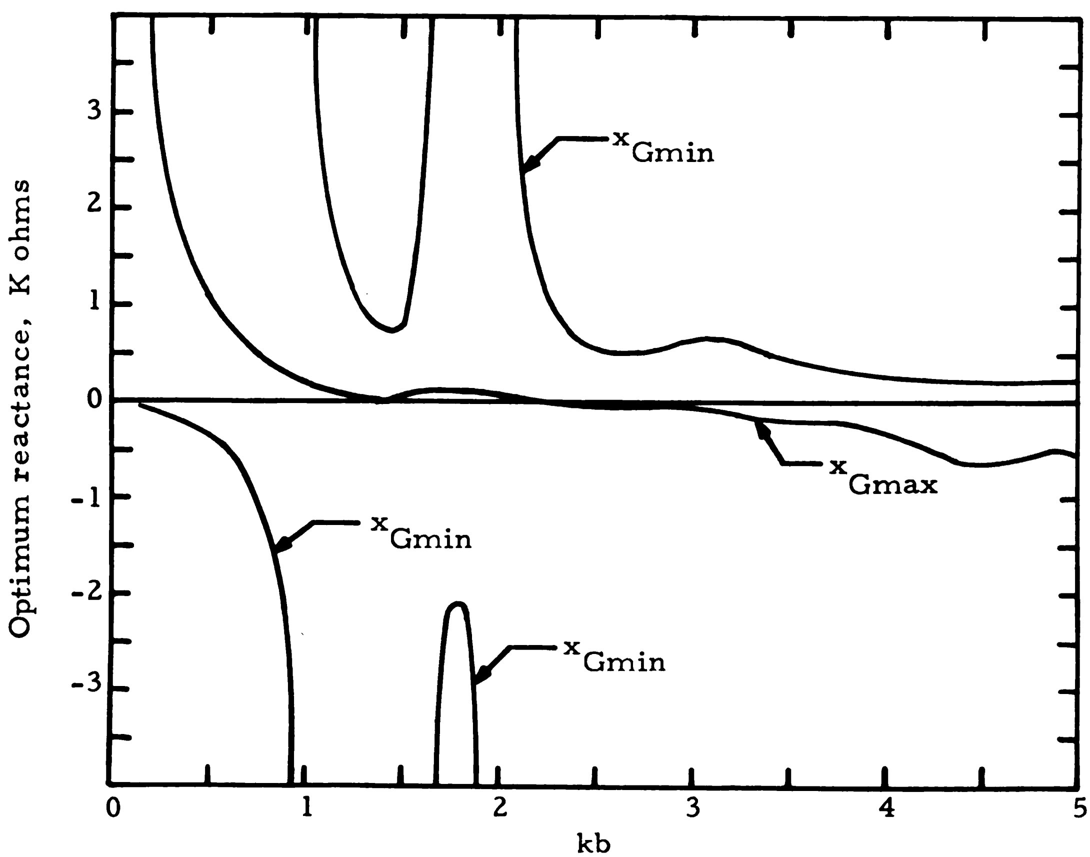


(b)

Figure 4.3. (a) Maximum and Minimum gain in direction $\theta = 90^{\circ}$, $\phi = 180^{\circ}$ of a loop antenna loaded at $\phi_o = 180^{\circ}$ with a purely reactive load as a function of kb. (b) Optimum load reactances for max. and min. gain in direction $\theta = 90^{\circ}$, $\phi = 180^{\circ}$.

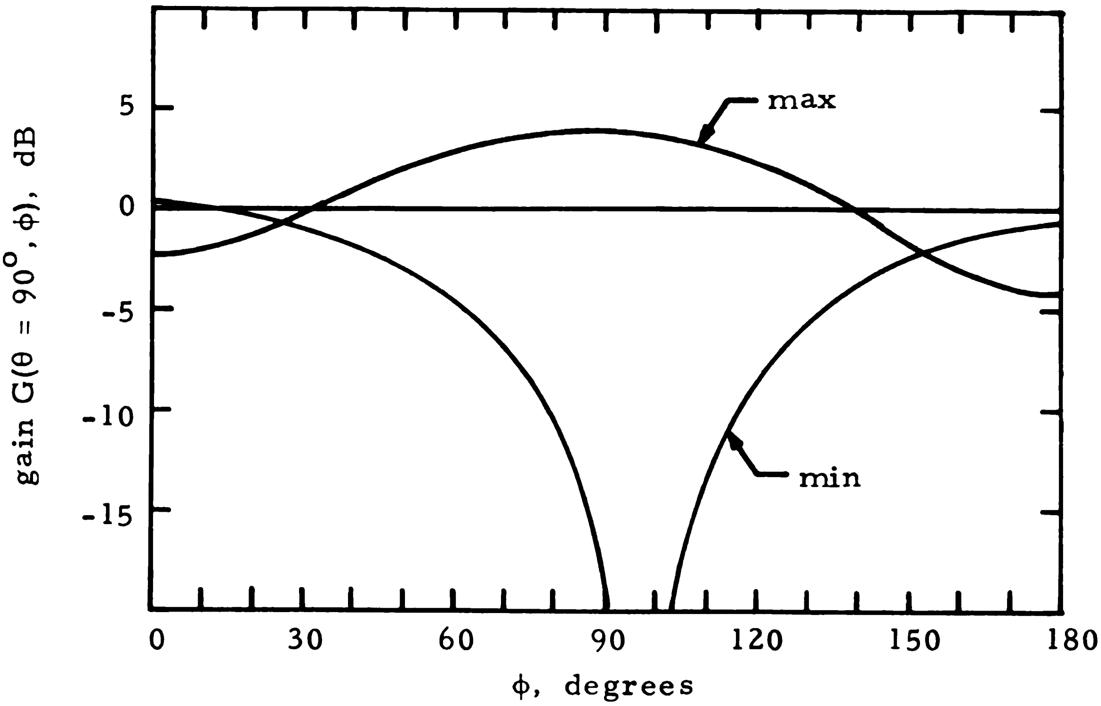


(a)

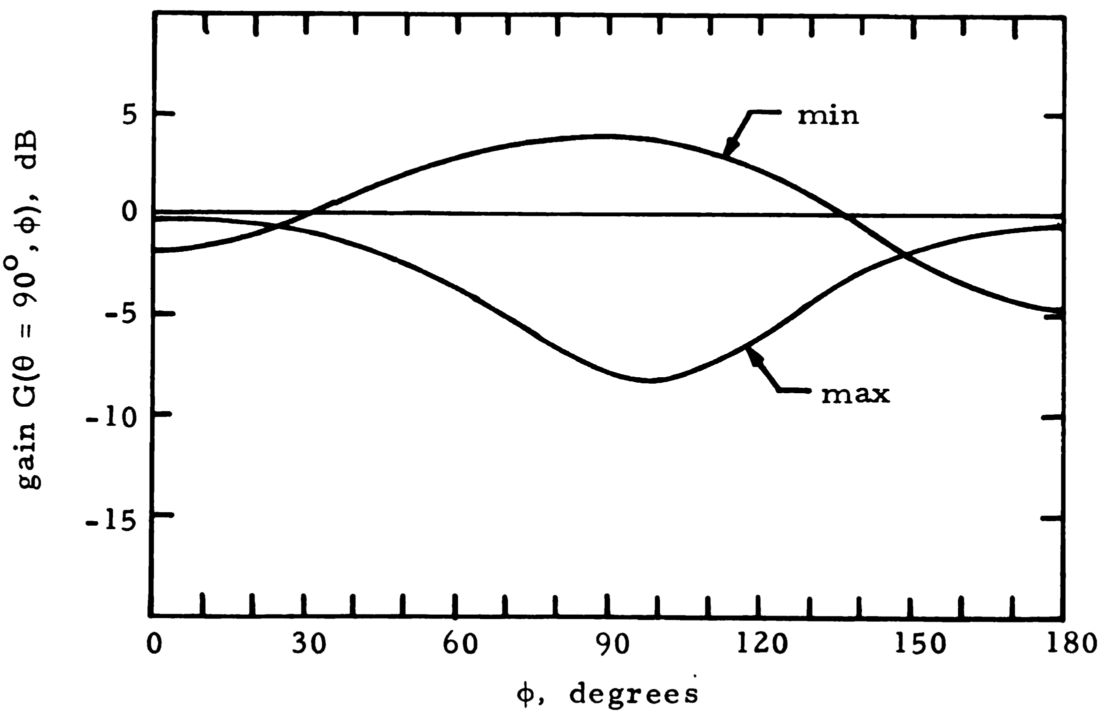


(b)

Figure 4. 4. Gain pattern of loop antenna kb = 1. 0 loaded at $\phi = 180^{\circ}$ with a purely reactive load for minimum and maximum gain at: (a) $\phi = 90^{\circ}$ and (b) $\phi = 180^{\circ}$.

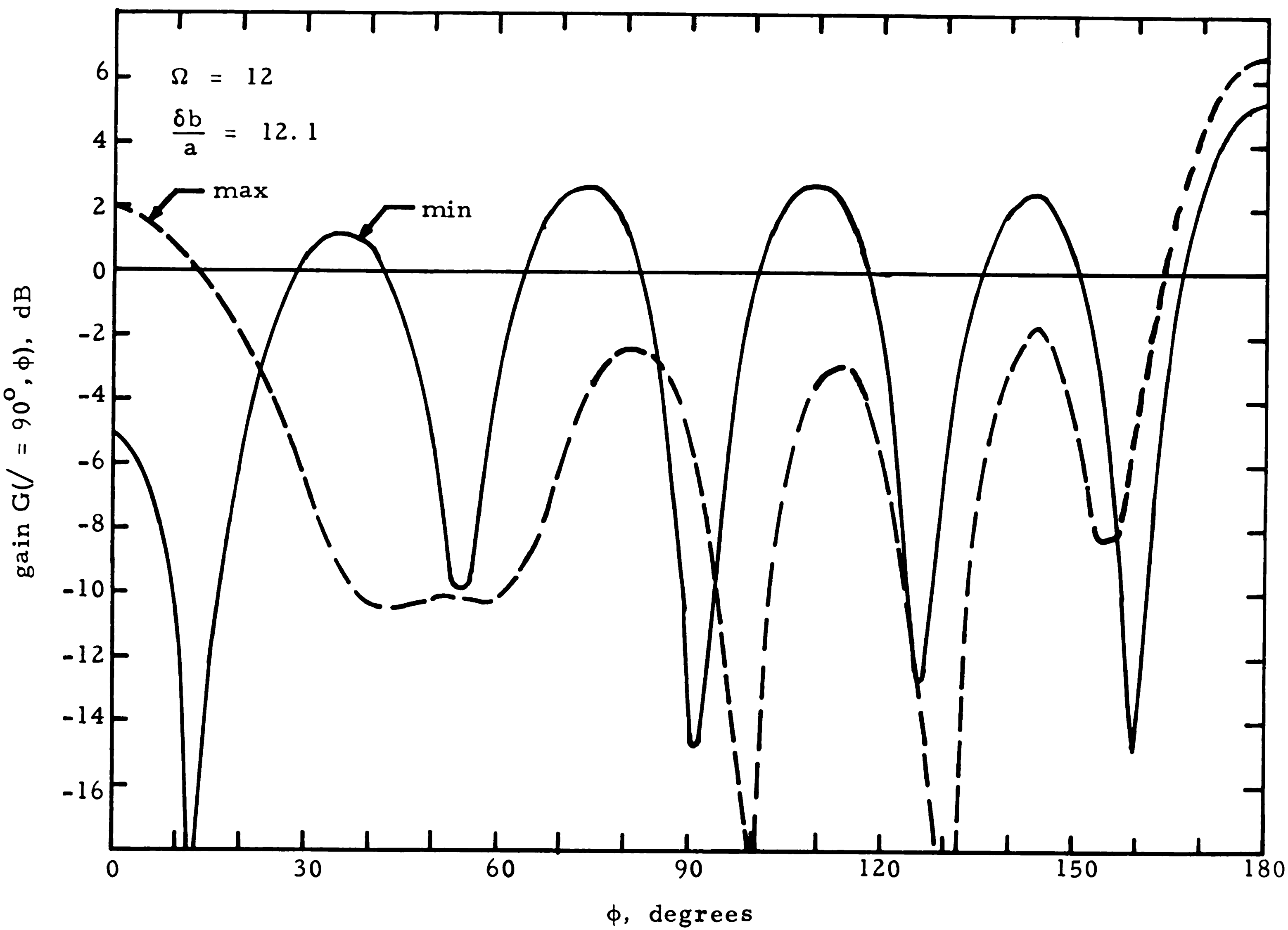


Figure 4.5. Gain pattern of a loop antenna kb = 5.0 loaded at $\phi = 180^{\circ}$ with a purely reactive load for minimum and maximum gain at $\phi = 90^{\circ}$.

Consider a loop antenna loaded with N arbitrary load impedances. The radiation pattern function of either the $\theta$ or $\phi$ component of the radiation zone electric field may be written as

$$F(\theta, \phi) = F_o(\theta, \phi) - \sum_{n=1}^{N} F_n(\theta, \phi) \overline{V}_n \tag{70}$$

[See equations (44) through (49) where $F_n$ represents either $F_{\theta n}$ or $F_{\phi n}$]. It is convenient to work with pattern functions that have been normalized to the unloaded pattern function. With this in mind, the following normalization is defined:

$$f = \frac{F(\theta, \phi)}{F_o(\theta, \phi)}$$

$$f_n = \frac{F_n(\theta, \phi)}{F_o(\theta, \phi)}$$

and equation (70) becomes

$$f = 1 - \sum_{n=1}^{N} \overline{V}_n f_n \tag{71}$$

The normalized unloaded loop radiation pattern is a unit sphere so that changes in the unloaded loop pattern are easily specified. This eliminates the need to know the exact values of the unloaded loop radiation pattern and for most applications the general shape of the unloaded pattern is all that is needed.

The value of the normalized pattern is specified in N directions. With equation (71) this yields the following system of N equations

$$f(\theta_m, \phi_m) = 1 - \sum_{n=1}^{N} \overline{V}_n f_n(\theta_m, \phi_m) \tag{72}$$

$$m = 1, 2, \ldots, N .$$

Defining

$$f_m = f(\theta_m, \phi_m) \quad \text{and} \quad f_{mn} = f_n(\theta_m, \phi_m) \tag{73}$$

equations (72) can be written in matrix form as

$$\begin{bmatrix} 1 - f_1 \\ 1 - f_2 \\ \cdot \\ \cdot \\ \cdot \\ 1 - f_N \end{bmatrix} = \begin{bmatrix} f_{11} & f_{12} & \cdots & f_{1N} \\ f_{21} & f_{22} & & \\ \cdot & & & \\ \cdot & & & \\ \cdot & & & \\ f_{N1} & & \cdots & f_{NN} \end{bmatrix} \begin{bmatrix} \overline{V}_1 \\ \overline{V}_2 \\ \cdot \\ \cdot \\ \cdot \\ \overline{V}_N \end{bmatrix} \tag{74}$$

The term $(1-f_n)$ represents the difference between the unloaded and loaded radiation patterns in the direction $(\theta_n, \phi_n)$. Equation (74) is easily solved and the load admittances are found from equation (30) to be

$$Y_n = \left(y_n - \sum_{n=1}^{N} y_{nm} \overline{V}_m\right) / \overline{V}_n \, . \tag{75}$$

Care must be taken in choosing the directions in which the radiation pattern is specified because the matrix in equation (74) can become singular when too much symmetry is introduced into the problem. This can be seen by examining equations (48) and (49).

Consider the design of a pattern which is relatively directive with respect to the pattern of the unloaded loop. An attempt will be made to

a. maximize the front to back ratio of the loaded pattern
b. minimize the beam width of the loaded pattern
c. eliminate or minimize the need for negative load impedances.

For simplicity the following discussion will be restricted to the pattern in the plane of the loop (i.e., $\theta = 90^\circ$). The problem is, given N loads, to determine the best set of N load positions and the best set of N pattern specifications to accomplish the above criteria.

It was found that one maximum point should be specified and remaining points specified as zeroes in the pattern. In many cases, an attempt to specify the pattern more exactly than this results in the development of large lobes in directions where none are desired. Little success was obtained using only two loadings while with three or more loadings favorable results were obtained. For numerous examples considered, it was determined that the modified pattern shape was predominantly determined by the directions in which the pattern was specified and the positions of the loadings had only a slight effect. However, the values of the load impedances necessary to produce a given pattern modification are strongly affected by the positions of the loads.

Consider now, a loop of size kb = 1.0 loaded with three impedances. It was determined that a slightly better directivity could be obtained in the $\phi = 0^{\circ}$ direction than in the direction $\phi = 180^{\circ}$. The best pattern specifications for several different loading positions were found to be $f_1(90^{\circ}, 0^{\circ}) = 1.0$, $f_2(90^{\circ}, 160^{\circ}) = 0.0$ and $f_3(90^{\circ}, 200^{\circ}) = 0.0$. Moving the points the pattern was specified at farther apart, it only slightly decreased the beam width, B. W., (the angle between half power points in the plane of the loop) with the back lobe increasing more rapidly. The load reactances resulting from the above pattern specification are shown as a function of load position in Figure 4.6. It can be seen that all the load resistances are positive in the region $80^{\circ} < \phi < 95^{\circ}$. Figure 4.7 displays the resulting gain pattern of the loop when the loads are located at $\phi_1 = 85^{\circ}$, $\phi_2 = 180^{\circ}$, and $\phi_3 = 275^{\circ}$. This pattern has a B. W. $= 110^{\circ}$ which is approximately the same as that for the unloaded loop. The loaded loop has a front to back ratio, F. B. R., (ratio of the magnitudes of the electric fields evaluated at $\phi = 0^{\circ}$ and $\phi = 180^{\circ}$) of 50 while the unloaded loop has a F. B. R $\doteq 1$. The loop load impedances are $Z_1 = Z_3 \doteq 387 - j\,1180$ ohms and $Z_2 = 108 - j\,140$ ohms and the input impedance is $Z_{in} \doteq 224 - j\,23$ ohms.

Next, the effect of changing kb was investigated. It was found that for the above pattern specifications and load configuration the resulting load impedances had positive real parts and were very smooth functions of kb for kb greater than 0.3 and less than 1.1. Outside this region the loop impedances become quite irregular functions of kb. The pattern retained its basic shape up to kb < 1.3 for these pattern specifications and load positions.

An example of a small loop (kb = 0.3) with these same pattern specifications and load positions as discussed above is shown in Figure 4.8. The load impedances are $Z_1 = Z_3 \doteq 39 + j\,291$ ohms and $Z_2 \doteq 678 - j\,459$ and the input impedance is $Z_{in} = 885 + j\,40$ ohms. The very small values of gain arise from the fact that the gain of an

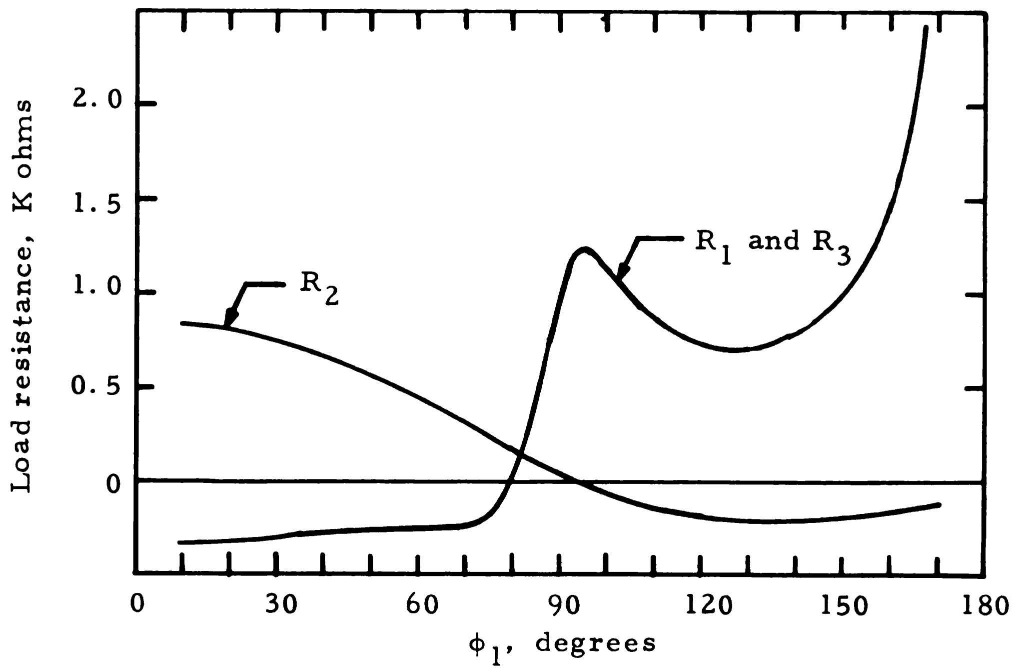


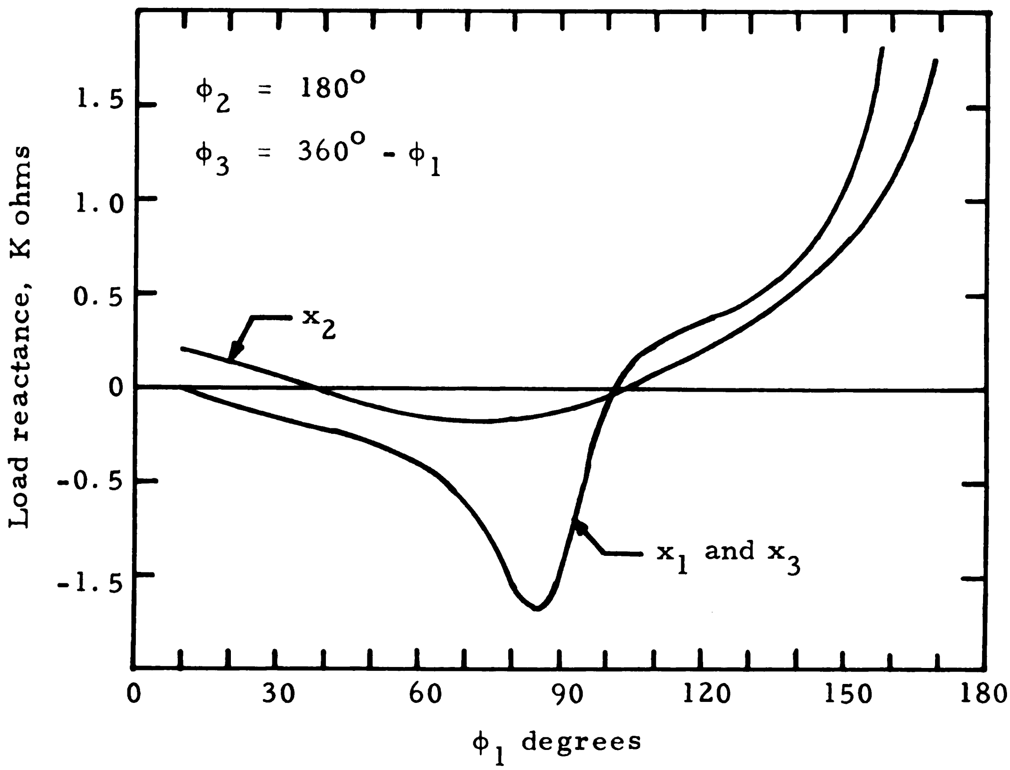


Figure 4.6. Load impedances as a function of load position for a loop antenna of size kb = 1.0 with the pattern specified as $f_1(90^\circ, 0^\circ) = 1.0$, $f_2(90^\circ, 160^\circ) = f_3(90^\circ, 200^\circ) = 0.0$, and $\Omega = 12$, $\delta b/a = 10$.

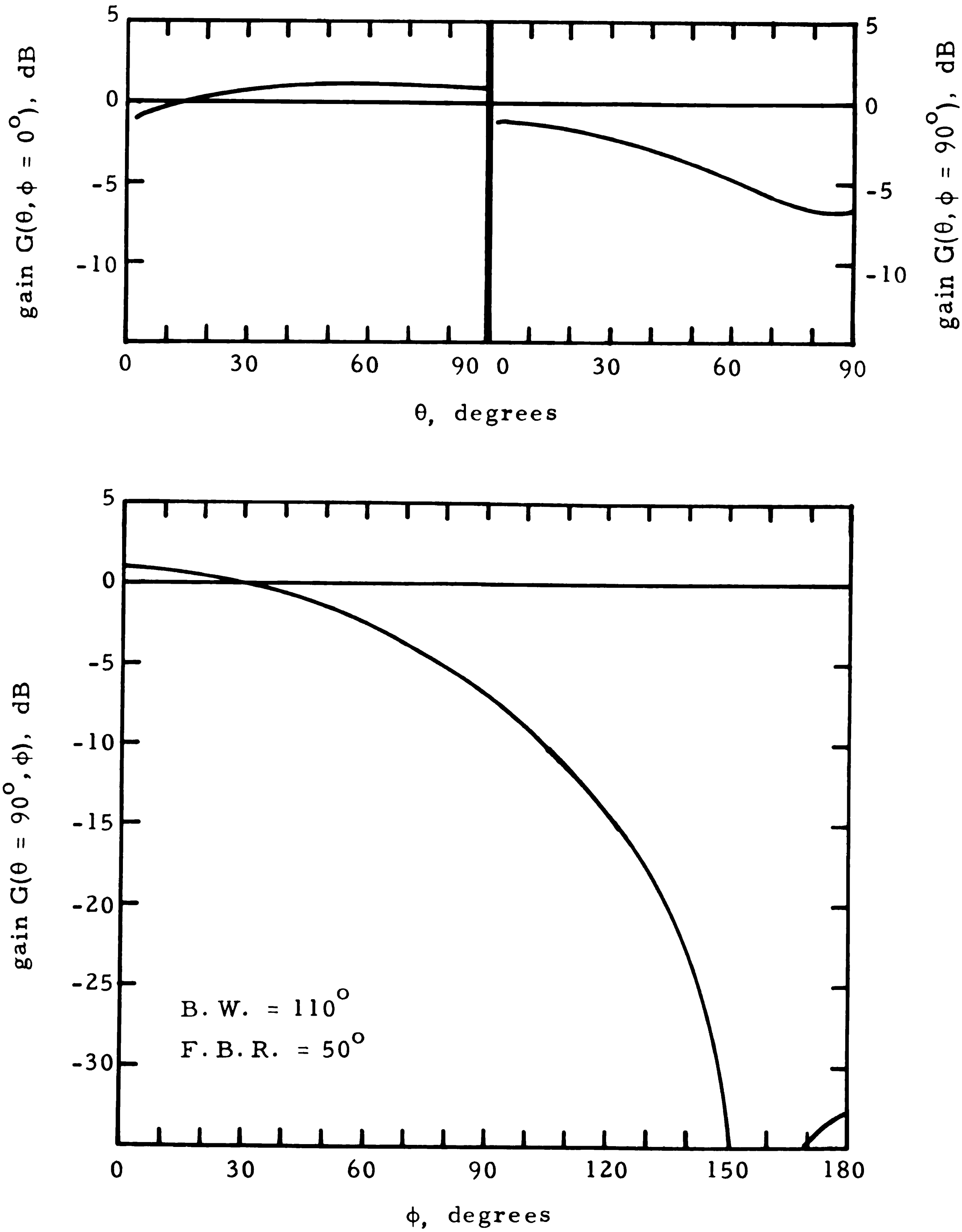


Figure 4.7. Gain pattern of a loop antenna, kb = 1.0, loaded with three impedances located at $\phi_1 = 85^o$, $\phi_2 = 180^o$, and $\phi_3 = 275^o$. The pattern is specified by $f_1(90^o, 0^o) = 1.0$, $f_2(90^o, 160^o) = f_3(90^o, 200^o) = 0.0$.

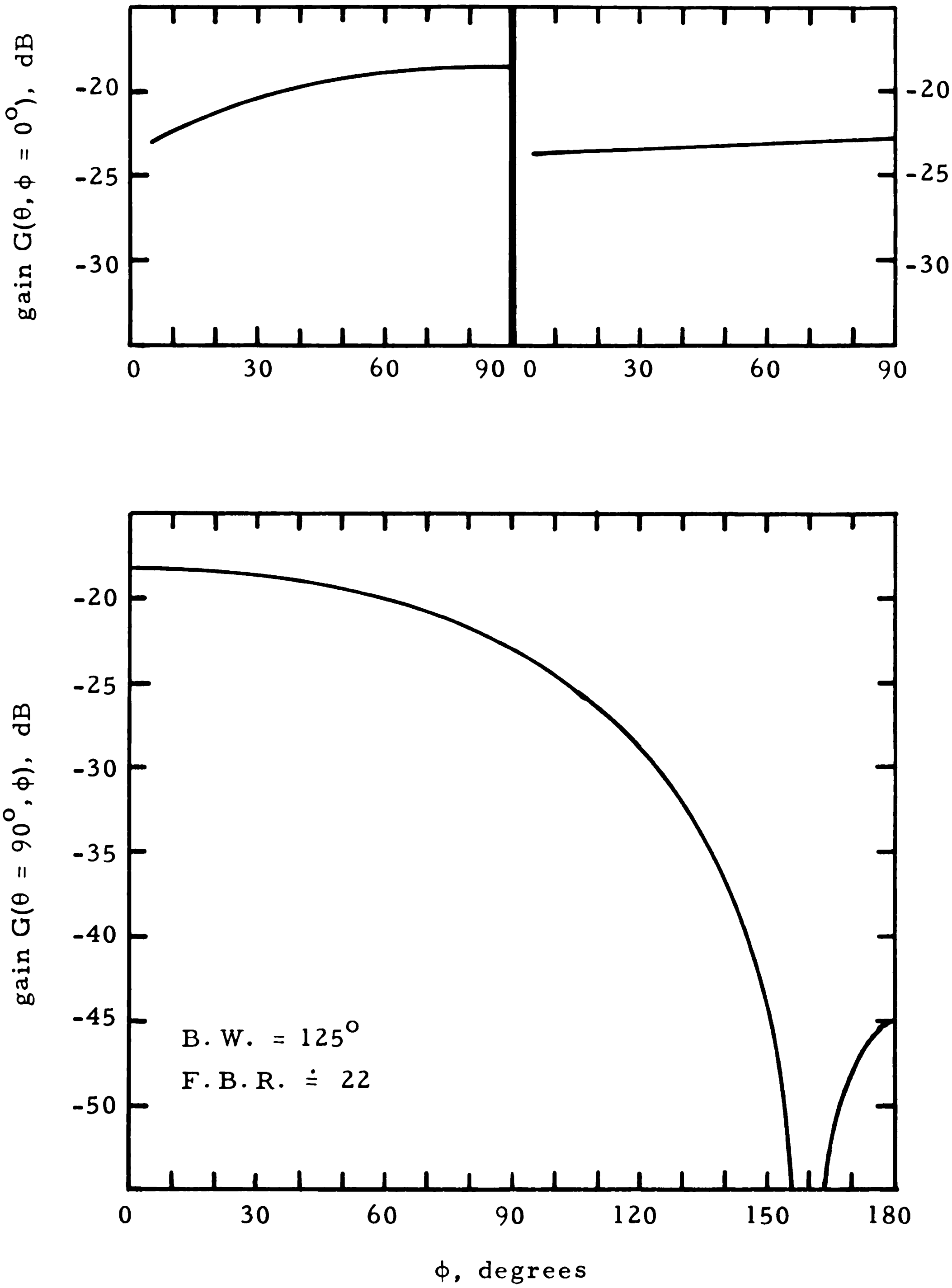


Figure 4.8. Gain pattern of a loop antenna, kb = 0.3, loaded with three impedances at $\phi_1 = 85^o$, $\phi_2 = 180^o$, and $\phi_3 = 275^o$. The pattern is specified by $f_1(90^o, 0^o) = 1.0$, $f_2(90^o, 160^o) = f_3(90^o, 200^o) = 0.0$.

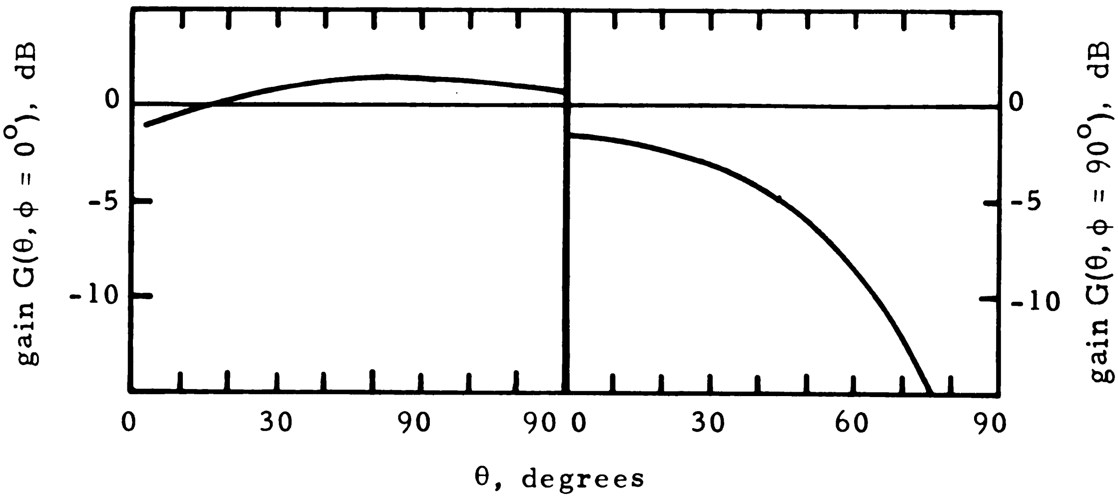


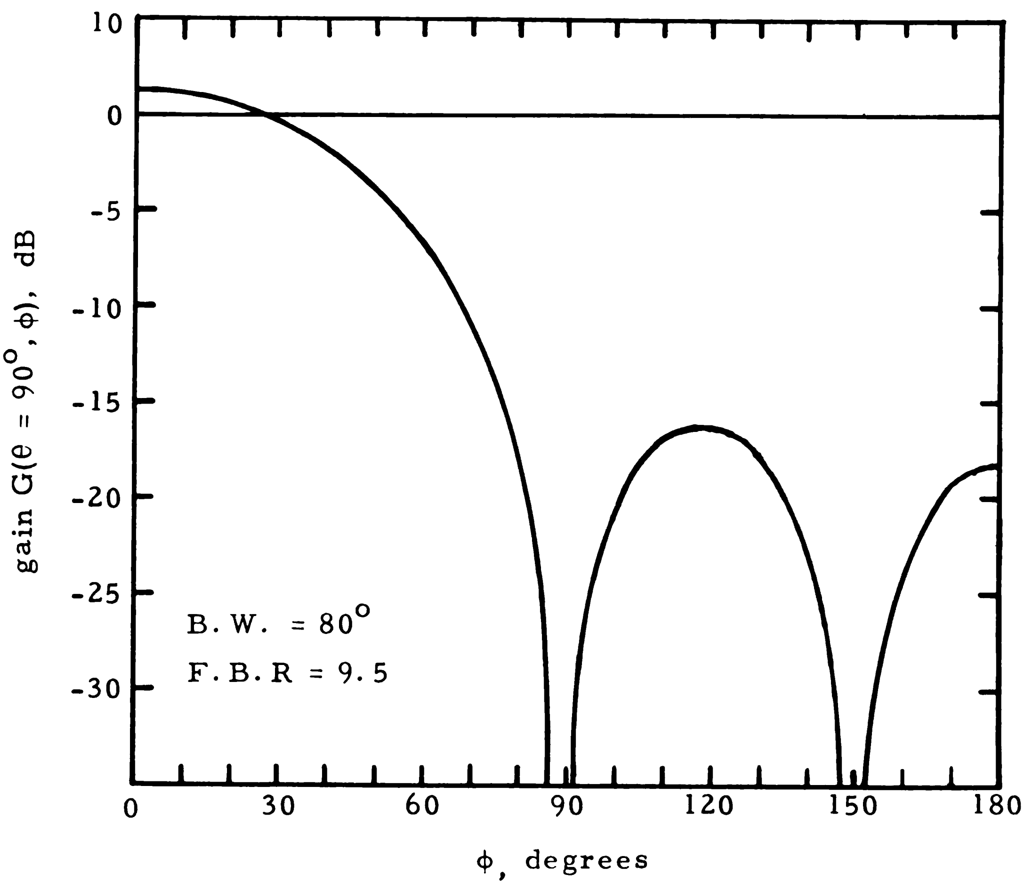


Figure 4.9. Gain pattern of a loop antenna, kb = 1.0, loaded with five impedances of $\phi_1 = 60^o$, $\phi_2 = 120^o$, $\phi_3 = 180^o$, $\phi_4 = 240^o$, and $\phi_5 = 300^o$ and the pattern specified by $f_1(90^o, 0^o) = 1.0$, $f_2(90^o, 90^o) = f_3(90^o, 150^o) = f_4(90^o, 210^o) = f_5(90^o, 270^o) = 0.0$.

antenna is equal to its directivity times its efficiency. The extremely small values of gain imply that the radiation resistance of the loaded loop is very small compared with the input resistance of the loaded loop.

Figure 4.9 displays the gain pattern of a loop (kb = 1.0) loaded with five impedances as indicated. The load impedances are $Z_1 = Z_5 = 244 + j\,226$ ohms, $Z_2 = Z_4 = 274 + j\,779$ ohms, and $Z_3 = -121 + j\,397$ ohms and the input impedance is $Z_{in} = 230 - j\,50$. Some effort was made to eliminate the one negative load resistance, but not all possible load configurations were explored. It can be seen that the beam width is much narrower than the case of three loads but at the expense of increased side lobes.

## 4.4. A Double Loaded Matched Loop.

It is well known that the maximum power will be transferred to an antenna if the impedance the antenna presents to the transmission system or generator driving it is the complex conjugate of the impedance of the transmission system or the impedance the generator presents to the antenna. When this condition exists the antenna is said to be "matched". In many cases there is a practical problem of matching the antenna. In particular, with electrical small antennas which characteristically have very small input resistances and large reactances the impedance transformers necessary to match the antenna are in many cases very lossy. This leads to a very low efficiency for the radiating system (which in this case is taken to include the antenna and its matching network).

It has been shown by Harrison[29] and Nyquist, Chen and others[30, 31, 32, 33] that the efficiency of electrically small dipoles, and slot antennas can be improved by impedance loading.

In this section the possibility of increasing the efficiency of a small loop by impedance loading is considered. The efficiency of the loaded loop is compared to that of an unloaded loop of the same size but matched at its input terminals with an impedance matching network. The loops themselves are considered lossless but the loading impedances and matching impedances are assumed to be lossy inductors and/or capacitors.

A different analytic technique than previously used is used to determine the values of the impedances necessary to match the loop.

Consider a loop loaded with two lumped inductors or capacitors which have finite Q. The Q of the loads is defined as

$$Q_1 = \frac{|X_1|}{R_1} = \frac{|B_1|}{G_1} \tag{76}$$

$$Q_2 = \frac{|X_2|}{R_2} = \frac{|B_2|}{G_2} \tag{77}$$

where $R_1$ and $R_2$ are the resistances that arise from the nonideal elements. The admittance of the loadings can be expressed in terms of their Q's and susceptance as

$$Y_1 = \frac{1}{Q_1} |B_1| + jB_1 \tag{78}$$

$$Y_2 = \frac{1}{Q_2} |B_2| + jB_2 \tag{79}$$

A constraint equation on the load voltages is obtained from equation (32) as

$$Y_{in} = y_o - \overline{V}_1 y_1 - \overline{V}_2 y_2 \tag{80}$$

where $Y_{in}$ is the specified, desired input impedance of the loop, and the normalized load voltages are related to the load admittances by

$$\begin{bmatrix} y_{11} + Y_1 & y_{12} \\ y_{21} & y_{22} + Y_2 \end{bmatrix} \begin{bmatrix} \overline{V}_1 \\ \overline{V}_2 \end{bmatrix} = \begin{bmatrix} y_1 \\ y_2 \end{bmatrix} \tag{81}$$

which is found from equation (30). The normalized load voltages can be eliminated from equation (80) by using equation (81). The resulting equation is

$$AY_1 + CY_1Y_2 + DY_2 + E = 0 \tag{82}$$

where A, C, D, and E are constants defined in this section as

$$A = y_{22}(y_o - Y_{in}) - y_2^2$$

$$C = (y_o - Y_{in})$$

$$D = y_{11}(y_o - Y_{in}) - y_1^2$$

$$E = \begin{vmatrix} y_{11} & y_{12} & -y_1 \\ y_{21} & y_{22} & -y_2 \\ -y_1 & -y_2 & (y_o - Y_{in}) \end{vmatrix}$$

Defining the notation

$$A = A^r + jA^i$$

$$C = C^r + jC^i$$

$$D = D^r + jD^i$$

$$E = E^r + jE^i$$

and writing

$$|B_1| = s_1 B_1 \qquad \text{where } s_1 = \pm 1$$

$$|B_2| = s_2 B_2 \qquad \text{where } s_2 = \pm 1$$

complex equation (82) can be written as two real equations. These equations may be manipulated into the form

$$B_1 = PB_2 + R \tag{83}$$

$$B_2^2 + SB_2 + T = 0 \tag{84}$$

$$P = -\left(\frac{\frac{1}{F}\left(\frac{D^r}{Q_2}s_2 - D^i\right) - \frac{1}{H}\left(\frac{D^i}{Q_2}s_2 + D^r\right)}{\frac{1}{F}\left(\frac{A^r}{Q_1}s_1 - A^i\right) - \frac{1}{H}\left(\frac{A^i}{Q_1}s_1 + A^r\right)}\right)$$

$$R = -\left(\frac{\frac{E^r}{F} - \frac{E^i}{F}}{\frac{1}{F}\left(\frac{A^r}{Q_1}s_1 - A^i\right) - \frac{1}{H}\left(\frac{A^i}{Q_1}s_1 + A^r\right)}\right)$$

$$S = \left(\frac{1}{H}\left(\frac{A^i}{Q_1}s_1 + A^r\right) + \frac{R}{P} + \frac{1}{HP}\left(\frac{D^i}{Q_2}s_2 + D^r\right)\right)$$

$$T = \left(\frac{R}{HP}\left(\frac{A^i}{Q_1}s_1 + A^r\right) + \frac{E^i}{HP}\right)$$

and

$$F = \left(\frac{C^r}{Q_1 Q_2}s_1 s_2 - C^r - \frac{C^i}{Q_1}s_1 - \frac{C^i}{Q_2}s_2\right)$$

$$H = \left(\frac{C^i}{Q_1 Q_2}s_1 s_2 - C^i + \frac{C^r}{Q_1}s_1 + \frac{C^r}{Q_2}s_2\right)$$

Equation (84) can be solved by trial and error with the four possibilities

a. $s_1 = s_2 = 1$

b. $s_1 = 1, \quad s_2 = -1$

c. $s_1 = -1, \quad s_2 = 1$

d. $s_1 = s_2 = -1$ .

The efficiency of this matching technique is given by

$$\text{eff} = \frac{\frac{1}{2}\left[|I(0)|^2 R_{in} - |I(\phi_1)|^2 R_1 - |I(\phi_2)|^2 R_2\right]}{\frac{1}{2}|I(0)|^2 R_{in}} \times 100\%$$

$$= \left[1 - |\overline{V}_1|^2 \frac{|B_1|}{Q_1 G_{in}} - |\overline{V}_2|^2 \frac{|B_2|}{Q_2 G_{in}}\right] \times 100\% \qquad (85)$$

The impedance transform network shown in Figure 4.10 can be used to base tune the unloaded loop.

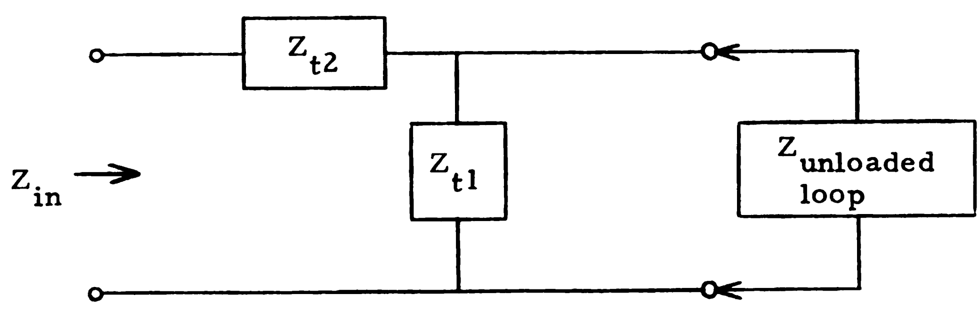


Figure 4. 10. Base tuning network.

The tuning impedances are assumed to be nonideal capacitors or inductors which have finite Q's. These impedances can be represented as

$$Z_{t1} = \frac{|X_{t2}|}{Q_{t1}} + j X_{t1} = \left(\frac{s_1}{Q_{t1}} + j\right) X_{t1} \tag{86}$$

$$Z_{t2} = \frac{|X_{t2}|}{Q_{t2}} + j X_{t2} = \left(\frac{s_2}{Q_{t2}} + j\right) X_{t2} \tag{87}$$

where $s_1 = \pm 1$ and $s_2 = \pm 2$.

Specifying a desired input impedance and given an unloaded loop impedance, the values of $X_{t1}$ and $X_{t2}$ may be found by conventional circuit theory. The exact solution is found to be the roots of a quadratic equation. It can be shown that the efficiency of this network is given by

$$\text{eff} = \left| \frac{Z_{t1}}{Z_{t1} + Z_{\substack{\text{unloaded}\\ \text{loop}}}} \right| \frac{R_{\substack{\text{unloaded}\\ \text{loop}}}}{R_{in}} . \tag{88}$$

This assumes $|Z_1| \neq 0$.

A numerical study was conducted, and it was determined that in the case of small loops the loadings necessary for a purely resistive input impedance are always inductive. However, when one load is placed at $\phi_1 = 0^\circ$ and the second at $\phi_2 = 180^\circ$ the loading necessary at the driving point becomes capacitive. This configuration is desirable since capacitors are usually less lossy than inductors.

A comparison is made in Figure 4.11 of the efficiencies of a loop loaded at $\phi_1 = 0^\circ$ and $\phi_2 = 180^\circ$ so that the input impedance is 300 ohms and the base matching network required to match the unloaded loop input impedance to 300 ohms. A Q of 300 ohms was assumed for all the elements. The corresponding reactances are shown in Figure 4.12. It is seen that the efficiencies are nearly identical for the loaded loop and the matching network. In reality the matching network is probably more efficient at least at lower frequencies where the Q of capacitors is greater than 300.

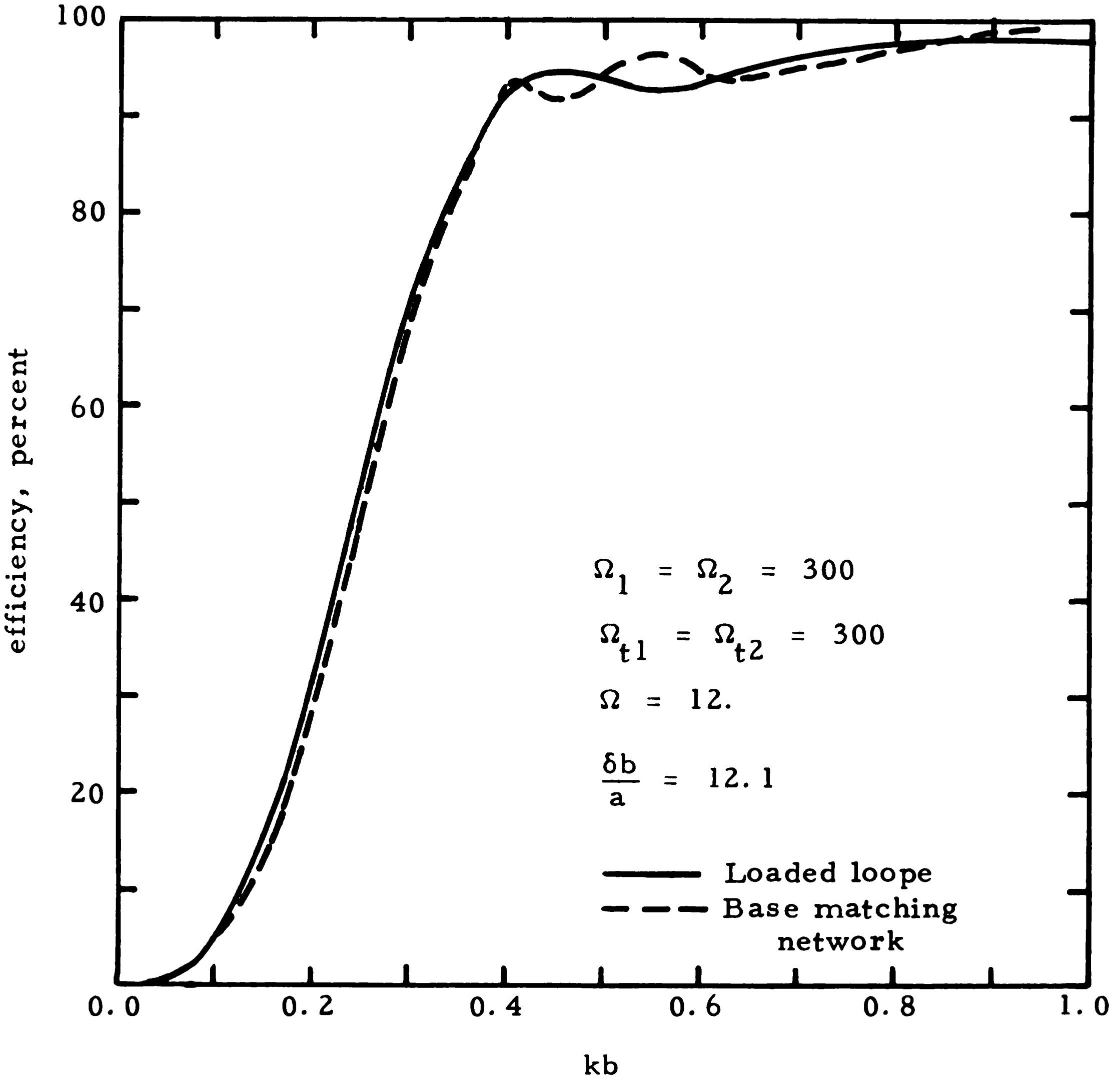


Figure 4. 11. Efficiency of loop loaded with two impedances at $\phi_1 = 0^\circ$ and $\phi_2 = 180^\circ$ to match antenna with 300 ohm input impedances. Compared to efficiency of base matching network.

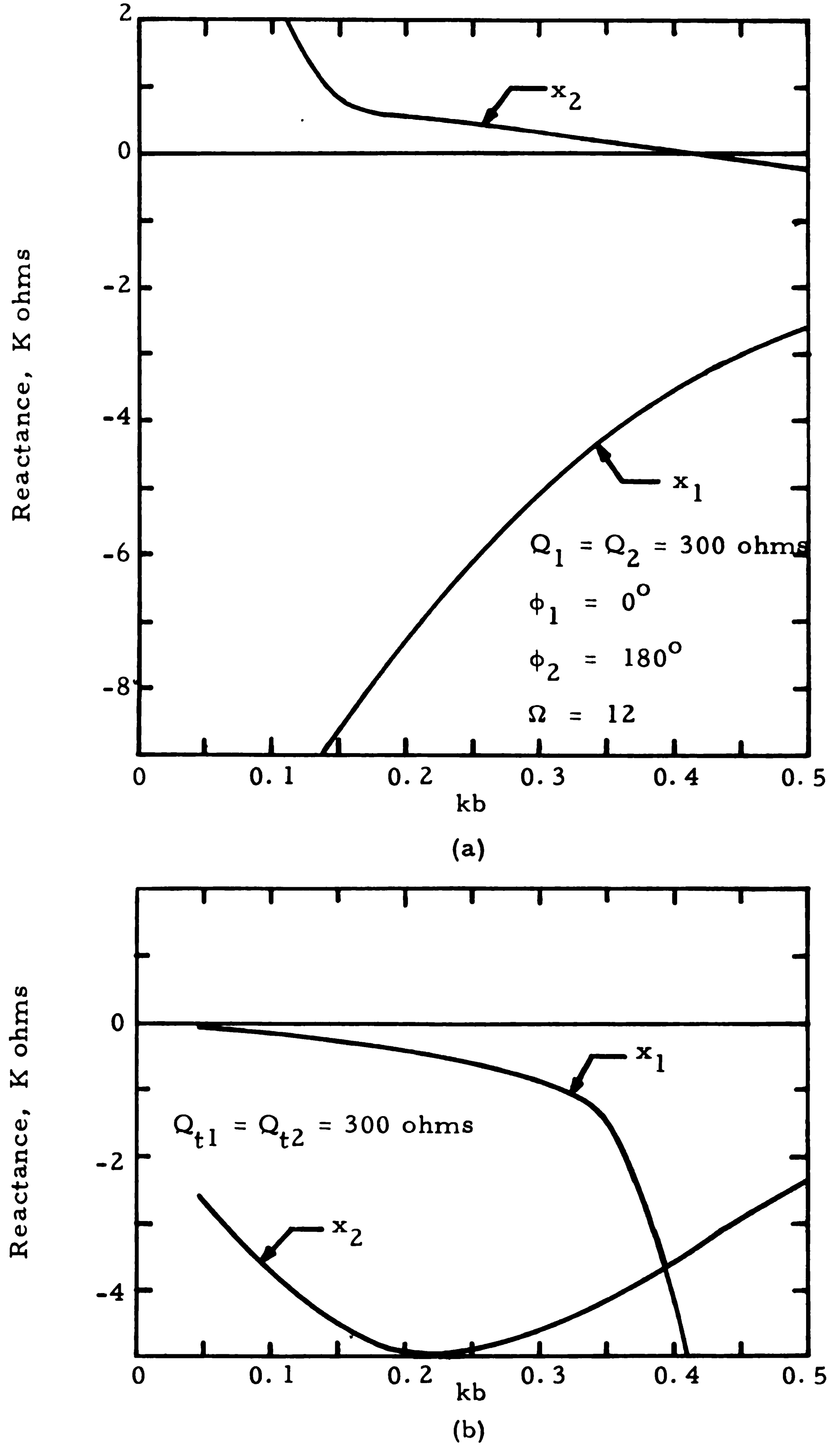


Figure 4. 12. (a) Load reactances necessary for 300 ohm input impedance to loop. (b) Matching network reactances necessary to match a loop antenna $\Omega = 12$, $\delta b/a = 12.1$ to 300 ohms.

# CHAPTER V

# CONCLUSIONS

In the preceding chapters, the circuit and radiation properties of a circular loop antenna were considered. A refined theory of the loaded loop antenna was developed which included a finite gap excitation. The effects of the finite gap excitation were considered and effective gap widths corresponding to the situation when the loop is driven by a two wire line and a coaxial line are proposed. A comparison of the finite gap theory including the effective gap widths is made with existing experimental input admittances. Excellent agreement between theory and experiment is obtained.

Synthesis procedures have been developed to facilitate the design of multi-loaded loop antennas. First, an expression for the maximum and minimum gain attainable from a loop loaded with a single impedance was developed. This expression gives upper and lower bounds on the amount of antenna gain pattern modification that can be accomplished by a single load impedance. It was found for the case of a purely reactive loading located at $\phi = 180^{\circ}$, that in the plane of the loop the antenna gain cannot, in general, be greatly modified in the directions near $\phi = 0^{\circ}$ and $180^{\circ}$ but can, in most cases, be significantly modified in directions near $\phi = 90^{\circ}$ and $270^{\circ}$.

A procedure was then developed for the design of specified radiation patterns. Examples were given showing that relatively directive patterns could be easily designed.

Finally, the possibility of loading a small loop antenna to produce a desired input impedance was considered. This technique does not appear promising as a means of improving the efficiency of the radiating system.

## REFERENCES


1. T. T. Wu, "Theory of the Thin Circular Loop Antenna," J. Math. Phys., 3, 1301-1304, (Nov.-Dec. 1962).

2. E. Hallen, "Theoretical Investigation into the Transmitting and Receiving Qualities of Antenna," Nova Acta Regiae Soc. Sci. Upsaliensis, 11, (1938).

3. J. E. Storer, "Impedance of Thin-Wire Loop Antennas," Trans. AIEE, 75, 606-619, (1956).

4. S. Adachi and T. Mushiake, "Theoretical Formulation for Circular Loop Antennas by Integral Equation Method," Sci. Rep. Res. Inst. Tohoku Univ., 9, 9-18, (1957).

5. S. Adachi and Y. Mushiake, "Study of Large Circular Loop Antennas," Sci. Rep. Res. Inst. Tohoku Univ., 9, 79-103, (1957).

6. R. W. P. King, C. W. Harrison, Jr., and D. G. Tingley, "The Admittance of Bare Circular Loop Antennas in a Dissipative Medium," IEEE Trans. Ant. Prop., AP-12, 434-438, (July 1964).

7. R. W. P. King, C. W. Harrison, Jr., and D. G. Tingley, "The Current in Bare Circular Loop Antennas in a Dissipative Medium," IEEE Trans. Ant. Prop., AP-13, 529-531, (July 1965).

8. S. Ito, N. Inagaki, and T. Sekiguchi, "An Investigation of the Array of Circular-Loop Antennas," IEEE Trans. Ant. Prop., AP-19, 469-476, (July 1971).

9. K. Iiauka, "The Circular Loop Antenna Multiloaded with Positive and Negative Resistors," IEEE Trans. Ant. Prop., AP-13, 7-20, (Jan. 1965).

10. K. Iizuka and F. LaRussa, "Table of the Field Patterns of a Loaded Resonant Circular Loop," IEEE Trans. Ant. Prop., AP-18, 416-418, (May 1970).

11. R. E. Collin and F. J. Zucker, Antenna Theory, Pt. I. (McGraw-Hill, New York, 1969), 461-463.

12. R. W. P. King and C. W. Harrison, Jr., Antennas and Waves (M. I. T. Press, Cambridge, Massachusetts, 1969), 544-548.

13. E. Jahnke and F. Emde, Tables of Functions, (Dover, New York, 1945), 211.

14. G. N. Watson, A Treatise on the Theory of Bessel Functions (Macmillan, New York, 1945), 308-309.

15. R. E. Collin and F. J. Zucker, Antenna Theory, Pt. I. (McGraw-Hill, New York, 1969).

16. R. W. P. King and C. W. Harrison, Jr., Antennas and Waves (M. I. T. Press, Cambridge, Massachusetts, 1969), 569-576.

17. G. Gilbert and G. Baker, Bessel Function (Fortran), M. S. U. Computer Lab. No. 00000223.

18. M. Abramowitz and I. A. Stegun, Handbook of Mathematical Functions (Dover, New York, 1965), 378-379.

19. M. Abramowitz and I. A. Stegun, Handbook of Mathematical Functions (Dover, New York, 1965), 378, Eq. (9.75).

20. H. K. Crowder and S. W. McCuskey, Topics in Higher Analysis (Macmillan, New York, 1964), 190 and 199.

21. K. Iizuka and R. W. P. King, "Terminal-Zone Corrections for a Dipole Driven by a Two-Wire Line," J. Res. Natl. Bur. Std. (U. S.), 66D, 775-782 (Nov.-Dec. 1962).

22. R. W. P. King, Theory of Linear Antennas (Harvard University Press, Cambridge, Mass., 1956), Chapt. II, Sec. 38.

23. T. T. Wu, "Input Admittance of Infinitely Long Dipole Antennas Driven from Coaxial Lines," J. Math. Phy., 3, 1298-1301, (Nov.-Dec. 1962).

24. R. E. Collin and F. J. Zucker, Antenna Theory, Pt. I. (McGraw-Hill, New York, 1969), Chapt. 10, Sec. 1 and 2.

25. P. A. Kennedy, "Loop Antenna Measurements," IRE Trans. Ant. Prop., AP-4, 610-618, (1956); Tables of experiment data in Cruft Lab. Tech. Rept. 213, Harvard University, May 1955.

26. R. E. Collin and F. J. Zucker, Antenna Theory, Pt. I. (McGraw-Hill, 1969), 473.

27. J. B. Sherman, "Circular Loop Antennas at Ultra-High Frequencies," Proc. IRE, 32 534-537, (Sept. 1944).

28. B. R. Rao, "For Field Patterns of Large Circular Loop Antennas: Theoretical and Experimental Results," IEEE Trans. Ant. Prop., AP-68, 269-270, (March 1968).

29. C. W. Harrison, Jr., "Monopole with Inductive Loading," IEEE Trans. Ant. Prop., AP-11 394-400, (July 1963).

30. C. J. Lin, D. P. Nyquist, and K. M. Chen, "Short Cylindrical Antennas with Enhanced Radiation or High Directivity," IEEE Trans. Ant. Prop., AP-18, 576-580, (1970).

31. C. J. Lin, D. P. Nyquist, and K. M. Chen, "Parasitic Array of Two Loaded Short Antennas with Enhanced Radiation or High Directivity," Fall URSI Meeting Commission VI, (1970).

32. T. Z. Hsieh, D. P. Nyquist, and K. M. Chen, "The Short-Slot Antenna with Enhanced Radiation or Improved Directivity," Electronic Letters, 7, (Jan. 1971).

33. T. Z. Hsieh, D. P. Nyquist, and K. M. Chen, "The Loaded Annular Slot: An Efficient Small Antenna," Spring URSI Meeting Commission V, (1971).

MICHIGAN STATE UNIVERSITY LIBRARIES
3 1293 03174 7482